universität wien

MASTERARBEIT / MASTER'S THESIS

Titel der Masterarbeit / Title of the Master's Thesis

Tracing mercury transformations in soil using mercury stable isotope analysis

verfasst von / submitted by

Flora Maria Brocza, BSc.

angestrebter akademischer Grad / in partial fulfilment of the requirements for the degree of

Master of Science (MSc.)

Wien, 2017 / Vienna 2017

Studienkennzahl lt. Studienblatt / degree programme code as it appears on the student record sheet:	A 066 815
Studienrichtung lt. Studienblatt / degree programme as it appears on the student record sheet:	Masterstudium Erdwissenschaften / Masterprogramme Earth Sciences
Betreut von / Supervisor:	Doz. Dipl.-Geoökol Dr. Jan Georg Wiederhold, MSc.

Acknowledgements

I would like to acknowledge the important role of Harald Biester and Jan-Helge Richard in the writing of this thesis. Their support and expertise during the sampling campain and during the discussion of the data was central to the success of this project. Thank you also to Stephan Krämer for the critical and helpful comments on the manuscript!

I have been lucky enough to touch upon uncountable open arms, open ears and open hearts during my academic journey. Friends, family and mentors alike: Your trust, patience and feedback have played an important role. Not only in the process of writing this thesis - also in my path as a person with a goal, a conviction and an ever-so-slowly growing toolset to work her way towards their fulfillment. Thank you friends and family near and far, especially Laurentius, Selma, Nina, and the lovely Environmental (Geo)scientists! Academically, I would like to thank my parents, for holding up to fiery arguments when my discussion style was yet to be refined; Werner Muller, who let me study his cattle farm at the age of 17; Taru Lehtinen, who told me to 'go out and do my thing' when I believed that this was not an option; Elena Petrishcheva, whose rigor and way of thinking set my path during my BSc. years. Last but not least, I want to thank Jan Wiederhold, who spent countless hours introducing me to his scientific field, discussing with me, and pointing out every conceptual and spelling mistake I made – all while showing me the kind of respect and never-ending patience that makes one feel confident and optimistic about one's work and, more generally, about doing science.

Abbreviations

BK . . . **B**ad **K**rozingen

SEP . . . **S**equential **E**xtraction **P**rotocol

DOM . . . **D**issolved **O**rganic **M**atter

NOM . . . **N**atural **O**rganic **M**atter

MDF . . . **M**ass **D**ependent **F**ractionation

MIF . . . **M**ass **I**ndependent **F**ractionation

w.w. . . . **w**et **w**eight

d.w. . . . **d**ry **w**eight

MC-ICP-MS . . . **M**ulti**c**ollector **I**nductively-**c**oupled **P**lasma **M**ass **S**pectrometry

PTD . . . **P**yrolytic **T**hermo-**D**esorption

Table of contents

List of figures

List of tables

Chapter 1

Introduction

1.1 Motivation for this project: Why this, and why now?

Mercury (Hg), 'quicksilver' by its old-fashioned name, has fascinated ancient cultures and alchemists of all continents in the form of a silvery liquid as well as the red pigment cinnabar (HgS). But mercury is more than just an archaeological curiosity: it is used in industrial processes to this day. While it is usually only present in the Earth's crust in the < 1 ppm range (Fitzgerald and Lamborg, 2014), mining of mercury ores has taken place for more than 3000 years (Cooke et al., 2013) and the global mercury flux to the atmosphere has been estimated to have tripled in size compared to pre-industrial times, up to 8900 ⅊ (AMAP/UNEP, 2013; Hintelmann and Zheng, 2011). Mining of gold and silver, burning of fossil fuels and coal and other anthropogenic activities have contributed to this. Mercury's chemical forms in our environment vary widely, from the well-known metallic liquid Hg^0 to molecules with different bonding partners, through gaseous, liquid and solid state and with vastly different distances that these compounds can travel. The rising level of mercury in our environments is thus increasingly raising health concerns: All forms of mercury are highly toxic to the human nervous system. Mercury may be inhaled as elemental mercury vapor. The most toxic mercury species - methyl mercury - is prone to accumulate in the aquatic food chain and reaches concerning levels in popular seafood species (Kirby et al., 2013). To counteract this, the United Nations are seeking to phase mercury out from industrial processes and strongly limit its production and use in daily life, and the Minamata Convention on Mercury has been signed by 128 countries at the time of writing (UNEP, 2013b). However, even if the international community succeeds in constraining new releases of mercury into the environment, the legacy of past mercury pollution will pose a problem for generations to come. The high mobility in the environment and easy volatilization of the element causes significant re-emission from legacy mercury stored in sediments and watersheds; together

with new releases from unregulated soures such as artisanal gold mining, mercury will continue to be a substance of concern (Fitzgerald and Lamborg, 2014). The multitude of mercury compounds and their differing toxicities make mercury a much-studied contaminant that needs careful investigation to avoid any risk to human and ecosystem health.
In many cases, the biogeochemical pathways of mercury transformations in the environment are still not fully understood (Bergquist and Blum, 2009). Owing to this situation, our goal is to deepen our understanding of the mercury cycle with all methods available to us. We want to better understand how mercury moves through the environment, and to understand its speciation, which is indicative of the risk that the pollutant may pose.
Stable isotopes have recently be shown to be a useful marker of the biogeochemical transformations of mercury (Hintelmann and Zheng, 2011). By determining the stable isotope fractionation which occurs between species of mercury while undergoing transformations, these transformations are recorded in the residual mercury pool and the newly formed mercury-containing product. This change in isotopic signature has been observed in natural systems, as well as in the laboratory, where a multitude of fractionation-inducing processes have been studied. However, not much of this knowledge about specific processes and their mark on soils' mercury pools has been taken back to the field and studied in mercury-contaminated field settings. This thesis studies a field site which is severely affected by legacy pollution: The studied residential area in Bad Krozingen, Germany, formerly a commercial facility for impregnation of wooden poles by submersion in mercury(II) chloride ($HgCl_2$), has been remediated on the surface by topsoil removal (Schöndorf et al., 1995). Only 50 cm below the apartment blocks and lawns, however, the mercury concentrations are still up to 800 $^{mg}/_{kg}$ soil in some places, and mercury is detected in the groundwater. The contamination originally consisted of the soluble $HgCl_2$, which has undergone transformations, as different mercury species such as HgS and Hg^0 have been detected on-site. The soil composition is poor in organic matter, which is known to strongly bind mercury in soil systems. This allows expectation of a more varied set of reactions to take place, beside binding to organic matter. Additionally, Hg concentrations and its distribution in soil and groundwater are well known (Biester and Scholz, 1997; Bollen et al., 2008). Still, much about the chemical speciation and binding forms is unknown and the method of mercury stable isotope analysis has never been applied to the site.
This thesis combines the 'classical' methods of soil extractions, concentration measurements, basic geochemical parameters and pyrolytic thermo-desorption with Hg stable isotope measurements. Metal stable isotopes have emerged in the past decade(s) with the advancement of multicollector inductively coupled mass spectrometers (MC-ICP-MS) and have the potential to determine the isotope ratios of the seven mercury isotopes and depict their variation.

Mercury isotopic ratios have shown to vary spatially and isotope fractionation has been demonstrated to be specific for certain transformation processes that the element undergoes (Bergquist and Blum, 2009). Using the newly generated data and already existing data, a better understanding of the speciation of mercury, as well as the processes producing it, is achieved. The isotope dataset produced in this thesis adds another layer to the existing dataset on the contamination case.

1.2 Site Description

1.2.1 History

The field site for this study is located in the town of Bad Krozingen, about 15 km southwest of Freiburg, in Baden-Württemberg, Germany. From 1904 until 1965, a wood impregnation plant was operating in Bad Krozingen (Bollen et al., 2008). Impregnation of wooden sticks used in vineyards, sleepers for railway tracks and telegraph poles was achieved using the kyanization method, for which the wood pieces are submerged in an aqueous solution of 0.67% $HgCl_2$ ('Sublimate'). The poles were then placed outside of the kyanization hall for drying, where some of the sublimate solution dripped onto the ground and leached into the soil and underlying groundwater. Additionally, leakage into the soil occurred when a fire at the kyanization facility during World War II was put out using the dilute $HgCl_2$ impregnation solution (Lenguin-Hoppe, 2000). While in the beginning of operations, the sublimate stocks were bought, after 1921, $HgCl_2$ was produced on site using liquid mercury ($Hg^0_{(l)}$) and chlorine gas ($Cl_{s\ (g)}$) (Lenguin-Hoppe, 2000). This accounted for additional contamination; however, it has been reported that this contamination is very local and has not affected the studied sites. Impregnation of the lower parts of poles by application of tar oils has lead to an additional contamination of the area by polycyclic aromatic hydrocarbons (Bollen et al., 2008; Schöndorf et al., 1995). Schöndorf et al. (1995) estimated that during the 60 years of operation 10-20 tons of $HgCl_2$ leaked into the ground.
From 1968 on, the 8 ha brownfield area of the now-closed impregnation plant was cleared for redevelopment into a settlement area (Lenguin-Hoppe, 2000). All buildings of the facility were removed and top soil was re-distributed over the whole area to level out the topography. During the process, spreading the soil contamination over the whole area occurred. All construction work on the 'Parksiedlung' residential area finished by 1981. At that point, ca. 1200 residents had moved in, making it Bad Krozingen's biggest residential area. Only in 1994, the extent of the mercury contamination was discovered and the LRA Breisgau-Hochschwarzwald conducted a larger-scale screening of the area. In the following years,

it was decided by the former owner, the residents and city officials to remediate yards and parks of the area by topsoil-removal. Geotextile was laid out at about 50 cm depth to avoid re-contamination of the upper layers from below, and the volume above was filled with uncontaminated soil.

1.2.2 Geology and extent of contamination

In spite of the surface remediation, the ground of the 'Parksiedlung' residential area remained still highly contaminated in the subsurface. Especially the location of the former kyanization plant is still contaminated with concentrations up to 11 000 $^{mg}/_{kg}$ mercury (Bollen et al., 2008) and the contamination has reached the groundwater, causing maximum concentrations of 230 $^{mg}/_{L}$ in a plume that is 1.3 km long and up to 100 m wide, as Bollen et al. (2008) have determined. Already Schöndorf et al. (1999) concluded on the basis of soil gas measurements that some samples contained high amounts of Hg^0, and that the absolute amounts of Hg in different surface soil samples was highly heterogeneous. The upper 1-3 meters of soil consist of material redistributed in the 1970's, and contain loess from underlying layers as well as construction materials and gravel. Below, unaffected by construction endeavors, homogeneous loess is encountered. The loess consists of carbonatic, mostly silty sediments with a low organic carbon content. The system is carbonate-buffered and thus has a high pH of 6.9-8.7 in the soil solution (Schöndorf et al., 1999), as shown in table 1.1 (Bollen et al., 2008).

	pH (−)	C_{org} (%)	Eh (mV)	O_2 (mg/l)	DOC (mg/l)	Cl^- (mg/l)
Groundwater	6.62±0.45 ($n = 103$)		454±55 ($n = 97$)	6.01±1.06 ($n = 107$)	0.57±0.04 ($n = 4$)	20±1 ($n = 8$)
Soil horizons						
Artificial filling	7.90±0.06 ($n = 4$)	2.50±2.20 ($n = 4$)				
Loess cover	7.89±0.10 ($n = 6$)	0.85±0.47 ($n = 8$)				
Unsaturated zone	7.55±0.20 ($n = 6$)	0.21±0.14 ($n = 10$)				
Saturated zone	7.27±0.38 ($n = 6$)	0.07±0.05 ($n = 7$)				
Aquitard	7.32±0.26 ($n = 6$)	0.16±0.09 ($n = 8$)				

FIG. 1.1 Soil and water chemistry at the sampling location in Bad Krozingen, as published by Bollen et al. (2008). The represented numbers represent medians and 1 S.D. of the collected data.

FIG. 1.2 Location of the study site on the map of Germany and within Bad Krozingen itself. Base map Google Earth, 2017. Map of Germany: https:www.suche-postleitzahl.org. The orange stars mark the drilling locations for the soil cores of this study.

1.3 Anthropogenic emissions and health effects of mercury

According to the Global Mercury Assessment 2013 (UNEP, 2013a), natural mercury emissions to the atmosphere only make up 10% of the total annual emissions. Anthropogenic sources account for 30% of the yearly; the rest, an overwhelming 60 %, are constituted by re-emissions from legacy mercury in the environment. Anthropogenic emissions are partly unintentional; for example, 24% of anthropogenic emissions are connected to coal burning, 10% to the smelting/mining of iron and other metals, lesser percentages by cement production and oil refining. On the other hand, 37% of anthropogenic yearly emissions are due to small-scale and artisanal gold mining, where mercury is used to amalgamate the gold contained in crushed sediments and later volatilized to free the gold again. Consumer products such as dental amalgams, halogen lamps and cosmetics enter the environment through landfills or cremation. Mercury use in chlor-alkali plants is increasingly phased out, but other industrial processes such as vinyl chloride monomer production still require the toxic metal. Mercury pollution is not a local phenomenon (Pirrone et al., 2010); once mercury is brought into the environment, it is likely to volatilize, to be transported thousands of kilomenters, and to be deposited again in a different region.

Mercury intake most commonly occurs over two pathways: First, it may be inhaled as elemental Hg^0 gas. Secondly, organic methyl mercury ('MeHg') may be ingested through the consumption of contaminated seafood. MeHg is produced through bacterial activity in surface waters and soils, and is the most toxic mercury species to humans. Once methylated, the lipophilic substance easily enters the food chain and accumulates in the fatty tissue, where it bioaccumulates. The bioaccumulation factors that have been determined by the

Nichols et al. (1997) report show that in trophic levels 3 and 4, mercury concentrations are in the range of a factor 10^6 higher than in the surrounding water. Hence, already low concentrations of MeHg in an aquatic environment can pose a health problem through fish. Globally, fish consumption is the most common exposure pathway to critical amounts of mercury (Kirby et al., 2013). The health effects of mercury exposure are numerous and have been studied extensively (Risher, 2003), since the element has been named a *Priority hazardous substance* by EU (Parliament, 2001) and *one of the top ten chemicals of major public health concern* by the WHO (WHO, 2011). Elemental Hg^0 enters the body through inhalation, while methyl mercury is primarily ingested through seafood. It may cause a set of neurological problems and has also been shown to cause cardiovascular problems. Chronic exposure to mercury through seafood has been linked to attention deficit hyperactivity disorder in children (Boucher et al., 2012). Acute mercury poisoning may lead to numb limbs, and hearing or speaking impairment, as tragically occurred in several cases during the Minamata contamination case (UNEP, 2013a).

1.4 Properties of Mercury

Mercury is a metal whose properties can largely change when it undergoes geochemical transformations in the environment. Its toxicity and bioavailablity depend strongly on the mercury species that are present in a system. Thus, it is important to know which species are present in the soil, and what their mobility and bioavailability are like.

1.4.1 Physico-chemical properties

As elemental mercury Hg^0, it as a melting point of -38.87 °C and the lowest boiling point of all metals (356.57 °C) (Skyllberg, 2011). It has a quite low solubility of ca. 60 ppb in water at room temperature. Mercury has a very stable electronic configuration where both f- and d-orbitals are filled: $[Xe]4f^{14}5d^{10}6s^2$. This almost "noble gas like" feature leads to several characteristics of elemental mercury: It only interacts weakly with other atoms (Skyllberg, 2011), forms a monatomic Hg^0 gas, is in liquid state at room temperature and has a comparably high vapor pressure (Huber et al., 2006). Mercury occurs in the oxidation states of 'metallic' Hg^0, 'mercurous' Hg^I and 'mercuric' Hg^{II}, where Hg^I in the form of Hg_2^{2+} is metastable and disproportionates to Hg^{II}, so fast that it is not detected by conventional methods (Skyllberg, 2011). The redox potential E^0 of Hg^0/Hg^{II} of 0.85V (Clever et al., 1985) is similar to that of Fe^{II}/Fe^{III}. Oxidation/reduction reactions are commonplace in natural systems and add to the variablilty of mercury species seen in the environment. There

are also methylated species of mercury CH_3Hg^+ and $(CH_3)_2Hg_{(aq)}$, which are well known for its high toxicity and potential to bioaccumulate in the aquatic food chain. The highest methylation rates are encountered at the redox interface in sediments, but methylation has also been shown in the water column, which, although displaying lower rates, is vastly larger (Ullrich et al., 2001). Mercury is a chalcophilic element; it has a strong affinity for sulfide and sulfur groups. Skyllberg (2011) compiled thermodynamic data on mercury species in soils and sediment which show that the thermodynamically most favorable inorganic Hg^{II} complexes are formed with sulfides, polysulfides and thiol groups, followed by chloride- and hydroxy complexes. Mercury favors complexes with the low coordination numbers 2, 3 and 4.

1.4.2 Biogeochemical cycling of Hg

Mercury's unusual physico-chemical properties lead to a complex cycle of biogeochemical transformations that take place in the environment. This section discusses the predominant forms of mercury in the reservoirs atmosphere, soils and aqueous systems.

Atmosphere

More than 95% of mercury in the atmosphere is present as $Hg^0_{(g)}$ in the atmosphere, the other 5% are particulate $Hg^{II}_{(p)}$ (Schroeder and Munthe, 1998). The residence time of Hg^0 in the atmosphere was determined by Schroeder and Munthe (1998) to be approximately one year and due to the fact that the mercury is present almost exclusively as a gas, rather than an aerosol, and displays low reactivity. Owing to its long retention in the atmosphere, once there, the mercury gas is distributed globally. When it is oxidized eventually – mainly by O_3, OH, Br and BrO (AMAP/UNEP, 2013) –, it is deposited via wet or dry deposition to terrestrial or ocean surfaces. The potential for re-emission to the atmosphere varies from reservoir to reservoir, which will be discussed in the follwing paragraphs. Mercury once brought into this cycle is bound to be re-emitted and deposited, thus stay in the cycle and likely represent legacy contamination for many years to come.

Soil

Soils are complex mixtures of mineral particles, organic matter at various stages of degradation, soil water and the soil gaseous phases (Scheffer and Schachtschabel, 2010). The opportunities for mercury to bind to this mixture, and to transform, are as variable as the

actual soil composition. Mercury may be present in dissolved, gaseous or solid forms, may form complexes, sorb to particles, or diffuse into them.

Oxidation states

Mercury is present in several oxidation states in soil systems. Oxidized Hg^{II} is rarely found in its free form but forms stable complexes with multiple anion species in the soil, which will be described more closely in the next paragraph. However, it does not necessarily need reducing conditions throughout the whole soil system for mercury to become reduced to metallic Hg^0. Schuster (1991) state based on their pH/eh diagram that even under moderately oxidizing conditions at pH > 5, Hg^0 is the most stable species. Due to its low solubility (0.06 mg/L at room temperature, (Skyllberg, 2011)) and high vapor pressure, saturation is easily reached and the possibility of degassing and loss from the soil system to the atmosphere is a likely scenario for soils which are shown to contain Hg^0 (Schuster, 1991), and has also been demonstrated to happen at the Bad Krozingen site. Pannu (2012) reviewed factors which influence the reduction of Hg^{II} to elemental Hg^0 in soils and identified soil physicochemical characteristics as well as abiotic factors like insolation and moisture to play a role in the rates of reduction.

Common ligands

The most common ligands of mercury are discussed here. $Hg(OH)_2^0$ is the dominant complex at neutral pH in a system where no organic matter, sulfides or chloride are present. As for halides, mercury has the highest affinities for halides with the highest atomic number; as chloride is widely more available in most natural systems than bromine or iodine, chlorine complexes are usuallally dominant. Due to the high solubility of $HgCl_2$ in H_2O of 74000 mg/L at 20°C (US-EPA, 1995), the resulting complex has a high mobility in the aqueous system.

Dissolved and particulate organic matter (DOM/POM) are present in the percent range in virtually all soil types (Scheffer and Schachtschabel, 2010); several functional groups of organic matter can bind to mercury; thiol groups have the highest affinity, but carboxyl, hydroxyl and phosphoryl groups also exhibit reasonably high binding constants. The role of OM in the cycling of soil mercury can hardly be understated and has been the subject of several studies and reviews (Ravichandran, 2004; Wallschläger et al., 1996). In terms of mobility, OM may bind Hg^{II} and render it immobile; on the other hand, it has been shown to be capable of reducing Hg^{II}, and also of promoting its photoreduction, both of which increase mobility highly and cause emissions of mercury from soils to the atmosphere (Ravichandran, 2004). OM also plays an important role in the (de-)methylation of mercury, shielding the

complexed Hg^{II} from methylating bacteria. DOM consists to 80% of humic substances (Ravichandran, 2004) and contains several functional groups which mercury may bind to, such as carboxyl, hydroxyl, phosphoryl and thiol groups; (Mishra et al., 2011). Thiol groups associated with dissolved organic matter (DOM) can reach micromolar concentrations in solutions. Due to their extraordinarily high affinity for mercury, they form stable complexes with mercury, $Hg(SR)_2$ being the dominant one at various chloride and pH conditions, according to thermodynamic modeling carried out by Skyllberg (2011). Figure 1.3 shows an exemplary species dominance diagram over a range of pH values and for varying chloride content in the system. It is clearly visible that while in a system without sulfur binding groups, chloride complexes dominate at lower pH values, while hydroxide complexes dominate at higher pH values and lower chloride concentrations. Once thiols enter the aqueous phase of a natural soil system, which is estimated by Skyllberg (2011) to contain an average of 0.005–0.1 nmol/L, their affinity for mercury is so high that sulfide-Hg complexes dominate the mercury speciation. This has been modeled to happen over the whole range of environmental conditions in freshwater and marine systems, even at thiol concentrations as low as 10 nmol/L. Owing to the strong binding to organic matter, soils may act as net sinks for mercury (Schuster, 1991) Nevertheless, re-emission can happen, as when Hg^{II} is reduced to Hg^0, which has high vapor pressure and low solubility in H_2O, thus is easily volatilized and released back into the atmosphere.

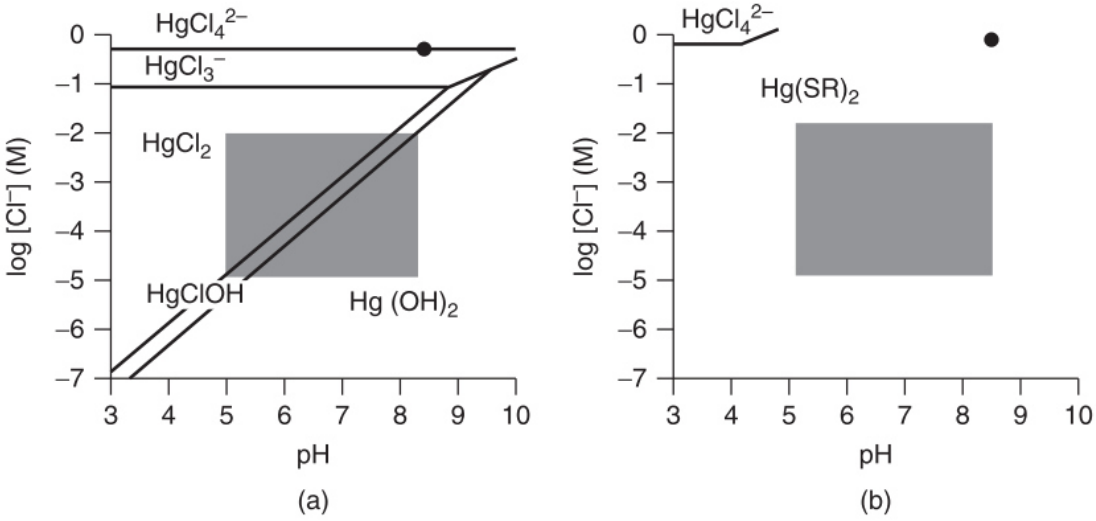

FIG. 1.3 Ph/eh diagram by Skyllberg (2011): Dominance diagram for aqueous phase species of Hg under natural oxic conditions (5-100 pM Hg) in the absence (a) and in the presence (b) of 10 nM of low molecular mass thiols (RS_{tot}). The black dots represent seawater conditions, the gray rectangle represents natural soils and freshwater conditions.

Sorption

Since the solution speciation of mercury is determined by the complexes discussed above, these also govern the sorption behavior of the element. Schuster (1991) found that increasing chloride content of the solution reduces the amount of mercury that is adsorbed to silica, and that the adsorption then only occurs at higher pH levels. As mentioned previously, mercury has an extraordinarily high affinity for reduced sulfur-groups on organic matter, which of course also applies to particulate OM in soil. Organic-rich soil horizons have been shown to contain the highest mercury amounts of all soil horizons (Navrátil et al., 2014). Schuster (1991) cites two studies where cation-exchange resin extracted 200 times less mercury than fulvic acid from soils contaminated by mercury mining. According to Skyllberg (2011), most natural systems have such a surplus of sulfur-binding sites on NOM compared to available mercury that oxygen-binding sites at Fe- and Al-oxide surfaces play only a minor role in the adsorption of mercury, unless the system is so highly contaminated that all binding sites at the NOM are occupied.

Solid forms

Mercury may also precipitate and form mineral phases in soils. The solubility of $HgCl_2$, the main contamination source, has been reported to be as high as 74000 mg/L water at room temperature Clever et al. (1985); US-EPA (1995). Consequently, mercury-chloride precipitates such as mercuric chloride (also called 'sublimate', $Hg^{II}Cl_2(s)$) and mercurous chloride ('calomel', $Hg_2^{I}Cl_2(s)$) are rare in soil systems, but nevertheless are possible under environmental conditions. Sublimate was commonly used in industrial processes such as the one which contaminated this study site, while calomel is rarely detected in contaminated sites although its stability field is within the range of naturally occurring species, according to thermodynamically calculated speciation diagrams, e.g. as found in Brookins (1988). More commonly, under reducing or even slightly oxidizing conditions, sulfide phases such as hexagonal cinnabar ($\alpha - HgS$) and cubic metacinnabar ($\beta - HgS$) may form. The solubility of these has been reported to be around $2 \cdot 10^{-21}$ mg/L (Drott et al., 2013; Hintelmann, 2010) and their stability is high, so if formed, they have been shown to prevail even under oxidizing conditions (Skyllberg, 2011). $\beta - HgS$ is commonly found in anoxic sediments. Montroydite (HgO), mercury oxide, only forms at highly contaminated, oxidizing sites; its solubility is constant at a pH > 4 at the quite high level of 44 mg/L (Hocsman et al., 2006). Thus, it will dissolve fast in contact with water in a soil setting. Mercury carbonate minerals are only found as alterations on cinnabar ore in silica carbonate mercury deposits (Roberts et al., 2001; Varekamp and Buseck, 1984).

Aquatic systems

Whether or not mercury will reach the groundwater from the overlying soil depends strongly on the soil properties as discussed in section 1.4.2 above, as well as on the level and speciation of the contamination. Once in the groundwater, the mechanisms governing mobility and bioavailability of mercury are mostly the same: organic matter and sulfide content will bind most mercury, slightly reducing conditions may foster the outgassing of Hg_g^0 or form 'pockets' of liquid Hg_l^0 in the aquifer pores. Barringer et al. (2013) have summarized the reactions taking place in groundwater, and summarized it in Figure 1.4.

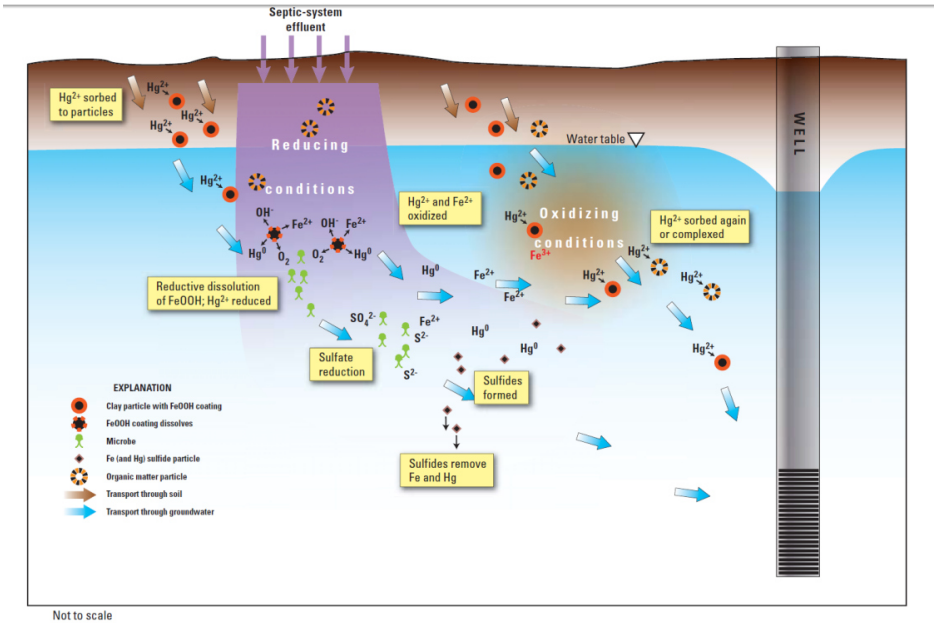

Figure 2. Mobilization of mercury from land surface to groundwater and biogeochemical transformations along flow paths in an unconsolidated sandy, acidic aquifer.

FIG. 1.4 Speciation scheme of mercury in groundwater by Barringer et al. (2013)

1.5 Mercury Isotopes

From sections 1.4.2 and 1.4, it has become clear that mercury's forms in nature are many, and that they vary greatly in terms of their properties and behavior. To study the provenance of a certain mercury pool, its speciation, and the chemical pathways by which this speciation came about has proved challenging over the last decades (Leermakers et al., 2005). Mercury isotope analysis is a relatively new tool by which some of these questions can be tackled (Yin et al., 2010). In this section, we will look more closely at what the isotopes of mercury

are, how they differ slightly in their behavior, and how these differences can be utilized to study mercury transformations and sources.

1.5.1 What are isotopes?

Isotopes of an element differ only in the number of neutrons in their nucleus and thus in their atomic weight (Wiederhold, 2015). Mercury has seven stable isotopes, the most abundant being ^{202}Hg. The stable isotopes of mercury and their relative abundances in the NIST standard "SRM 3133" (NIST) are ^{196}Hg (0.16%), ^{198}Hg (10.04%), ^{199}Hg (16.94%), ^{200}Hg (23.14%), ^{201}Hg (13.17%), ^{202}Hg (29.73%) and ^{204}Hg (6.83%). Their subtle mass differences cause isotopes of elements to behave slightly differently from each other, causing fractionation when chemical reactions or bonding sites favor heavier or lighter isotopes over the other (Blum et al., 2014; Hintelmann and Zheng, 2011). Since the abundances of all isotopes except ^{196}Hg is bigger than 5 % and thus quite evenly spread, all of the isotopes with the exception of ^{196}Hg can be routinely used in isotope ratio calculations, making it possible to look at multiple isotope ratios for each sample. This presents a big advantage over other metal isotope systems, as fractionation may not be mass-dependent and proportional between all isotope ratios, but deviate from the pattern of mass-dependent fractionation, which is scalable to any ratio of two mercury isotopes of interest (Wiederhold, 2015).

1.5.2 Isotope fractionation

In stable isotope geochemistry, isotope ratios are always interpreted relative to an isotope standard with known composition. Since the differences in isotope abundance are usually very small, it is convention to report them as parts per thousand ('‰'), called the 'delta notation' (Blum et al., 2014; Wiederhold, 2015).

$$\delta^{xxx}Hg\ [‰] = \left(\frac{\frac{^{xxx}Hg}{^{202}Hg_{\,sample}}}{\frac{^{xxx}Hg}{^{202}Hg_{\,standard}}} - 1 \right) * 1000 \tag{1.1}$$

Stable isotope fractionation occurs when the ratio between two isotopes of an element changes with respect to the standard that the sample is compared to (Fry, 2006; Wiederhold, 2015, e.g.). It occurs when isotopes of an element behave differently during a reaction, and thus, a shift in the isotopic ratio between product and reactant is induced. In most observed cases, this difference is due to 'mass-dependent fractionation' (MDF), e.g.: The difference in behavior depends on the difference in mass of the isotopes that are related to each other. However, deviations from this pattern have been observed, and processes have been observed in natural environments and the laboratory where odd-mass isotopes

were preferentially depleted or enriched in the studied samples. This effect is called mass-independent fractionation (MIF) and is in most cases linked to processes in the environment that include photochemistry (Bergquist and Blum, 2009). It is calculated by subtracting the theoretical δ^{xxx}Hg value based on scaling of the δ^{202}Hg ratio from the observed δ^{xxx}Hg value. The scaling factors are derived from the theoretical MDF factors according to transition state theory (Blum and Bergquist, 2007; Blum et al., 2014):

$$\Delta^{199}Hg = \delta^{199}Hg - \left(\delta^{202}Hg \cdot 0.2520\right) \tag{1.2}$$

$$\Delta^{200}Hg = \delta^{200}Hg - \left(\delta^{202}Hg \cdot 0.5024\right) \tag{1.3}$$

$$\Delta^{201}Hg = \delta^{201}Hg - \left(\delta^{202}Hg \cdot 0.7520\right) \tag{1.4}$$

$$\Delta^{204}Hg = \delta^{204}Hg - \left(\delta^{202}Hg \cdot 1.4930\right) \tag{1.5}$$

MIF may be due to the magnetic isotope effect (MIE), in which the reaction path of odd-mass isotopes differs from that of even-mass isotopes due to their non-zero magnetic spin (Hintelmann and Zheng, 2011). The nuclear volume effect (NVE), which is smaller than MIE, is due to the fact that the nuclei charge radii of uneven isotopes are slightly smaller than would be expected based on their mass, assuming a linear relationship between them, as holds true for the even isotopes of mercury (Bergquist and Blum, 2009). Figure 1.5 illustrates the different fractionation mechanisms and their magnitudes. The difference between the stable isotope ratios of two pools may be due to kinetic or equilibrium fractionation between them (Hintelmann and Zheng, 2011):

Kinetic fractionation is observed between the reactant and product of an incomplete process, where both pools are present in the system. One isotope has a different reaction rate than the other, causing a shift between them. Once the reaction is complete, only the product is in the system, and no more fractionation is observable: the product will have the signature of the completely reacted reactant.

Equilibrium fractionation is observed between two species that are in thermodynamic equilibrium, thus exchanging isotopes in reversible reactions. This process may also induce fractionation between the isotopes, with heavier isotopes preferring the stronger bonding environment of one of the reaction partners.

Isotopic fractionation can be caused either by mercury pools with different signatures mixing, or by biogeochemical processes which induce kinetic or equilibrium fractionation. Wiederhold (2015) presented a review on the processes which may cause fractionation in heavy metal isotopes. It concludes that redox processes, complexation and organic matter binding, sorption, precipitation, dissolution of minerals, condensation, evaporation and diffusion are

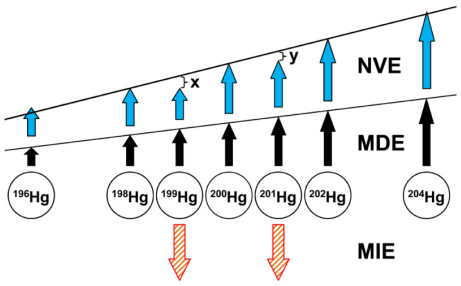

FIG. 1.5 Illustration of the effects fractionating the Hg isotopic signature of samples. Graph from Wiederhold (2015). 'MDE' refers to Mass-Dependent Effects, which are scaled to the weight of the isotopes. 'NVE' and 'MIE' are mass-independent effects that work by different mechanisms that preferentially deplete ore enrich odd-mass isotopes. 'NVE' ... Nuclear Volume Effect, MIE ... Magnetic Isotope Effect.

the prime causes for differentiation of isotope pools. Generally speaking, changes in oxidation states, bonding partners, or changes in the aggregation state may induce fractionation. Thus, virtually all biogeochemical processes introduced in section 1.4.2 can induce isotope fractionation between pools and indeed, the broad range of studied natural and anthropogenically influenced materials have proven to vary extensively in their isotopic signatures, as stated in Sun et al. (2016), Blum et al. (2014), and many others. Hintelmann and Zheng (2011) provide an overview over studied fractionating reactions pertaining to mercury until 2012. The fractionation factors resulting from kinetic fractionation have been studied for several biotic and abiotic reaction pathways. Multiple pathways of Hg^{II} reduction (Blum and Bergquist, 2007; Zheng and Hintelmann, 2009), (de-)methylation of mercury (Kritee et al., 2008), volatilization of Hg^0 (Zheng et al., 2007) are examples. Studied equilibrium fractionation processes include complexation of Hg^{II} by thiols (Wiederhold et al., 2010), sorption of Hg^{II} to goethite (Jiskra et al., 2012) and equilibrium volatilization of metallic mercury (Estrade et al., 2009).

1.6 Analytical methods to analyze mercury in soils

After discussing the wealth of information that may be gained about mercury transformations from looking at speciation and isotopic composition of the compounds, it's time to take a look at the tools available to measure them! At first, the total amount of mercury in a sample has to be assessed; after that, several methods may be deployed to provide information on the mercury speciation within a sample and to measure mercury stable isotope ratios. Here, the most common methods are introduced.

1.6.1 Determining mercury concentrations

Mercury concentrations can be measured either with a solid mercury analyzer or in solutions, via several detection mechanisms like atomic absorption spectrometry (AAS) or atomic fluorescence spectrometry (AFS). The AAS setup used in this thesis - a Flow Injection Mercury System (FIMS) - is explained in the method section 2.5.1.

1.6.2 Determining mercury speciation

X-Ray Spectroscopy

X-ray absorption spectroscopy (XAS) is the most direct method to determine speciation of mercury, as it allows detection and quantification of oxidation states and between Hg-S and Hg-O or Hg-N bonds (Skyllberg, 2010) and requires no sample modification prior to analysis. However, the concentration of mercury compounds in natural samples is, except for mining areas or highly contaminated sites, so low that direct identification of species via X-ray Absorption Fine Structure Spectroscopy (XAFS) and Near Edge Structure (XANES) is not possible (Leybourne et al., 2016). Some scientists have focused on μXAS, which has a smaller focus and thus requires concentrations of 100 $^{mg}/_{kg}$ only in smaller areas of the sample. All XAS methods however need synchrotron radiation to excite the samples and thus require large infrastructure. Other methods to determine speciation in environmental soil samples require only bench-top infrastructure, but provide only indirect evidence of speciation and more extensive sample modification is necessary.

Pyrolytic thermo-desorption

Pyrolytic thermo-desorption (PTD) is specific to mercury analysis. It utilizes the generally low volatilization temperatures of mercury compounds that vary among the different mercury species (Biester and Scholz, 1997). The solid sample is heated slowly by small increments, and the released mercury at each temperature is measured. By comparison to standards which represent pure mercury species, the temperature of thermal desorption of the unknown mercury-containing sample gives information on its chemical speciation. PTD and an extensive PTD standard set are discussed in section 4.1.1 of the discussion.

Sequential extraction

Sequential extraction procedures (SEP) have been applied to the research of heavy metals in the environment since the 1970's (Bacon and Davidson, 2008; Rauret et al., 1999; Tessier et al., 1979). They rely on the idea that differently bound species of metals in general and

mercury in particular can be leached from the soil by an array of extractants that vary in their properties. Each extractant is designed to leach an operationally defined group of species, and thus, the sample is split into easily interpretable sub-pools.
For this thesis, the author was interested both in the mercury speciation of the soil samples as well as the fraction's isotopic ratios. As samples have to be introduced into the MC-ICP-MS as aqueous solution, sequential extraction was used as a main tool for speciation. Since the limitations of this technique in terms of accuracy and reproducibility are well known, pyrolysis was also conducted on different aliquots of the samples to provide values for comparison, correction and to add an additional tool for the interpretation of the data.

1.6.3 Determining mercury isotope ratios

MC-ICP-MS

The method for mercury isotope ratio determination with the highest measurement precision and accuracy is multicollector inductively-coupled plasma mass spectrometry, short MC-ICP-MS (Irrgeher and Prohaska, 2015; Wiederhold, 2015). The plasma source is suited to ionize even heavy metal atoms such as mercury, and the mass spectrometer is equipped with multiple faraday cups to measure all isotopes of mercury simultaneously. In addition, the system can be coupled with a cold vapor system for sample introduction that reduces dissolved Hg^{II} to Hg^0 vapor, which is then introduced into the plasma and essentially eliminates interferences from other elements of similar masses, which do not volatilize. This way, matrix effects on the measurements are minimized (Foucher and Hintelmann, 2006). Exact information on quality control on the measurements can be found in the method section 2.5.2.

1.7 Revisiting the Bad Krozingen contamination case

Equipped with the knowledge about mercury's behavior in the environment and the tools to study these variation, we can ask meaningful questions about Bad Krozingen. As established, the soil properties exert an important influence on the speciation of mercury in the soil. This study concerns itself only with the soil cover and vadose zone sediments of the BK field site; these have been described as silty, carbonate-containing homogeneous fluvial sediments. Their organic carbon content has been reported by Bollen et al. (2008) to be around 0.2-0.9 % , so it's relatively low. This is an important piece of information, as organic matter has been reported to be the dominant binding partner to Hg^{II} in soils (Navrátil et al., 2014). In combination with the extraordinarily high reported soil concentrations of up to 11000 $^{mg}/_{kg}$ mercury in some soil samples (Bollen et al., 2008), it is thus unlikely that all mercury is

bound to soil organic matter and a more complex speciation has to be assumed.
Already the first papers about BK in the late 1990's reported that the speciation of mercury in the soil had changed significantly from the original $HgCl_2(aq)$ contamination source. Schöndorf et al. (1995) conducted soil gas measurements which detected gaseous Hg^0 and Biester and Scholz (1997) conducted pyrolytic thermo-desorption on soil samples that also revealed the presence of metallic Hg^0, indicating that the once-oxidized Hg^{II} contamination had been partly reduced to metallic mercury, even though the soil conditions were reported as oxic. The circumstances of this reduction have only been speculated about, but the exact mechanisms are unknown. The characterization of the BK soil material has been undertaken in multiple ways. As mentioned already, soil gas measurements have been conducted (Schöndorf et al., 1995), and mercury concentrations have been obtained in several soil cores and for the groundwater, where a contamination plume has been identified. In terms of speciation, Schöndorf et al. (1999) conducted sequential extractions aimed at assessing the bioavailability of the present mercury. They report results on total digests with aqua regia to determine the total Hg concentration, and on extracts with water and digestive model juices, to obtain information on the bioavailability and connected health risks of the present mercury. Biester and Scholz (1997) and Bollen et al. (2008) compared these results to results of pyrolytic thermo-desorption, which revealed that most of the mercury in the samples was Hg^{II} bound to the soil matrix, but also confirmed the presence of metallic Hg^0 in some samples. While we see that several methods have been used to study the BK mercury speciation, both the transformations which have lead to the reduction of mercury in the subsurface, as well as the bonding partners of the Hg^0 and Hg^{II} species in the soil remain unclear. This presents a perfect opportunity to use stable isotopes for a close re-examination of the site: The areas of highest contamination, as well as the approximate speciation of the site are known; and concentration measurements, sequential extraction and pyrolytic thermo-desorption provide quality control and additional information on the samples which can then be interpreted for their stable isotope variations. Comparing this information to laboratory studies on mercury isotope fractionation during biogeochemical reactions is a promising way to shed light on the transformations which have taken place.

1.8 Objectives

As established throughout the introduction, mercury stable isotopes present an opportunity to study the transformations that mercury undergoes in controlled laboratory settings (Hintelmann and Zheng, 2011).

Appreciating that mercury's behavior in the environment is highly complex and less well constrained than in laboratory settings, this thesis seeks to explore the possibility of tracing biogeochemical transformations of mercury in a field site.

To apply this knowledge to natural systems, careful characterization of the mercury speciation in the soil is required. The field site in Bad Krozingen is well suited for this, due to the known source of mercury pollution and the data available on the distribution of the contamination, which provides evidence that transformation processes such as reduction have taken place. Mercury speciation and stable isotope signatures in Bad Krozingen are studied and critically assessed. The extent of mercury stable isotope fractionation between the samples and identified mercury pools will be explored as to whether the observed variations can be attributed to specific processes. The following questions will be addressed in this thesis:

Question 1:
Is sequential extraction a suitable - and sufficiently specific - tool to divide the soil mercury pool into portions for mercury stable isotope analysis?

Question 2:
Do the stable isotopes of mercury vary significantly over the soil cores of the studied site, the different depths, and also the extracted fractions?

Question 3:
Can observed variation in mercury stable isotopes be attributed to biogeochemical processes which have been reported in literature?

To answer Question 1, different sequential extraction protocols will be applied to soil samples from this study. Their results will be compared to results of pyrolytic thermo-desorption on the same samples and with mercury isotope measurements. This way, it will be assessed which information about the binding forms of mercury the extractions behold, and whether this can be interpreted meaningfully in terms of mercury transformation processes which have taken place in the soil. Addressing Question 2, bulk soil samples and sequentially extracted mercury pools are measured for their stable isotope composition and compared to each other, keeping in mind the available speciation information and the specifics of the contamination case. The observed stable isotope variations will be discussed in the light

of mercury isotope fractionation literature, and it will be assessed whether the data of this thesis leads to the identification of specific transformation processes that have taken place in the soil. Exploring the specific contaminated site in Bad Krozingen, it will finally be discussed why the gained information holds relevance to future mercury tracing studies in natural systems.

Chapter 2

Methods

2.1 Field methods

All analyses presented in this thesis were done on material from two soil cores taken on June 3^{rd}, 2016 in the town of Bad Krozingen, Germany in collaboration with Prof. Harald Biester and Dr. Jan-Helge Richard of TU Braunschweig (Germany). An introduction to the site and its contamination history is given in 1.2. Figure 2.1 shows the two drilling locations. Core K2 is located in the most polluted area near the former kyanization hall. Core K3 is located in the former storage area for impregnated wood, with less contaminated soil. The cores were taken with a pile driving device from HPC AG. Once a 1 or 1.5 m core was recovered (see figure 2.2), it was divided into 20 cm long sections, which were homogenized gently with a stainless steel spatula, filled into 180 mL PP sample containers (figure 2.3) and stored inside a cooling box on-site for transport. Whenever substantial amounts of core loss occurred during the pulling of the core, this was attributed to the lower end of the core. All samples were split, with half of the material going to Braunschweig for pyrolytic thermo-desorption analysis, the other half to Vienna. In the Vienna laboratory, the samples were stored in the refrigerator until further processing.

2.2 Soil handling

To minimize loss of elemental mercury, no sieving, milling or drying of the soil samples was conducted. Instead, the samples were homogenized a second time with a stainless steel spatula. This was done in a well ventilated laboratory. Approximately half of each sample was filled into a smaller PE container and stored in a -20 °C freezer for long-term storage. The other half was kept in the fridge at +4 °C for extractions and analysis.

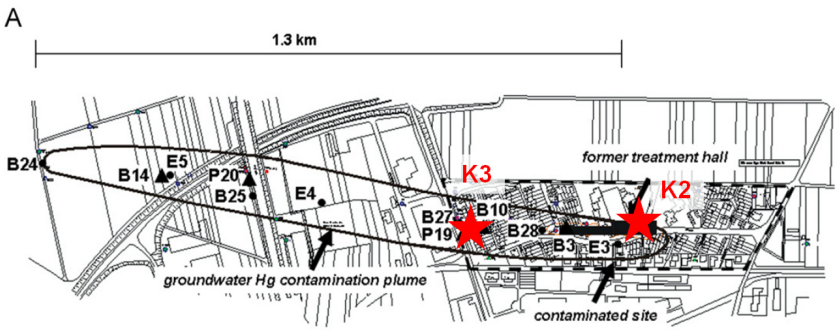

FIG. 2.1 Plan of the 'Parksiedlung' contaminated area in Bad Krozingen, Germany. The red stars indicate the locations of the drill cores K2 and K3. Source: modified after Richard (2011) (original map by HPC engineers, 2005).

2.3 Water content

For the determination of water content, 5 g of the wet material of each sample were weighed into 100 mL glass beakers and put into a drying oven in a fume hood for at least 48 h at 105 °C to the point of constant mass. Once the mass of the dry sample wasn't changing anymore, the samples were let to cool to room temperature in a desiccator, weighed, to determine water content and dry mass, and afterwards discarded. For extractions, soil was weighed into the sample tubes based on wet weight. The determined water contents were then used to calculate dry mass concentrations sample by sample in a final calculation step.

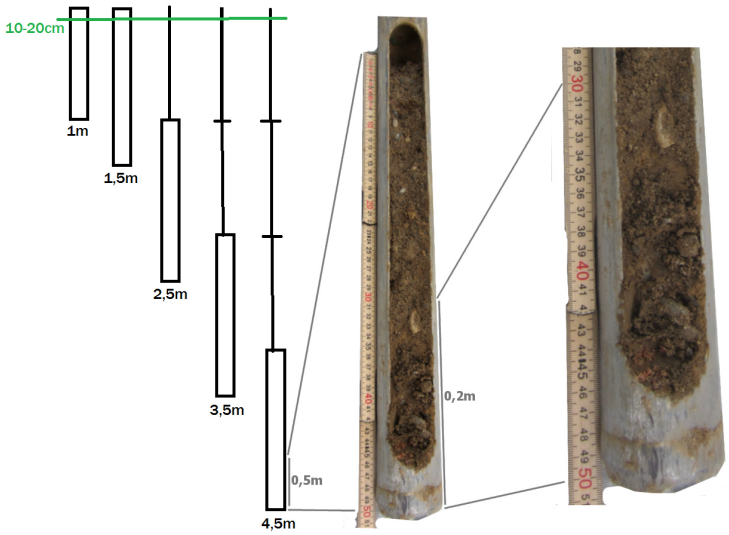

FIG. 2.2 Schematic drawing of the borehole depth and how different core lengths were used. Core K2 corresponds to the 4.5 m core, K3 to the 3.5 m core.

2.4 Extractions

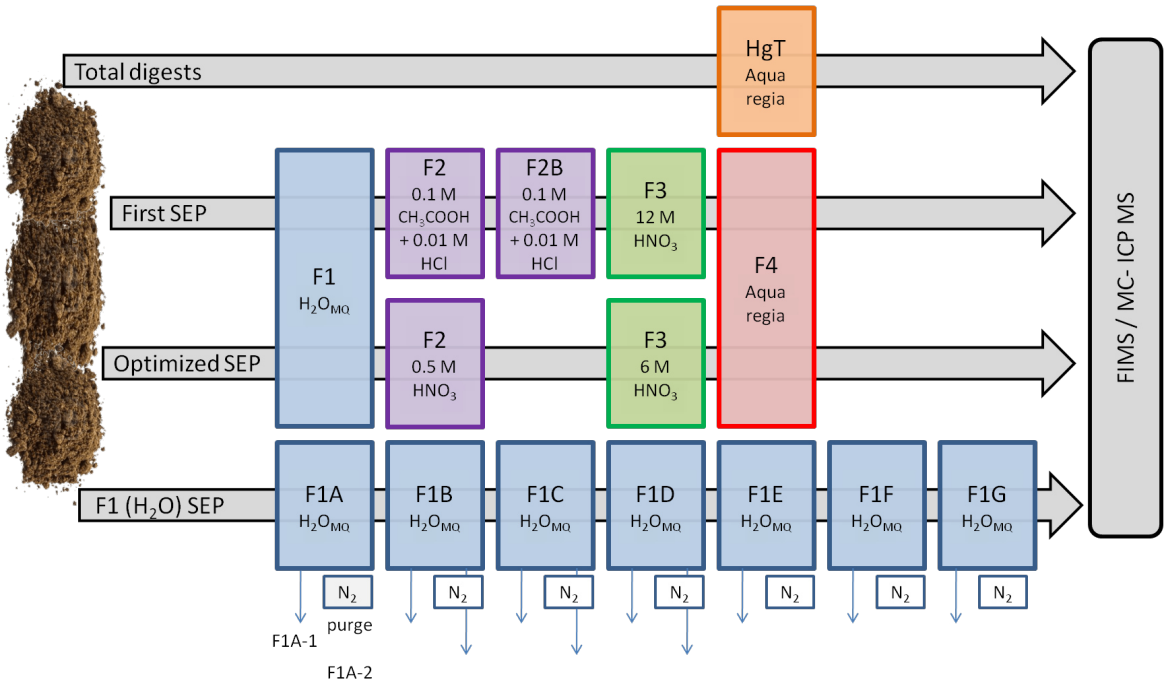

FIG. 2.4 Sequential extraction schemes. Colors denoting the different extracts are used throughout the thesis when extracted data is presented. SEP . . . Sequential Extraction Protocol.

FIG. 2.3 All samples were loosely homogenized with a stainless steel spoon. An aliquot of each soil sample was packed on site for the laboratory on Braunschweig, another one for the laboratory in Vienna.

Extractions were undertaken with various reagents, with the objective to either leach all or just specific pools of mercury from the soil that could later be interpreted in terms of their speciation. The general procedure consisted of mixing a known amount of wet soil with the reagent inside a centrifugation tube, shaking the solution for a certain amount of time, centrifuging it afterwards to separate the extractant solution from the residual soil, filtering it and storing the now mercury-containing solution for analysis. All extractions were carried out using analytical-grade reagents and ultrapure water. The ultrapure water came from a Millipore system with > 18 MΩ·cm resistivity and <2 ppb TOC. In all extracts, mercury was stabilized in the resulting solution with bromine monochloride, 0.2 M $BrCl$ in $HCl_{conc.}$. This reagent has been shown in multiple studies Bloom et al. (2003); Leermakers et al. (1990) to stabilize mercury in solution by both oxidizing Hg^0 to Hg^{II}, keeping it in solution by complexing it, and minimizing adsorption of mercury to the container walls. In the following chapters, this reagent will in short be called $BrCl$.

BrCl The 0.2 M bromine monochloride solution was prepared following the protocol of Bloom et al. (2003) by adding 5.4 g KBr crystals slowly to 500 mL of $HCl_{conc.}$ and stirring it for 1 h in a fume hood using a magnetic stirrer. Then, 7.6 g of $KBrO_3$ were added slowly to the solution, as the process releases Cl_2 and Br_2. The solution was then stirred for another hour in the fume hood, before the lid was put back on and the solution was stored in the fridge until further use. Both potassium reagents were heated in a muffle furnace at 220 °C for 24 h (Leopold et al., 2010) to drive out any possibly present mercury contamination .

2.4.1 Aqua regia digests

To determine total mercury content of the samples, soils were digested with aqua regia. 12 mL aqua regia (see below) were mixed directly in the 50 mL HDPE centrifugation vials with 1 g of soil and covered but not sealed with pierced parafilm to avoid spillage but allow for Cl_2 and $NOCl$ gases to escape. The samples were shaken overnight (18 $\pm$ 4 h) at 15 rpm on a horizontal shaker in a fume hood, then diluted with 8 mL H_2O_{MQ} and centrifuged at 3000 rpm (3992 g) (HiCen21C, HeroLab, Wiesloch, Germany). They were filtered through 0.45 μm PTFE filters (Sartorius AG, Göttingen, Germany). The hydrophobic PTFE filters were wetted with ethanol and flushed twice with H_2O_{MQ} before usage. The filtrate was stored in acid-washed borosilicate vials with teflon-lined lids and analyzed within two weeks of extraction on a cold-vapor flow injection AAS (FIMS 100, Perkin Elmer, Waltham, USA).

Aqua Regia For 12 mL of aqua regia, 8 mL HCl_{conc}, 3 mL $HNO_{3\ conc}$ and 1 mL 0.2 M $BrCl$ in HCl_{conc} were pipetted directly into the centrifugation vials.

2.4.2 Sequential extractions

Extractant solutions

Two series of sequential extraction procedures (SEP) were carried out with different protocols that will be described in this section. The first set of sequential extractions ('First SEP') was carried out based on the five-step sequential extraction for mercury in soils by Bloom et al. (2003). It is one of the most widely used extraction protocols for mercury. Since the sampling site had been previously characterized as low in organic matter (Bollen et al., 2008) and pre-tests on older cores from the site had shown that Bloom's 'F3' fraction, designed to leach mercury from organic matter, yielded low mercury concentrations, it was omitted. (The pre-test results can be found in Appendix A.) After the First SEP, the Optimized SEP will be presented. Before describing specifics about the two SEPs, their common features are described.

Extraction procedure

For both sequential extraction runs, 1 $\pm$0.01 $g_{w.w.}$ of each sample was weighed into 50 mL HDPE centrifugation vials. 25 mL of extractant were added for steps F1, F2 and F3. For F4, 12 mL of extractant were used and the extraction was identical to the aqua regia digests (section 2.4.1). The vials were closed, shaken by hand to wet the whole sample, then placed on an end-over-end shaker at 15 rpm overnight for 18 $\pm$ 4 h. The next day, samples were centrifuged at 3000 g and filtered into acid-washed borosilicate vials with teflon-lined lids.

The filters were pre-flushed with the extractant solutions in the cases of F1 and F2. Where PTFE-filters were used, these were wetted with ethanol, then flushed twice with H_2O_{MQ}. Where cellulose acetate filters were used for F3 and F4 steps they were flushed with diluted extractant solution that matched the concentration of the sample after dilution.

2.4.3 First sequential extraction

For extraction steps F1 and F2, pH was measured with an Ag/AgCl electrode. In the Bloom et al. (2003) protocol, F2 is designed to resemble stomach acid conditions with a pH of ≈ 2. This presented a problem in the First SEP, since the high carbonate content of the samples buffered the extracted solutions to pH values of 5.3 ± 0.4 (see table 3.4 for all pH values). It was decided to repeat step F2 of the Bloom protocol. The new step was called 'F2B' and is treated as an extra extraction step. To stabilize the samples for measurement and storage, they were oxidized with 1%(v/v) *BrCl*, as described in the first paragraph of section 2.4. The same day, the next extractant solution was applied and the procedure repeated. At step F4, the samples were placed overnight on a lateral instead of an end-over-end shaker to prevent spilling. It was covered loosely with parafilm to avoid sample contamination, but enable emerging gases to escape. The solution was diluted with 8 mL H_2O_{MQ} before centrifugation, due to the high acidity of the extract. The protocol is visualized in figure 2.4 and was as follows:

F1: 25 mL H_2O_{MQ}, 18 h in end-over-end shaker, centrifuged at 3000 g for 15 min, filtered through 0.45 μm cellulose acetate syringe filter, 0.025 mL 0.2 M *BrCl* added.

F2: 25 mL 0.01 M *HCl* + 0.1 M CH_3COOH, 18 h in end-over-end shaker, centrifuged at 3000 g for 15 min, filtered through 0.45 μm cellulose acetate syringe filter, 0.025 mL 0.2 M *BrCl* added.

F2B: repetition of F2, to dissolve residual carbonate present in sample, and consequently lower the pH to similar values as described by Bloom et al. (2003).

F3: 25 mL 12 M HNO_3, 18 h in end-over-end shaker, centrifuged at 3000 g for 15 min, filtered through 0.45 μm PTFE syringe filter, 0.4 mL 0.2 M *BrCl* added.

F4: 12 mL aqua regia (8 mL *HCl*, 3 mL HNO_3, 1 mL 0.2 M *BrCl* in concentrated *HCl*), 18 h in lateral shaker, 8 mL H_2O_{MQ} added, centrifuged at 3000 g for 15 min, filtered through 0.45 μm PTFE syringe filter.

2.4.4 Optimized sequential extraction

Upon examination of the First Extraction results, the SEP was optimized to achieve better distribution of mercury among the extracted phases, so the maximum number of samples would reach the minimum concentration of mercury required for isotope measurements. F2 was adjusted to higher acid strength so it would be capable to dissolve all carbonate present in the samples, and to eliminate a problem encountered due to the mixing of the chloride residue from step F2 with F3 solution, which created an undesired 'aqua regia' effect (Mikac et al., 2003). F3 was adjusted to lower acid strength due to literature suggestions that 12 M HNO_3 would dissolve some small-grained HgS sulfides (Hall et al., 2005). F1 and F2 were centrifuged on a swing-bucket centrifuge (CR 4.22, Jouan SA, Saint-Herblain, France) instead of the fixed-rotor HiCen21C to provide better settling of the solids and avoid the loss of the fine soil fraction. The optimized steps are as follows:

F1: 25 mL H_2O_{MQ}, 18 h in end-over-end shaker, centrifuged at 3500 rpm (2360 g) for 15 min, filtered through cellulose acetate syringe filter, 0.250 mL 0.2 M $BrCl$ added

F2: 25 mL 0.5 M HNO_3, 18 h in end-over-end shaker, centrifuged at 3500 rpm (2360 g) for 15 min, filtered through 0.45μm cellulose acetate syringe filter, 0.250 mL 0.2 M $BrCl$ added

F3: 25 mL 6 M HNO_3, 18 h in end-over-end shaker, 25 mL H_2O_{MQ} added, centrifuged at 3000 g for 15 min, filtered through 0.45 μm cellulose acetate syringe filter, 0.500 mL 0.2 M $BrCl$ added

F4: 12 mL aqua regia (8 mL HCl, 3 mL HNO_3), 1 mL 0.2 M $BrCl$ in concentrated HCl, 18 h in end-over-end shaker, 36 mL H_2O_{MQ} added, centrifuged at 3000 g (HeroLab) for 15 min, filtered through 0.45 μm cellulose acetate syringe filter

One sample of each core was chosen to be extracted in 6 replicates. Three of the replicates were terminated after incomplete extraction, and the soil residue from the samples was sent for pyrolytic thermo-desorption (PTD) analysis. This 'sequential PTD' extraction scheme is represented in figure 2.5.

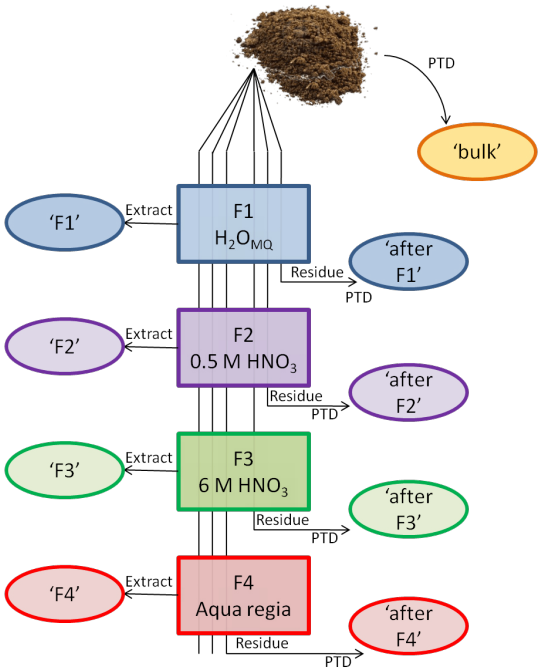

FIG. 2.5 Scheme showing how samples were obtained for bulk analysis and for sequential pyrolytic thermo-desorption (PTD) during the Optimized PTD.

TABLE 2.1 Overview of the sequential extraction protocols and comparison of this thesis' schemes with the method of Bloom et al. (2003).

First SEP		**Optimized SEP**	
F1 = $F1_{Bloom}$	H_2O_{MQ}	$F1_{Opt}$	H_2O_{MQ}
F2 = $F2_{Bloom}$	0.1 M CH_3COOH + 0.01 M HCl	$F2_{Opt}$	0.5 M HNO_3
F3 = $F4_{Bloom}$	12 M HNO_3	$F3_{Opt}$	6 M HNO_3
F4 = $F5_{Bloom}$	Aqua Regia	$F4_{Opt}$	Aqua Regia

2.4.5 Sequential water extractions

To see if diffusion or concentration equilibria were playing a role in the amount of mercury extracted in the 'F1' water step, a sequential extraction run just with ultrapure water was conducted. Originally, only three steps were planned and the extracts were then stored. Due to the fact that there was still a considerable amount of Hg in the extracted pools, the series was extended to seven steps after two weeks had passed. For the extracts, 2 g of soil

were weighed into 50 mL HDPE centrifugation tubes. They were filled with 50 mL H_2O_{MQ} and shaken on an end-over-end shaker for 18 $\pm$ 4 hours. Then, they were centrifuged on a swing-bucket centrifuge for 15 min at 3000 g and filtered through 0.45 μm cellulose acetate syringe filters. 25 mL of the solution were filled into a clean HDPE centrifugation vial and acidified with 250 μL BrCl solution. The other 25 mL of the solution were purged with N_2 in a fume hood, to drive out any present Hg^0 (compare f.ex. Begu et al. (2016)), and then acidified and stored. The flow rate from the bottle to the 5-fold valve was adjusted to ca. 160 cc/min (calibrated with He at 5 PSI and 70 °F) so that a steady stream of bubbles was emerging from the tip of the five pasteur pipette which were fixed to the end of the tubing connected to the gas bottle.

2.5 Analysis

2.5.1 Mercury concentration analysis with FIMS

Concentration analyses were conducted with a cold-vapor flow injection mercury system, the Perkin Elmer FIMS 100 at the Department of Environmental Geosciences, Vienna, Austria and measured by atomic absorption spectroscopy (AAS). Samples were diluted to an expected mercury concentration of 1 µg/L in a 1% BrCl solution. The Hg-containing solution mixed with the reducing solution of 2.5% $SnCl_2$ in 1 M HCl, and the resulting, reduced Hg^0 vapor passed through a hydrophobic membrane into the AAS detector. The instrument was calibrated with mercury standard solutions from 0.1 µg/L to 10 µg/L. Samples exceeding 10 µg/L during a measuring session were re-diluted and re-measured within the calibration range. The instrument precision was checked periodically (at least every 10 samples) by re-measurement of the 1 µg/L (in some sessions the 5 µg/L) calibration standard. The deviation of this measurement also presented the basis for the % standard deviation calculation that was then applied to all of the session's samples. Based on repeated measurements of the 1 µg/L calibration standard in all sessions, the analytical precision of the method was found to be 2.7% (1 SD, n=45).

2.5.2 Mercury isotope analysis with MC-ICP-MS

For isotope measurements, the Nu Plasma II multi-collector inductively-coupled plasma mass spectrometer (MC-ICP-MS) (Nu Instruments, UK) at the department of Environmental Geosciences, University of Vienna, Austria was used. The sample introduction system is a HGX200 cold vapor injection system with frosted glasspost design (Teledyne Cetac, Omaha, USA) that quantitatively reduces a dilute, mercury-containing 1% $BrCl$ solution with 2.5 %

$SnCl_2$ in 1 M HCl to mercury vapor.
Mass bias correction is achieved by introduction of a Tl standard solution of known isotopic compostion (NIST SRM 997) via an Aridus II desolvating nebulizer system (Teledyne Cetac, Omaha, USA) into the plasma interface and correcting for the shift in isotope ratios between the true ratio of the standard and the value measured in the mass spectrometer.
Further details on the method can be found in Wiederhold et al. (2010), which is based on Foucher and Hintelmann (2006). The MC-ICP-MS was fine-tuned on every measuring day, including the adjustment of the source position, adjusting the peak shapes, tuning the instrument focusing for maximum signal and stability, and setting the baseline by conducting pre-amplifier gain calibration. Each measurement represented the average value of 36 5-second measurements after 3 min. of sample solution uptake, followed by 5 min. of sample washout with 1% $BrCl$ solution. All Hg δ values are reported relative to the standard reference material NIST 3133 (NIST), which represents the 0-point of the δ scale. NIST 3133 was used during the daily fine-tuning of the machine focusing, and measured before and after every sample, using standard-sample-bracketing for later data correction. Adding the measuring, uptake and washout times for one standard and one sample, the total time of one sample measurement amounted to 25 min. Precision of the measuring sessions was controlled by periodical measurement of the secondary standard 'ETH Fluka'. The standard deviation of 'ETH Fluka' was then used as a measure of the session's precision. The overall precision for all presented δ^{202}Hg data in this thesis averaged to $\pm$ 0.14 ‰ (2 SD, n=38), but the standard deviations for the single measurements are reported relative to the sessions in which they were measured in. All measured 'Fluka' standards are reported in table C.3 in the appendix.

2.5.3 Mercury speciation analysis with PTD

All pyrolytic thermo-desorption (PTD) measurements were conducted at Prof. Harald Biester's laboratory at the Institute of Geoecology of TU Braunschweig, Germany. For bulk sample analysis, aliquots of the soil samples were combusted without prior drying. Further information on the pyrolysis method of the Braunschweig laboratory can be found in Biester and Scholz (1997). For pyrolysis on sequential extracts, the sample intended for measurement was treated as all others in the sequential extraction run. After the specific extractant was added, the sample shaken and centrifuged, the supernatant was decanted for Hg analysis on the FIMS. Instead of adding the subsequent extractant, the sediment cake was transferred into a 2 mL PE vial to send to Braunschweig. For F3 (6 M HNO_3) and F4 (aqua regia) sediment residue, an extra centrifugation step with 50 mL added H_2O was added to decrease the acidity of the sediment. Figure 2.5 visualizes the sampling scheme.

2.5.4 Dissolved organic carbon

For dissolved organic carbon (DOC) measurements, an aliquot (8 mL) of unacidified water extracts (see section 2.4.4) was measured for non-purgeable organic carbon and total nitrogen (TN) on a Shimadzu TOC-L (Shimadzu, Kyoto, Japan) at the Department of Geography, University of Vienna. The extracts were prepared according to the protocol for step 'F1' in section 2.4.4 and were stored in the refrigerator until being measured within 24 hours.

Chapter 3

Results

3.1 Reporting of results

In this chapter, all collected data is presented. Section 3.2 reports concentration measurements on all core samples, followed by data on sequential extracts, accompanying data on dissolved organic carbon and pH measurements of selected extracts. For more brevity and clarity, the focus of the results and discussion sections are on the Optimized SEP. Only Optimized SEP results are reported in text and graphs. The First SEP results can be found in table B.1 in the appendix. Section 3.3 presents all thermo-desorption pyrolysis data, both on bulk samples and during the Optimized SEP steps. The last results section 3.4 reports stable isotope measurements on the previously characterized bulk and Optimized SEP samples.
Unless specified otherwise, the concentration units 'ppb' and 'ppm' refer to the mass/mass concentrations '$\mu g/kg$' and 'mg/kg', and mass/volume concentrations are labeled '$\mu g/L$' and 'mg/L'. Concentrations refer to dry weight ('d.w.') of soil, unless specified otherwise by the subscript 'w.w.', meaning 'wet weight'.

3.2 Mercury concentrations

Depth profiles of mercury concentrations

Along the two soil cores K2 and K3, total mercury concentrations of every sample were measured. The results are reported in table 3.1 and plotted in figure 3.1. All measured samples were above background levels but the maximum concentrations varied between the two cores. K3, the core further removed from the contamination source, had maximum concentrations of almost 100 mg/kg Hg. Core K2, at the contamination hotspot, had 8 times higher maximum concentrations of 801 mg/kg. Comparing the two cores, the depth of maximum contamination

differed as well. While the highest concentrations were in a depth of ca. 2.5 m in K2, they were within the uppermost meter in core K3. Based on the total mercury concentrations of the samples, the most contaminated samples were chosen for sequential extraction.

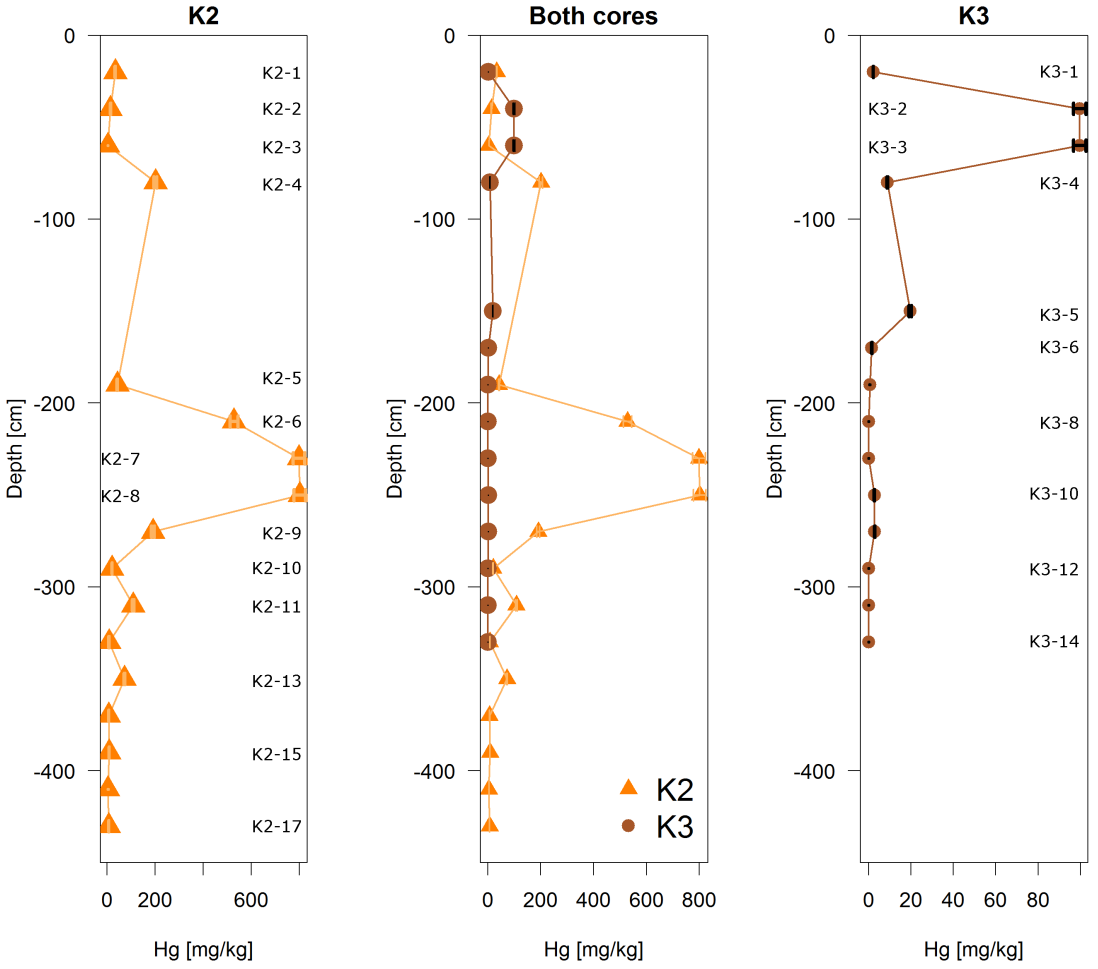

FIG. 3.1 Mercury concentration profiles of cores K2 and K3. Symbols are located at the vertical mid-points of the samples, which each span 20 cm of the cores. Error bars represent the analytical precision of ±2.7% (1 SD, n=45) based on repeat measurements of the calibration standard during all measuring sessions and are smaller than the plotted symbols, where they are not visible. Note that the x-axis scale on the right-hand panel is smaller, to display the less contaminated core K3 in more detail.

TABLE 3.1 Concentration data of cores K2 and K3. The measurements had an analytical standard deviation of ± 2.7% (1 SD, n=45) based on repeat calibration standard measurements - although the sample heterogeneity has been found to exceed this. The depths given are midpoints of 20 cm core sections.

Depth midpoint [cm]	**Name**	**Hg conc. wet weight** [$\mu g/kg$]	**Water content** [%]	**Hg conc. dry weight** [$\mu g/kg$]
-20	K2-1	29.3	14.1	34.0
-40	K2-2	12.7	12.1	14.4
-60	K2-3	3.5	2.8	3.6
-80	K2-4	173.6	13.9	201.5
-190	K2-5	35.5	16.8	42.6
-210	K2-6	421.5	20.2	528.2
-230	K2-7	624.3	21.8	798.5
-250	K2-8	635.4	20.7	801.5
-270	K2-9	157.5	17.6	191.1
-290	K2-10	17.2	17.1	20.8
-310	K2-11	89.1	17.8	108.3
-330	K2-12	6.7	18.0	8.1
-350	K2-13	60.2	17.5	72.9
-370	K2-14	5.4	20.2	6.7
-390	K2-15	7.4	17.4	9.0
-410	K2-16	3.7	18.0	4.5
-430	K2-17	6.0	19.2	7.4
-20	K3-1	2.2	4.6	2.3
-40	K3-2	90.3	9.4	99.6
-60	K3-3	84.1	15.6	99.6
-80	K3-4	8.4	5.2	8.9
-150	K3-5	16.8	14.2	19.6
-170	K3-6	1.3	14.6	1.5
-190	K3-7	0.5	14.8	0.6
-210	K3-8	0.1	13.3	0.1
-230	K3-9	0.1	12.3	0.1
-250	K3-10	2.5	11.3	2.8
-270	K3-11	2.6	11.7	2.9
-290	K3-12	0.1	13.9	0.1
-310	K3-13	0.1	16.5	0.1
-330	K3-14	0.1	15.0	0.2

Mercury concentrations of Optimized SEP pools

The samples chosen for the First and Optimized sequential extractions were K2-5 to 10 (180 to 300 cm depth) in core K2 and samples K3-2 to 5 (30 to 160 cm depth) in K3. They were sequentially extracted as described in sections 2.4.3 and 2.4.4. Figure 3.3 shows the Optimized SEP results. In K2, the SEP extracted only 1-2 % of the total mercury in the 'F1' pool, the water leach. Steps 'F2' to 'F4' yielded a more even distribution. It is noteworthy that during the Optimized SEP, sample K2-7 contained significantly more mercury (950 $^{mg}/_{kg}$ Hg) during the SEP than during the aqua regia digest (624 $^{mg}/_{kg}$), which illustrates the heterogeneity between subsamples of the same soil. In K3, most mercury (53 - 90%) was leached only in the last step, showing that the present mercury was bound more tightly to the soil samples and was less mobile in core K3 than in K2. Samples K2-8 and K3-3 were extracted in 3 replicates each. On another 3 replicates, the SEP was only conducted partially, and the remainder of the leached soil was sent to TU Braunschweig for pyrolysis measurements. Figure 3.2 shows the full and partial replicates of K2-8 and K3-3, which are in good agreement with each other.

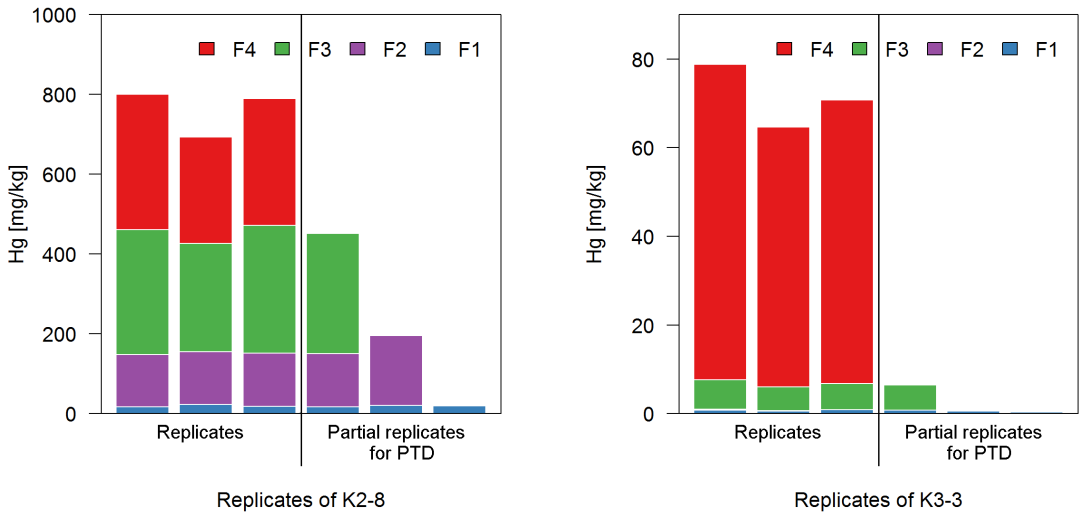

FIG. 3.2 Replicates of the samples K2-8 (left) and K3-3 (right). To the right of the panels, extractions were terminated after specific steps to send samples for pyrolytic thermo-desorption (PTD) analysis.

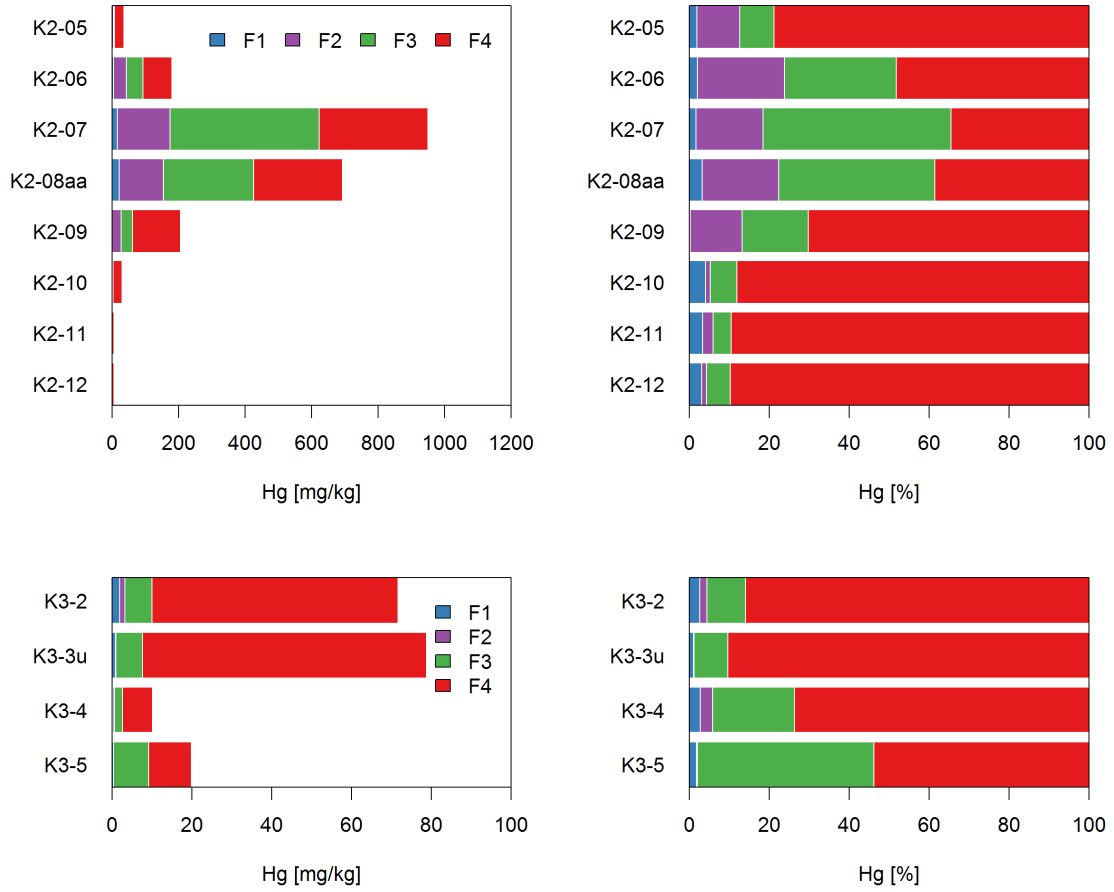

FIG. 3.3 Results of the Optimized SEP. The left-hand panels display the absolute amount of mercury extracted into the different, color-coded pools. The right-hand panels display the extracted mercury normalized to 100%, so the pool sizes can be compared relative to each other. Samples in one panel are presented in order of increasing depth in the profile, cores K2 and K3 are plotted separately.

Mercury concentrations of sequential F1 extracts

Due to the higher-than-expected amount of water-extractable mercury that was found in the hotspot samples of K2, sequential water extractions were carried out. The results are listed in table 3.2 and plotted in figure 3.4. The label 'F1' signifies that the extractant solution was ultrapure water; the suffixes 'A-G' signify the number of the extract in the sequence. Thus, 'F1A' was the first extraction step, 'F1G' the last one. Only sample K2-8, which showed the highest absolute mercury concentrations and, as will be described in sections 3.3 and 4.1.1, the highest percentage of Hg^0, was investigated. The replicates were in good agreement, showing % variations of $\leq \pm$ 12% (1 SD, n=3) for all extraction steps. Extract 'F1D' is highlighted pink in the plots due to its longer equilibration time of 66 hours before

and another 338 hours (≈ 2 weeks) after centrifugation; interestingly, though, it fit well with the other extracts and did not show deviation from the trend of decreasing H_2O-extractable mercury concentrations which were observed in with every extraction step.
The observed differences in mercury concentrations between purged and immediately acidified subsamples were not significant and did not lead to systematically lower concentrations which were expected due to the loss of elemental Hg^0 from the samples.

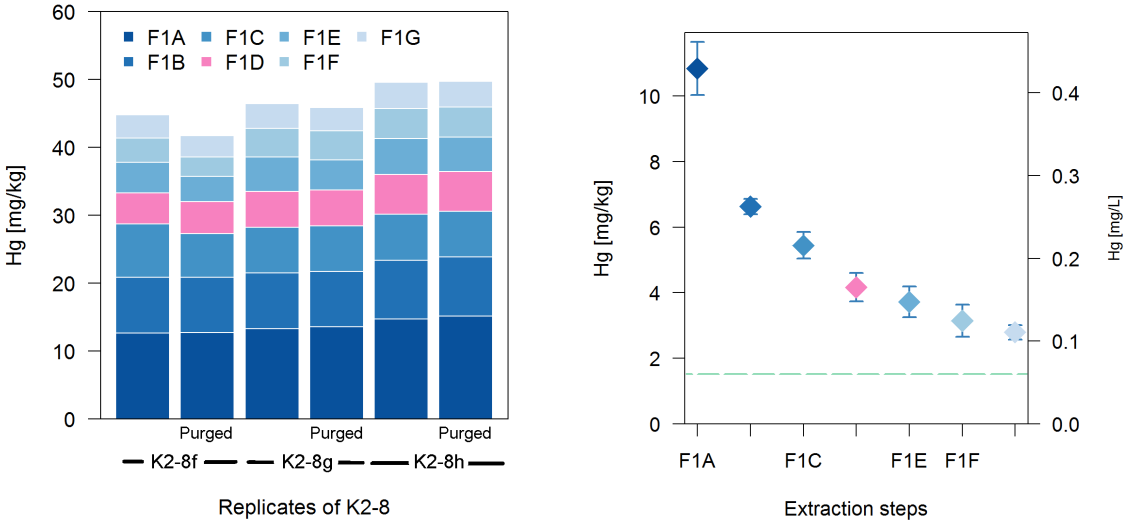

FIG. 3.4 Results of the sequential water extraction. The left panel shows all extracted replicates, on the right-hand side, their means and standard deviation (1 SD, n=6) are shown. Step 'F1D' is marked pink in the plot due to the much longer equilibration time. The light- green dashed line in the right-hand panel signifies solubility of Hg^0 in aqueous solutions, based on Skyllberg (2011).

TABLE 3.2 Results of the 7-step sequential F1 extraction.

	F1A		F1B		F1C		F1D		F1E		F1F		F1G		Total	
	Sol. conc. [$\mu g/L$]	Soil conc. [$\mu g/kg$]	Sol. conc. [$\mu g/L$]	Soil conc. [$\mu g/kg$]	Sol. conc. [$\mu g/L$]	Soil conc. [$\mu g/kg$]	Sol. conc. [$\mu g/L$]	Soil conc. [$\mu g/kg$]	Sol. conc. [$\mu g/L$]	Soil conc. [$\mu g/kg$]	Sol. conc. [$\mu g/L$]	Soil conc. [$\mu g/kg$]	Sol. conc. [$\mu g/L$]	Soil conc. [$\mu g/kg$]	Sum [$\mu g/kg$]	Sum [%]
HgT		801531														
K2-8af[1]	398	12661	258	8212	247	7879	143	4555	141	4491	113	3605	107	3397	44799	5.59
K2-8ag[1]	417	13270	258	8214	211	6722	167	5307	160	5100	133	4231	113	3598	46442	5.79
K2-8ah[1]	461	14692	273	8705	212	6746	184	5854	168	5339	139	4424	121	3839	49600	6.19
K2-8af[2]	399	12721	255	8138	203	6450	147	4695	118	3758	90	2859	97	3096	41717	5.2
K2-8ag[2]	427	13593	255	8128	211	6713	166	5291	139	4412	135	4298	107	3421	45855	5.72
K2-8ah[2]	475	15122	275	8766	210	6698	184	5858	160	5088	138	4396	120	3808	49735	6.21
Mean	429	13676	262	8360	216	6868	165	5260	148	4698	125	3969	111	3526	46358	5.78
1 SD	32	1023	9	293	16	507	17	553	18	589	20	621	9	281	3038	0.38
$\%_{\text{residual}}$ *		1.71	0	1.06		0.88		0.68		0.61		0.52		0.46		
$\%_{\text{of total}}$ +		1.71	0	1.04		0.86		0.66		0.59		0.5		0.44		

[1] ... Samples acidified with 1 % BrCl directly after filtering

[2] ... Samples purged for 30 min. after filtration, then acidified with 1 % BrCl.

* ... Percentage of mercury in the extract, relative to the amount which is still in the sample after the previous extraction steps:
$100*Hg_{F1(i)}$ / (HgT - $\sum_{i-1} Hg_{F1(i-1)}$), e.g. for F1B: $100*Hg_{F1B}$ / (HgT - Hg_{F1A})

+ ... Percentage of total mercury that is represented by the extracted fraction, e.g. for F1B: 100 * Hg_{F1B} / HgT

DOC concentrations of F1 extracts

Dissolved organic carbon measurements were conducted on 8 mL of un-acidified F1 extracts of the Optimized SEP, as described in 2.5.4. As shown in table 3.3, the hotspot samples of core K2 exhibited lower values than those of K3, owing both to the more organic-rich soil composition of K3 and the fact that K3's samples stem from closer to the surface.

TABLE 3.3 DOC measurements on F1 (H_2O_{MQ}) extracts of Optimized SEP. 'DOC' ... Dissolved Organic Carbon ('non-purgeable organic carbon', see 2.5.4), 'TN' ... Total Nitrogen

K2	**DOC** [mg/L]	**TN** [mg/L]	**K3**	**DOC** [mg/L]	**TN** [mg/L]
K2-5	1.27	0.84	K3-2	2.97	0.96
K2-6	1.39	1.00	K3-3	2.43	1.06
K2-7	2.27	0.88	K3-4	2.20	0.64
K2-8	1.05	0.66	K3-5	2.04	0.45
K2-9	1.10	0.21			
K2-10	1.04	0.18			
K2-11	0.96	0.27			
K2-12	1.25	0.28			

pH of Optimized SEP pools

pH measurements were conducted during the First and Optimized SEP to control whether the acidity of the extracts after extraction corresponded to the suggested values given by Bloom et al. (2003). Measurements were only undertaken in the fractions F1 to F2, since it was critical to overcome the buffering capacity of the soils by dissolving all contained carbonate. The results are displayed in table 3.4. It can be seen that during the First SEP, the added solutions did not suffice to dissolve all carbonate. Even after the repetition of 'F2' (labeled as 'F2B'), the pH was between 3.1 and 5.0, well above the extractant solution's pH. The Optimized SEP's 0.5 M HNO_3 solution produced similar pH values of 1.09 ± 0.04 (1 SD, n=21) in all samples.

TABLE 3.4 Table of pH values measured during the first steps of the SEP protocols.

	First SEP						**Optimized SEP**			
	F1 (H_2O_{MQ})		**F2** (0.1 M HAc + 0.01 M HCl)				**F1** (H_2O_{MQ})		**F2** (0.5 M HNO_3)	
	pH_{F1}	n	pH_{F2}	n	pH_{F2B}	n	pH_{F1}	n	pH_{F2}	n
Reagent	6.30				2.53				1.05	
N2711	7.56		2.49		2.55				1.03	
									± 0	2
K2-5	9.24		2.87		4.16				1.06	
K2-6			5.27		4.32				1.07	
K2-7	8.90		5.01		4.51				1.08	
K2-8	8.52		5.60		4.74		8.03		1.15	
	± 0.09	3	± 0.03	3	± 0.06	3	± 0.01	3	± 0.02	5
K2-9	8.69		5.19		4.93				1.14	
K2-10	8.93		5.64		4.99				1.15	
K2-11	8.85		5.66		5.04				1.12	
K2-12			5.69		4.97				1.11	
K3-2	7.92		4.93		3.42					
	± 0.15	3	± 0.30	3	± 0.52	3				
K3-3	7.78		5.13		4.06		7.7		1.07	
							± 0.04	3	± 0.01	5
K3-4	7.90		4.49		3.14				1.05	
K3-5	7.62		5.15		4.05				1.08	

3.3 Pyrolytic thermo-desorption results

Pyrolytic thermo-desorption (PTD) was conducted on all soil samples of this study. The PTD curves for each sample are presented in graphs where the extinction measured by the Hg detector is plotted against a temperature axis. Due to variable amounts of the samples being combusted during PTD analysis, all results were normalized in a standard procedure so that the highest peaks of each sample curve represents '100% extinction' on the y-axis. PTD measurements are interpreted relative to standards of pure laboratory mercury chemicals, which are run in every measuring session. The peaks of the known chemicals are used to determine at which temperatures these chemicals are released from the sample into the detector. Figure 3.5 shows the standards measured during the analysis of core K2. The standard Hg^0 mainly volatilizes before 100 °C. its peak shows a smaller-magnitude 'tail', though, that is released only between 100-200 °C. This happens due to diffusion of the metallic Hg^0 into the quartz matrix with which it is mixed. $HgCl_2$ is mainly released between 150 and 300 °C. However, a small peak between 50 and 150 °C is also detected. This is due to reduction of the store-bought $HgCl_2$ to Hg^0, as has been observed in the Braunschweig laboratory multiple times (Harald Biester, pers.comm.). All measurements were carried out in replicates as seen in the example plot in the right panel of figure 3.5. The replicates are plotted as dashed lines, their mean as a thick, blue, solid line. In the core K2 results, the session standards are plotted for reference in the background as thin, gray lines.

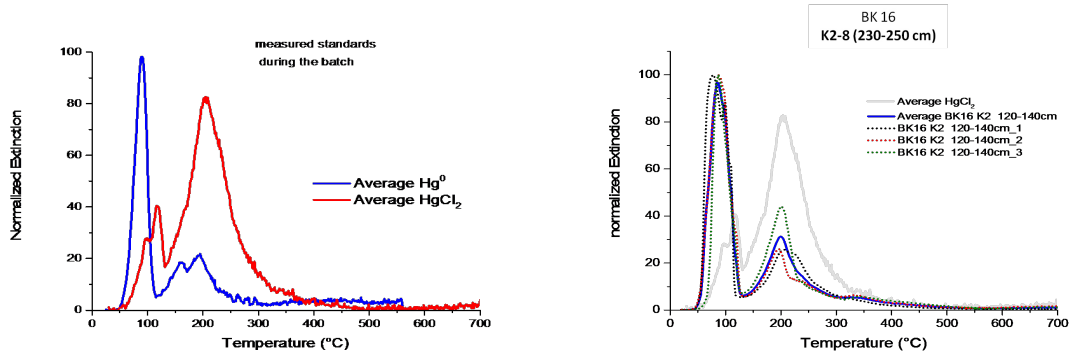

FIG. 3.5 The left panel shows curves of the Hg^0 and $HgCl_2$ standards measured during pyrolytic thermo-desorption (PTD). The main $HgCl_2$ peak occurs slightly above 200 °C, but an earlier peak at 100 °C of the same substance is caused by partial degradation of the mercury chloride to Hg^0. The Hg^0 release occurs mostly before 100 °C. However, due to diffusion into the quartz matrix of the sample, some of the elemental mercury is only released later, between 100 and 200 °C. The right panel shows the sample result for K2-8. The dashed lines represent two separate replicates, the blue thick line the average of the sample. The gray background lines are the standard results.

PTD results of bulk samples

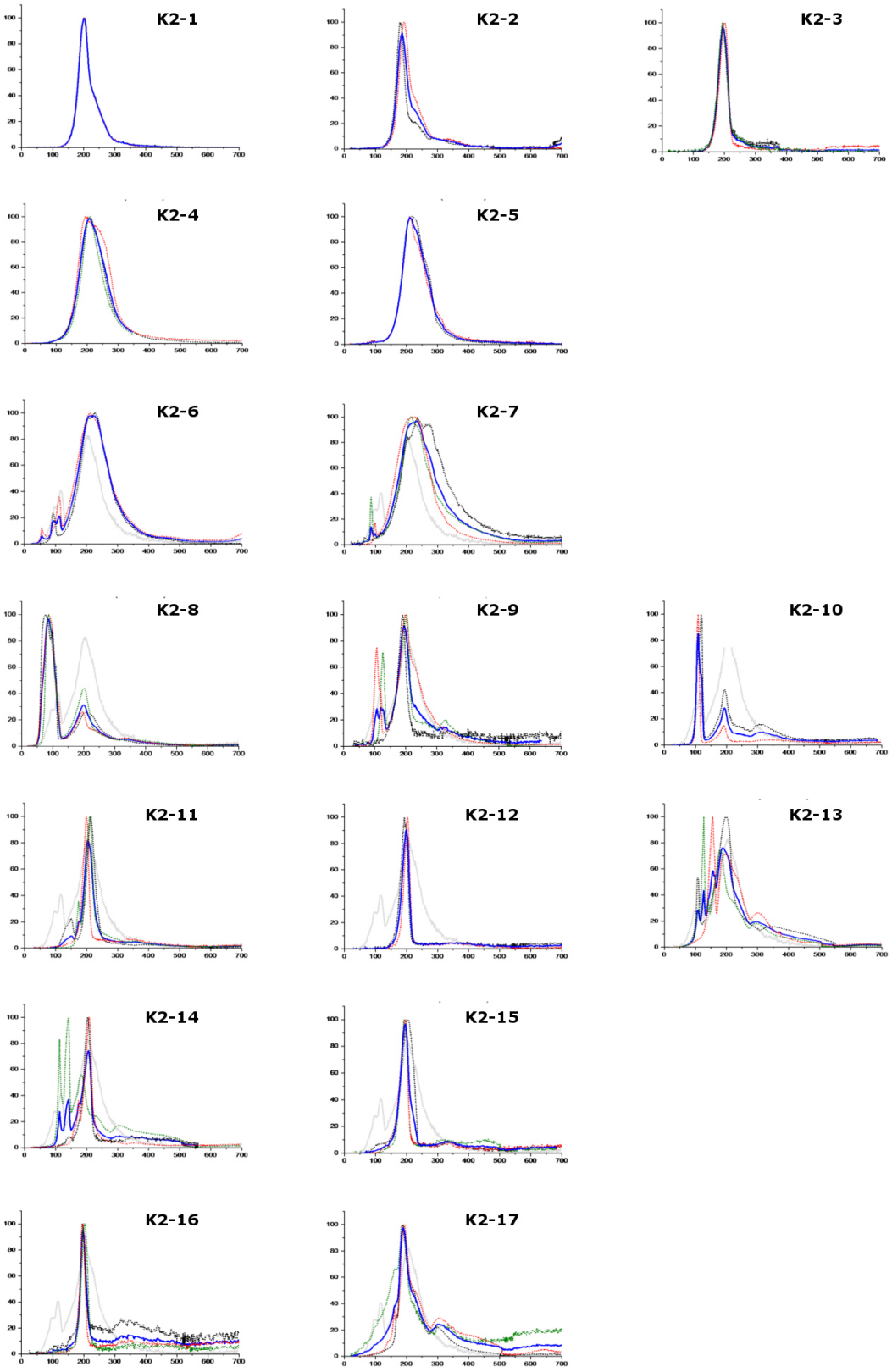

FIG. 3.6 Pyrolytic thermo-desorption (PTD) curves of all samples in core K2, with numbers 1–17 indicating increasing depth. Samples plotted in the same rows also show similar features. Details on the interpretation of the curves can be found in the caption of figure 3.5.

All PTD data obtained from core K2 is plotted in the overview figure 3.6. The samples are plotted in order of progressing core depth, K2-1 being the shallowest. They are grouped in a way that curves with similar features appear next to each other. It is evident that the majority of mercury in core K2 is released at around 200 °C. However, the peak shapes of the highest peak at around 200 °C vary, progressing from very sharp peaks in samples K2-1 to 3 to broader peaks in samples K2-4 to 7. Starting at sample K2-6, another earlier peak at around 100 °C is also visible. This peak makes up less than 30% of the 200 °C peak in samples K2-6, -7 and -9, but represents the majority of mercury in samples K2-8 and K2-10. Some samples at greater depths, such as K2-10, K2-13 to 15 and K2-17 also show significant mercury release at temperatures around 350 °C. In every case, these only make up small fractions of the total mercury in the samples.

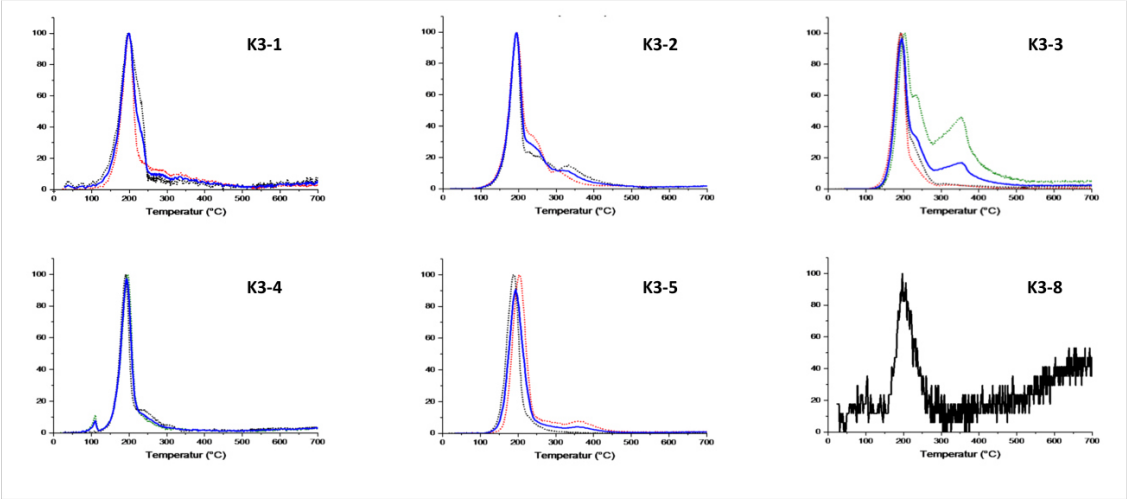

FIG. 3.7 Pyrolytic thermo-desorption (PTD) curves of all samples in core K3, in order of increasing depth. Samples after K3-5 contained very little mercury and are omitted but look very similar to K3-8.

Figure 3.7 displays the pyrolytic thermo-desorption (PTD) results of core K3. In contrast to core K2, the 100 °C peak is absent from core K3, with the exception of a peak less than 10% of the main peak in sample K3-4. The 200 °C peak that releases close to 100% of the mercury is well-defined over the whole depth profile, and even visible in those samples exhibiting low total mercury concentrations such as sample K2-8. Sample K3-3 is the only sample which exhibits considerable release of mercury at around 350 °C at up to 50% of the 'main' peak at ca. 200 °C in one replicate.

PTD results of Optimized SEP pools

Samples K2-8 and K3-3 were chosen for the sequential after different steps of the Optimized SEP, as described in section 2.4.4 and the extraction scheme in figure 2.5. PTD due to their interesting features in the bulk sample PTD analysis: K2-8 was the sample that exhibited the largest peak at 75 – 100 °C. K3-3 exhibited the largest peak at 350 °C of the whole sample set in one of the measured replicates. Figures 3.8 and 3.9 display results of PTD measurements that were undertaken after each step of the Optimized SEP, as described in section 2.5.3. While the 'bulk' curve represents the original composition of the sample, the replicates measured after a number of extraction steps only represents whatever mercury was left in the sample at that point. To visualize this, these PTD curves were scaled: while the highest peak is plotted at 100% extinction for the 'bulk' samples, the subsequent samples are scaled to the amount of mercury that is estimated to be left in the sample, based on concentration measurements done on other replicates of the extracted samples. Table 3.5 describes how the scaling factors were calculated. It is important to note that the scaling only serves for interpreting qualitatively, not quantitatively: As all curves are normalized to the highest peak - which may be a different one for different samples - and as the peaks are different in their width, the area under the curves is not comparable directly. Nevertheless, it serves as a 'guide to the eye' in qualitative interpretation of the data. Due to the scaling according to how much mercury was left in the soil after a specific extraction step, the fraction 'after F4' is forcedly scaled to 0 and is not plotted in figures 3.8 and 3.9. There is some residual mercury visible in this fraction in the raw data, but it exceeds the background only by a factor of 4 and thus the exclusion of a curve 'after F4' was deemed reasonable. Analyzing the PTD results, it is important to consider that even though the fractions represent steps that occur after each other in the extraction, they were done in this case on un-homogenized subsamples of two soil samples, since PTD is destructive and cannot be conducted several times on the same batch of sediment. While the absolute amount of mercury in the replicates was similar, it was not identical, and it is possible that the mercury was bound differently in the different sub-samples.

TABLE 3.5 Table showing percent values of mercury extracted in each Optimized SEP step, from which the scaling factor ('Scaling') for the PTD curves is derived. n=3; 'Scaling' ... Scaling factor; '$\%_{Fract.}$' ... Percent of Hg extracted in specific fraction ; 'cum. $\%_{extr.}$' ... cumulative Hg that has been extracted at the indicated extraction step; Calculation of scaling factor: Scaling factor = $\frac{(100-\%Hg_{cum.})}{100}$

	F1 H_2O_{MQ}		**F2** $0.5MHNO_3$		**F3** $6MHNO_3$		**F4** aqua regia	
	Hg in F1 (n=3)	1SD	Hg in F2 (n=3)	1SD	Hg in F3 (n=3)	1SD	Hg in F4 (n=3)	1SD
K2-8								
$\%_{Fract.}$	2.56	0.57	17.44	1.53	39.61	0.86	40.39	1.97
cum. $\%_{extr.}$	2.56		20.00		59.61		100.00	
Scaling	**0.97**		**0.80**		**0.40**		**0.00**	
K3-3								
$\%_{Fract.}$	1.03	0.16	0.10	0.07	8.44	0.06	90.43	0.18
cum. $\%_{extr.}$	1.03		1.13		9.57		100.00	
Scaling	**0.99**		**0.99**		**0.90**		**0.00**	

Sequential PTD results of K2-8

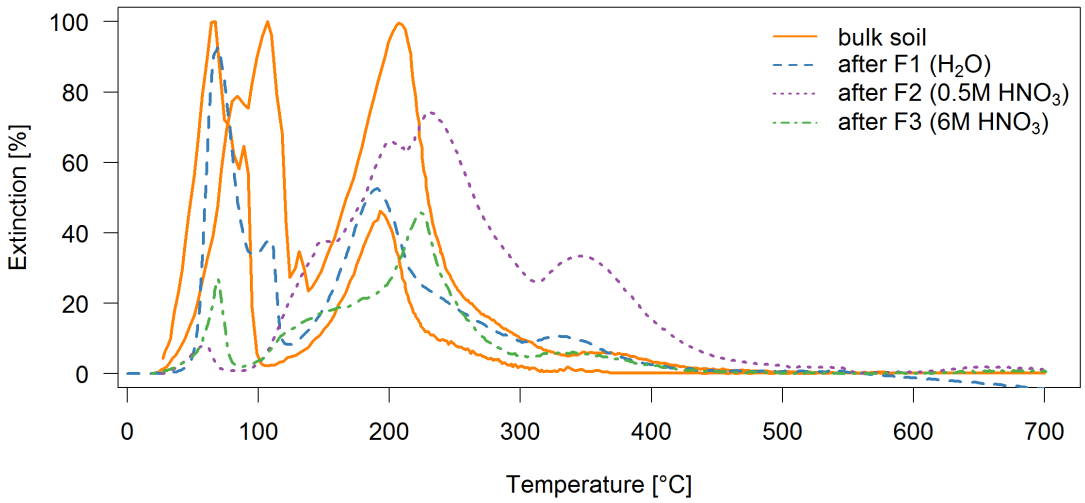

FIG. 3.8 The figure shows the release of mercury from the sample K2-8 at different temperatures at all stages of the extraction procedure. The measurements were done on replicates, not on the same sample.

Sample K2-8 was selected for PTD according to its well-pronounced Hg^0 peak, as can be seen in figure 3.6. The bulk PTD measurements conducted during Optimized SEP look different

from the one conducted during the bulk measurements: While the 'original' PTD curve showed a sharp Hg^0 peak that showed higher maximum extinction than the 'matrix-bound Hg^{II}' peak, the bulk measurement conducted during the SEP shows an uneven peak around 100 °C with four distinct sub-peaks at different temperatures. This reflects the heterogeneity of the Hg^0 peak, which was released at slightly different temperatures between the two subsamples of the same extraction vial sent for analysis. Examining the temperature ranges with the highest mercury releases, the following can be stated: While the 100 °C and 350 °C peaks are relatively sharp and well-defined, with their maxima occurring within a small temperature range, the 120–300 °C area shows multiple peaks that overlap and are not clearly resolvable from one another. Their maxima do not overlap in all subsamples, posing difficulties for interpretation. Looking at the 100 °C peak, the 'bulk' and 'after F1' sample clearly show the larger peaks, with those 100 °C peaks 'after F2' and 'after F3' diminished, suggesting that some of the mercury released at around 100 °C is removed in every step of the SEP. The peak at around 350 °C demonstrates the heterogeneity of the sample, being present in the residues after F2, F3 and F4, but not in the bulk sample, where it ought to be if the sample were perfectly homogeneous. This may either be due to inhomogeneity between the subsamples, or due to an artifact which occurs during extraction via precipitation of a more heat-resistent mercury phase such as α-HgS. The change in size of this peak is therefore difficult to interpret. It can only be noted that in the 'after F3' curve, it likely overlaps with the peaks around 120 – 300 °C. This is a collection of overlapping peaks that seem to be highly variable from sub-sample to sub-sample. There seem to be three overlapping peaks in this area that show up at different temperatures. The earliest occurs at around 150 °C, the next at around 195 °C and the last at around 250 °C. The interpretation of these peaks in terms of speciaton will be discussed in section 4.1.1 of the discussion. Since it has been shown e.g. by Biester and Scholz (1997); Richard et al. (2016) that there are numerous mercury species and binding forms of mercury species being released in this temperature range, nothing more specific can be said about these peaks. The one at around 200 °C is only visible in 'bulk', 'after F1' and 'after F2', while the one at 250 °C seems to only show up in the later extracts. It is, however, not clear if this presents a shift of the earlier peak or, again, sample heterogeneity.

Sequential PTD results of K3-3

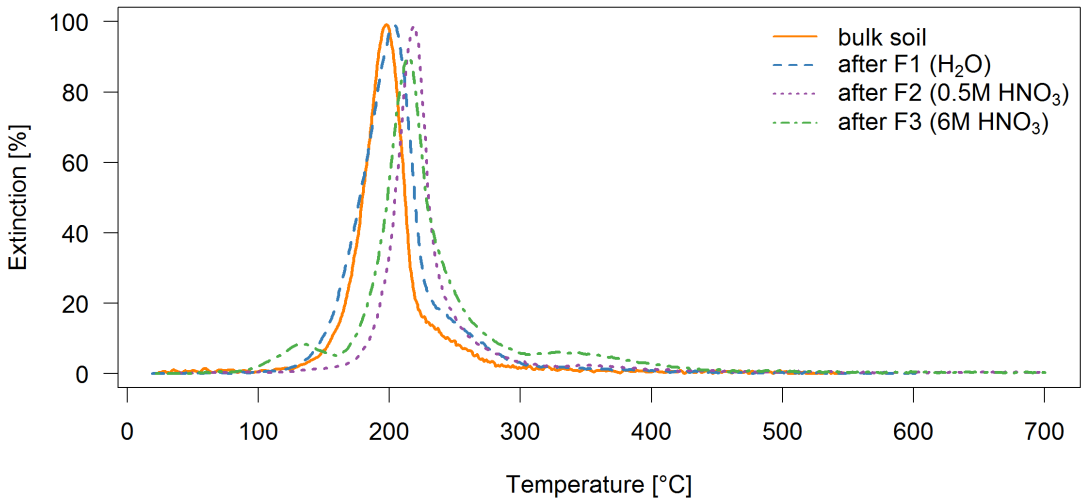

FIG. 3.9 The figure shows the release of mercury from the sample K3-3 at different temperatures at all stages of the extraction procedure. The measurements were done on replicates, not on the same sample.

In figure 3.9, K3-3 presents only one prominent feature: 100% of the mercury are released at around 200 °C. This is contrary to the expectation that this sample would show signficant release of mercury at temperatures > 350 °C, as in the first round of PTD (figure 3.7). It seems like there is a shift of the 200 °C peak towards higher temperatures in the later extraction steps, possibly suggesting that the less thermally stable mercury would be leached out by weaker extraction steps already. The replicate which was measured after F3 is more heterogeneous in its composition, displaying a small peak at 130 °C and slightly elevated extinction at around 350 °C. It has to be stated that the selectivity of the Optimized SEP was not optimal for core K3. Only few percents of mercury were leached from the soil in F1 and F2 and F3, leaving the bulk of mercury in the soil until the aqua regia extract. This is the reason why hardly any size reduction of the peaks 'after F1', 'after F2', 'after F3' is visible in the temperature curves. On the other hand, the scaling approach taken, which normalizes the highest peak of the diagram to the fraction of mercury which is still left in it, is more easily interpretable in this sample than in K2-8: As there is only one peak, no relative size changes between peaks, and subsequent changes in the reference peak for scaling occurred. Thus, there is more consistency to the area underneath the curve. Due to the non-selectivity, the scaling is only minimally different.

3.4 Mercury stable isotope results

Mercury stable isotopes were measured on the bulk samples of cores K2 and K3, as well as on the SEP samples. Here, only stable isotope results of the Optimized SEP results are presented and displayed in detail. Information relating to the First SEP can be found in table C.4 in appendix C.2. The complete dataset with δ^{202}Hg, Δ^{199}Hg, Δ^{200}Hg, Δ^{201}Hg and Δ^{204}Hg can be found in appendix C. The given standard deviation refers to the reproducibility of the secondary standard 'Fluka' in the session in which the sample in question was measured. δ^{202}Hg and Δ^{199}Hg data are first presented in juxtaposition with the total mercury concentration in the soil profiles (Figures 3.10 and 3.11). Figures 3.12 and 3.13 then visualize δ^{202}Hg of the extracted fractions of the two cores, and display the isotopic signatures as well as the pool sizes.

Depth profiles of mercury stable isotopes

Hg isotope ratios were measured on the most contaminated samples, where the digests were concentrated enough so a measurable solution with low acid and high mercury content could be produced. Total digests of the samples were measured in July 2016. In core K2, the total digests of K2-4 to 12 were measured and samples K3-2 to 5 were measured in K3. The Optimized SEP extracts were produced and measured in November and December 2016. SEP extracts could be measured on samples K2-5 to 10 for core K2, and on K3-2 and K3-3 for core K3. SEP extracts were only measured if all extracts (F1-F4) contained > 5 µg/L Hg. It is important to recognize that the pool sizes between the different fractions may be quite different, which is visualized in Figures 3.12 and 3.13. For the Optimized SEP dataset, theoretical bulk values were calculated by weighting the measurements according to the fraction of mercury of the sample that they represented, and adding them.
Comparing measured and calculated bulk signatures, differences can be seen in some samples - especially for the Δ^{199}Hg data in figure 3.11. Since significant differences between subsamples of the same soil sample had been noted as well in the concentration data (figure 3.2) and PTD datasets (e.g. as discussed in 3.3), this was interpreted as sample inhomogeneity.
Looking at the δ^{202}Hg signature of total digests in K2 (orange circles) and comparing the isotopic signatures of the samples with the absolute amount of mercury in them, it seems that samples with high concentrations of mercury are isotopically lighter and vice-versa, creating an almost symmetrical pattern. This trend is not observed in core K3, where the most contaminated samples also have heavier signatures. The absolute δ values also differ between K2 and K3: while K2 has minimum values of bulk sample digests of -0.45 $\pm$ 0.09 ‰ (K2-8, 240-260 cm) and a maximum value of 0.10 $\pm$ 0.09 ‰ (K2-10, 280-300 cm), K3

samples are significantly heavier with a minimum of -0.12 ± 0.03 ‰ (K3-5, 140-160 cm) and a maximum of 0.08 ± 0.03 ‰ (K3-3, 50-70 cm).

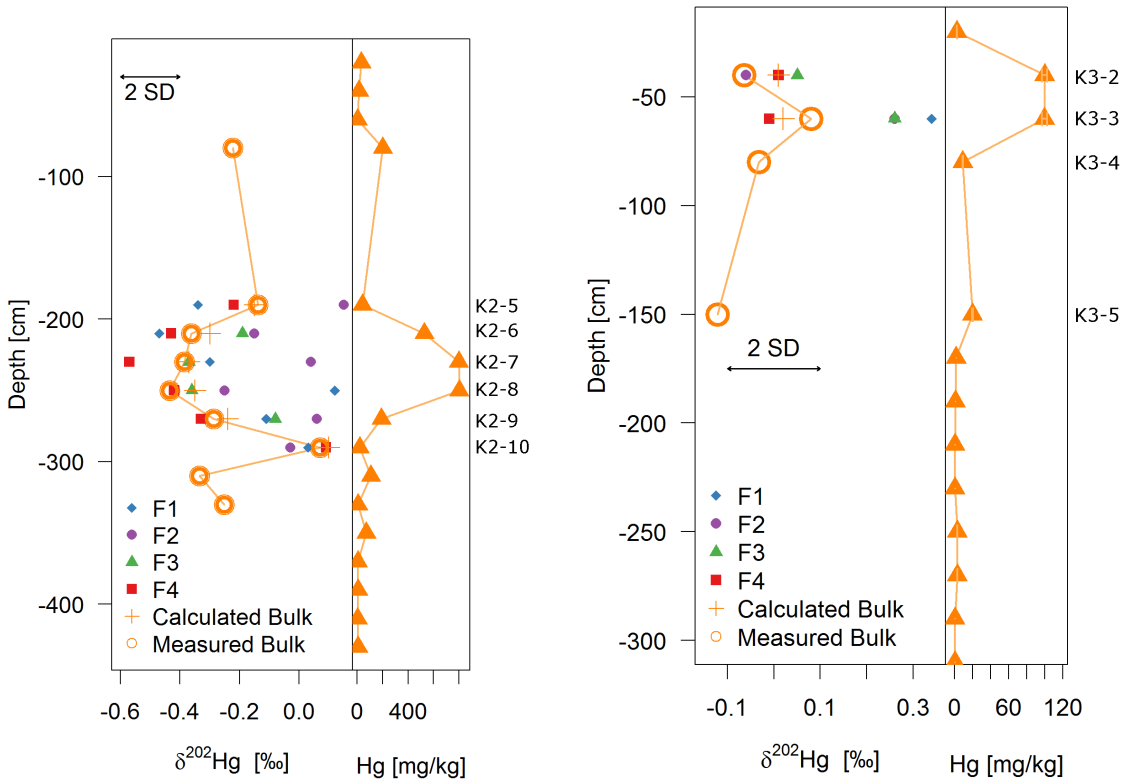

FIG. 3.10 δ^{202}Hg data on bulk and sequentially extracted samples, and their position within the cores. The left panel represents core K2, the right core K3. Details of this overview figure are represented in figures 3.12, 3.13 and in the discussion. The 'Measured Bulk' results are based on measurements of aqua regia total digests of the samples conducted in July 2016. 'Calculated Bulk' is the weighted sum of the four extracted sample fractions that were measured in November & December 2016. 2 SD represents the reproducibility of the in-house secondary standard.

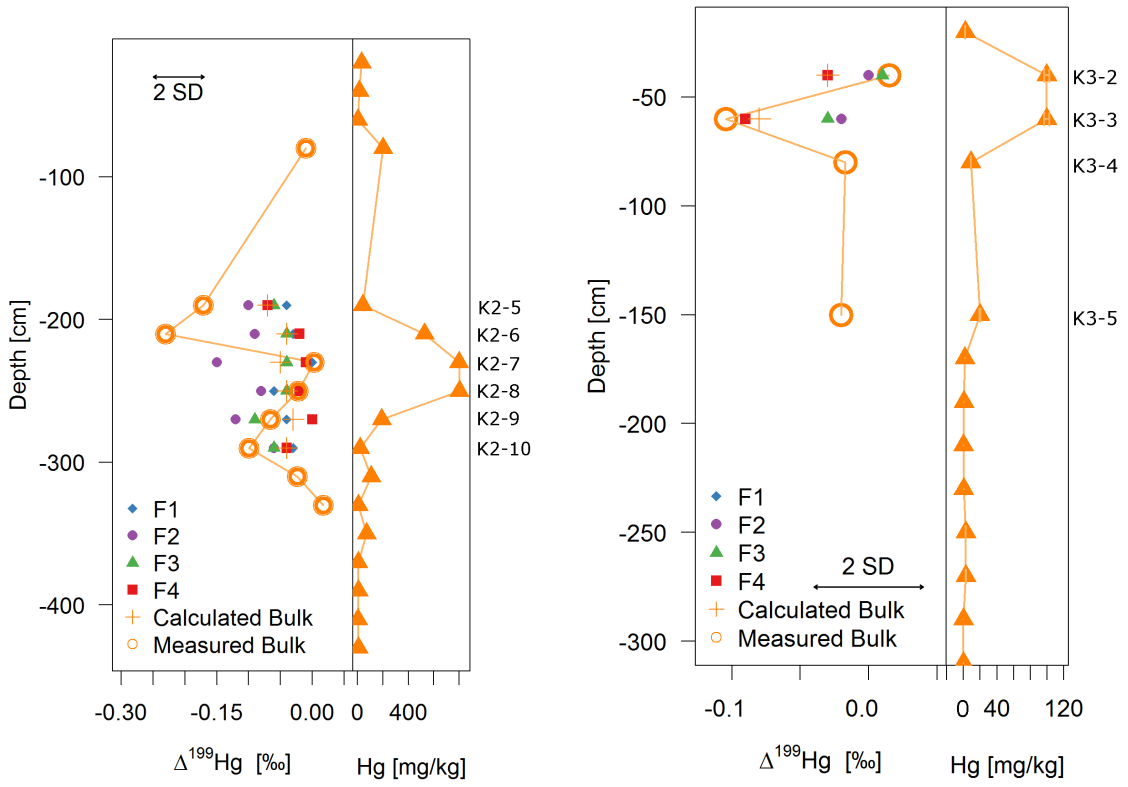

FIG. 3.11 Δ^{199}Hg data on bulk and sequentially extracted samples, and their position within the cores. The left panel represents core K2, the right core K3. The 'Measured Bulk' results are based on measurements of aqua regia total digests of the samples conducted in July 2016. 'Calculated Bulk' is the weighted sum of the four extracted sample fractions that were measured in November & December 2016. 2 SD represents the reproducibility of the in-house secondary standard.

Mercury stable isotopes of Optimized SEP pools

Figures 3.12 and 3.13 show the sequentially extracted pools of the Optimized SEP and the calculated mean signatures of the samples, including information on the amount of mercury extracted in each SEP pool, which is represented through the sizes of the plotted symbols.

K2 In K2, the most contaminated samples were sequentially extracted. The samples K2-7 and -8 at depths -220 cm and -240 cm were the most contaminated, as can be seen in the right panel of figure 3.12, where the pools are scaled according to the absolute amount of mercury in them. The F4 fraction contains most mercury, in addition to displaying the lightest δ^{202}Hg signatures in the whole extraction series.

K3 In K3, most mercury was only leached into solution in step 'F4', which makes up > 90 % of total mercury in all samples of the Optimized SEP. The two extracted samples seem to be complementary in terms of which fractions are light and which are heavy.

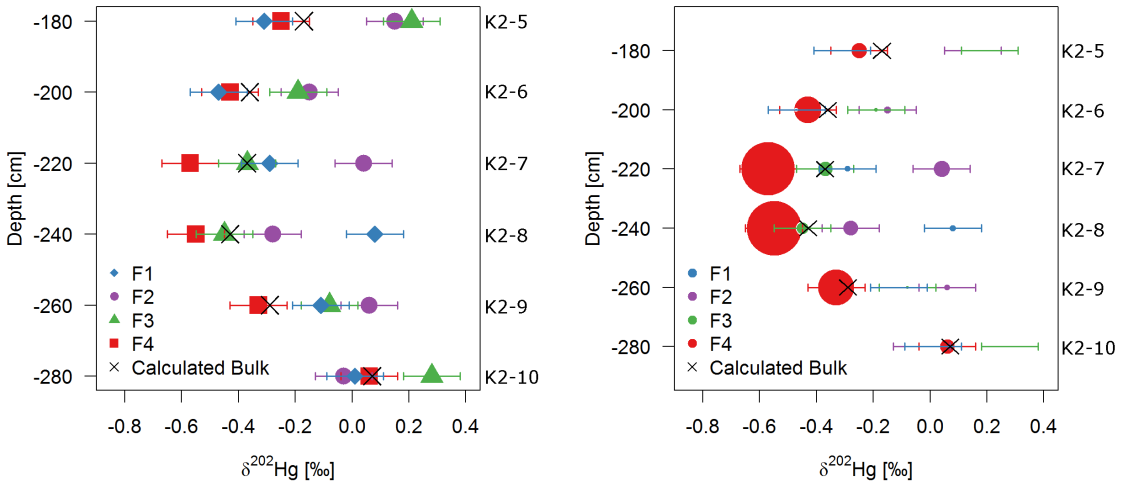

FIG. 3.12 δ^{202}Hg values of all Optimized SEP extracts in core K2. The left panel displays the datapoints with 2 SD error bars based on the reproducibility of the in-house secondary standard. In the right panel, the extracted pools are scaled to their absolute pool size. 'Calculated Bulk' refers to the mean signature of the sample, calculated by averaging the weighted, measured fractions.

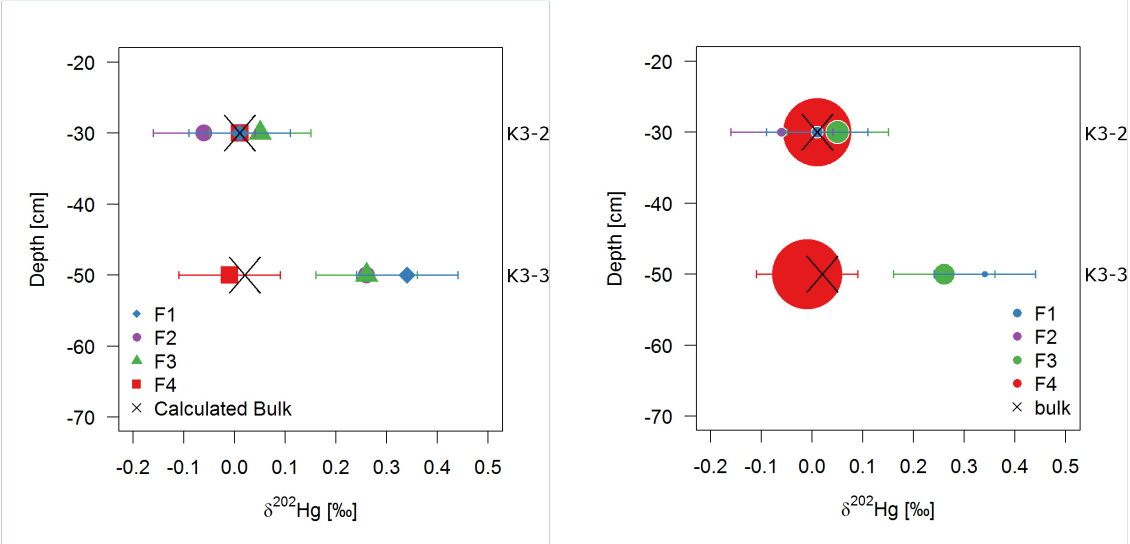

FIG. 3.13 δ^{202}Hg values of all Optimized SEP extracts in core K3. The left panel displays the datapoints with 2 SD error bars based on the reproducibility of the in-house secondary standard. In the right panel, the extracted pools are scaled to their absolute pool size. 'Calculated Bulk' (left panel) and 'bulk' (right panel) refer to the mean signature of the sample, calculated by averaging the weighted, measured fractions.

Mercury stable isotopes of sequential F1 extracts

The isotope measurements on the sequential water extracts (section 2.4.5) are plotted in figure 3.14. They are all heavy relative to the bulk signature of the sample K2-8 and each subsequent step is lighter than the one before. The only exception is 'F1D', which had a much longer equilibration time than the others, as described in section 3.2. It is marked pink in the graph.

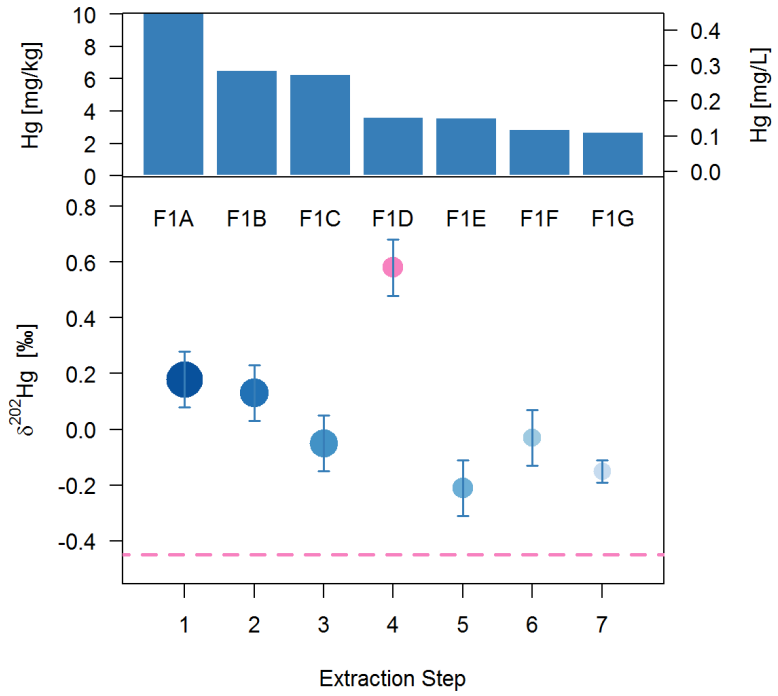

FIG. 3.14 δ^{202}Hg of sequential water extracts, as well as the absolute amount of mercury extracted in the extraction step. F1D had a longer equilibration time than the other extracts and is marked pink. The dashed line at -0.43 ‰ δ^{202}Hg indicates the bulk sample signature of K2-8.

Chapter 4

Discussion

4.1 Mercury speciation

Is sequential extraction a suitable - and sufficiently specific - tool to divide the soil mercury pool into portions for mercury stable isotope analysis? - This is the central question which is sought to be answered in this section. Before exploring how the original $HgCl_2$ contamination has transformed at the Bad Krozingen field site, the current speciation of the site has to be known. To achieve this, a good understanding of the information, which the collected PTD and Optimized SEP results can provide about mercury speciation of the samples, needs to be established. The findings, which are visualized in the end of this section (figure 4.2), will serve for further reference for the rest of the discussion. They provide the basis for interpreting the mercury isotope data in terms of process tracing in the following chapters.

4.1.1 Speciation according to PTD

Pyrolytic thermo-desorption (PTD) curves provide information on the temperatures at which a sample's mercury is released into the detector. Comparing these to the PTD release curves of standard compounds, the mercury speciation of a sample can be determined - or at least limited to several species that show similar PTD release temperatures. Figure 4.1 is a collection of PTD curves for mercury-containing substances relevant for this thesis. They were measured in Harald Biester's research group at TU Braunschweig in different measuring sessions, using the same method as the samples of this study (Biester and Scholz, 1997; Richard et al., 2016). Published compilations of measured standard materials from Braunschweig can also be found in Bavec and Gosar (2016). Coufalík and Komárek (2014) compiled data on measured standards, but without elaborating on the methods used for determining the temperature-release curves. Reis et al. (2012) and Reis et al. (2015) also

published records of PTD measurements. Comparing measured data with literature values, the observed temperature ranges with high mercury release can be interpreted in terms of their species content. In the following paragraphs, the three observed temperature ranges are discussed separately.

70 - 100 °C The only Hg species known to volatilize at such low temperatures is metallic Hg^0. However, it is known that $HgCl_2$ may partly be reduced to Hg^0 and even store-bought stocks of $HgCl_2$ contain traces of Hg^0 and thus also partly volatilize at < 100 °C (Harald Biester, pers. comm.). This could also be observed in the $HgCl_2$ standard curve measured for reference in the presented dataset (figure 3.5).

150 - 250 °C With the exception of a few samples that contained high amounts of Hg^0, all samples studied during this thesis released the majority of contained mercury in the temperature range between 150-250 °C. The peak shapes varied from comparably sharp peaks with clear maxima, as in K3, to broader peaks or peaks displaying more than one maximum in this range. Numerous mercury species, such as $HgCl_2$, Hg_2Cl_2 (Coufalík and Komárek, 2014), metacinnabar β-HgS and $Hg(NO_3)_2 \cdot H_2O$ (see figure 4.1) have been found to volatilize in this temperature range. Hg^{II} bound to different matrices such as humic substances (Coufalík and Komárek, 2014; Reis et al., 2015) and sorbed to $Fe(OH)_3$ (Richard et al., 2016) also falls into this category. These peaks are not distinguishable in a natural sample with unknown speciation due to their overlapping volatilization ranges. Biester and Scholz (1997) coined the descriptive term 'matrix-bound Hg^{II}' for mercury species released in this temperature range in their study, which included soil from Bad Krozingen.

250 - 350 °C Several samples in core K3 of this study showed PTD peaks around 350 °C (figure 3.7). Mercury released in this temperature range can be assigned to α-HgS, according to different studies that measured natural and synthetic $\alpha-$cinnabar samples (Biester and Scholz, 1997; Coufalík and Komárek, 2014; Reis et al., 2012). PTD on mercury sulfates also showed that part of the mercury was released in this temperature range (Coufalík and Komárek, 2014). The exact temperature may vary depending on crystallinity and, again, the matrix.

Peaks at >350 °C are not observed in this study. According to standard curve measurements conducted by Harald Biester, they could be caused by HgO phases or $HgSO_4$. It can thus be assumed that these phases are not present in the studied soil and will be excluded from further consideration.

All PTD curves obtained in this study could be categorized in the way described above. While all samples released mercury in the 150-250 °C range, release at lower and higher temperatures served as a distinctive characteristic between samples. Release below 100 °C was only observed in the most highly contaminated samples of core K2 and was attributed to the presence of Hg^0 in the soil. In core K3, which did not contain evidence of significant Hg^0 presence, three samples released mercury at around 350 °C, hinting at the presence of α-HgS. This way, the mercury speciation of the samples can be constrained based on PTD curve results.

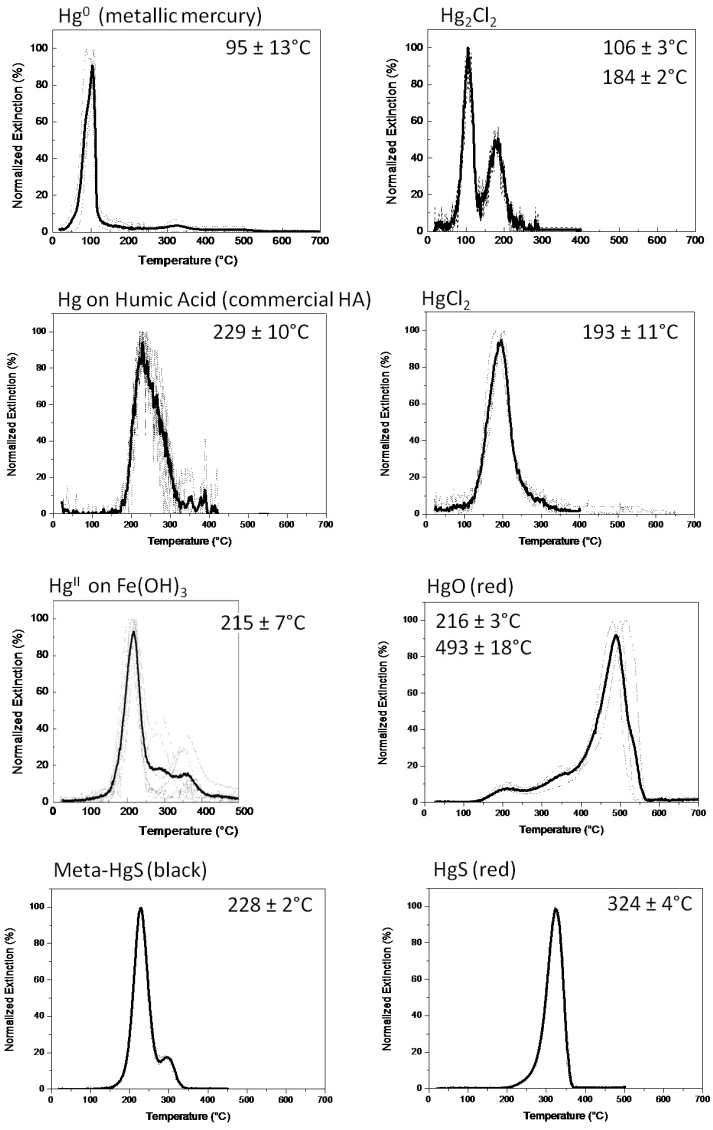

FIG. 4.1 Pyrolytic thermo-desorption results of pure chemicals, as measured at TU Braunschweig. The curves for Hg^0, $HgCl_2$, Hg^{II} on $Fe(OH)_3$, Meta-HgS and red HgS were published in Richard et al. (2016).

4.1.2 Speciation according to sequential extraction

To evaluate the Optimized SEP results, we will revisit some literature on sequential extractions. The goal of any sequential extraction is to produce sub-pools of an element in a sample which hold meaningful information about the metal in solution. This might be information about the speciation, about its environmental behavior, or others (Bacon and Davidson, 2008). The term 'speciation' itself is worthy of closer examination. Templeton et al. (2000) describe two uses of the word – *to indicate the analytical activity of identifying chemical species* and *to indicate the distribution of species in a particular sample or matrix*. They suggest replacing the first use by the term 'species analysis', while reserving the term 'speciation' in the sense of 'species distribution' of a sample. For the practical purposes of describing the outcome of sequential extractions, however, it is useful to look towards the suggestion of Ure (1991), who defines three classes of speciation in the following ways:

> *(1)* functionally*, i.e. by their role, e.g. plant-available species or exchangeable cations, (2)* operationally*, by the reagents or the procedures used to identify, isolate and quantify them, e.g. by the use of acid ammonium oxalate to extract elements associated with the "moderately reducible" components of soil, or the isolation of a physical fraction such as a "soil solution" or (3)* as specific chemical compounds or oxidation states *of an element, e.g. tri-butyl tin, or ferrous iron. Ure (1991)*

Bacon and Davidson (2008) argue on the basis of the Ure (1991) definition that all sequential extractions provide information on operationally defined speciation. Bloom et al. (2003), whose extraction will be discussed in detail below, use a different nomenclature, stating that their SEP divides the mercury present in a sample into *behavioral classes*. Their extracted pools are called 'water soluble' Hg (corresponding to an operational definition), 'stomach acid soluble' and 'organo-chelated' Hg (functionally defined), 'elemental' and 'sulfidic' Hg (compound specific). The claim is validated with data of different mercury compounds in various matrices, which showed clear distributions between the fractions. Bacon and Davidson (2008), however, take a very critical stance on the specificity of SEP:

> *It is extremely important to appreciate that sequential extraction only divides the PTE [potentially toxic elements, comm. F.B.] content of a test sample into portions soluble in particular reagents under particular conditions. Whilst these reagents are often selected with the intention that they should target well-defined mineral phases – and may indeed do so in many cases – such specificity cannot be guaranteed. Bacon and Davidson (2008)*

They present abundant literature where SEP proved non-specific for the targeted mineral phases. The given reasons why sequential extraction does not quantitatively determine the trace metals associated with specific mineral phases in environmental solids are: (1) redistribution of analytes among phases during extraction; (2) non-selectivity of reagents for target phases; (3) incomplete extraction; or (4) precipitation of 'new' mineral phases during extraction.

So far, this discussion has been relevant to extractions for all trace metals. A widely applied and extensively validated SEP for mercury is that of Bloom et al. (2003), which also provided the starting point for extractions conducted in this thesis. Bloom et al. (2003) extracted several pure mercury compounds ($HgCl_2$, HgO, $HgSO_4$, $HgAu$, Hg_2Cl_2, CH_3Hg, humic-bound Hg, Hg^0, $HgSe$ and HgS) and reported in which steps they were extracted using their SEP. They noted that even though some compounds were clearly preferably leached into one extracted pool, several factors such as the amount of a mercury species that is present in the sample exerted an influence on the SEP outcome. For example, when low amounts of $HgCl_2$ were present in a sample, it was extracted across the four pools $F1_{Bloom}$—$F4_{Bloom}$, but with > 52 mg/kg $HgCl_2$ present in the soil, the vast majority of the species was leached already in $F1+F2_{Bloom}$, which are the pools of highly mobile mercury (Bloom et al., 2003). Hall et al. (2005) found that grain size may influence the SEP result, reporting that small-grained HgS may be leached already in $F4_{Bloom}$, even though it is meant to only be leached in the final aqua regia step. Kim et al. (2003) have compared PTD results with 'Bloom SEP' results for different Hg-contaminated soils and synthetic mercury compounds. They found that the mineral schuetteite ($Hg_3(SO_4)O_2$) in a gold mine tailings sample was released evenly through several SEP fractions rather than in one specific step, and assumed encapsulation of the mineral in the host rock as the cause.

Taking into account these shortcomings in terms of determining the exact species in solution in each extracted pool, and also taking into account that the presented Optimized SEP was adjusted according to pre-tests and is no longer the same as Bloom's protocol (see section 2.4), there is still important information on the sample speciation to be gathered through combined PTD and SEP.

The following paragraphs first introduce the mercury species which are expected to dissolve in each step. Then, literature data on such extracts is compared to the results of the Optimized SEP of this study, and the possible mercury speciation of this thesis' samples is discussed.

$\mathbf{F1}_{Opt}$, $\mathbf{H_2O}_{MQ}$

Operationally defined as 'water-extractable pool' by Bloom et al. (2003), ultra-pure water has been observed to extract compounds with a high water solubility such as $HgCl_2$, free

inorganic Hg^{II} (Bloom et al., 2003; Fernández-Martínez and Rucandio, 2013), and mercury bound to dissolved organic matter (DOC) (Skyllberg, 2011). Yin et al. (2013) conducted water extractions of contaminated soil and referred to the speciation diagrams of Schuster (1991) that show $HgCl_2$, $Hg(OH)_2$ and $HgOHCl$ as the dominant species in aqueous solutions. However, especially DOC has been well documented to exert a strong influence on the distribution of mercury in aqueous systems (Ravichandran, 2004, f.ex.) and some studies have assumed that 100 % of H_2O-extractable mercury is bound to organic matter (Wallschläger et al., 1996). Of its different functional groups, especially thiol binding sites have an exceptionally high affinity for mercury and form $Hg(SR)_2$ complexes (Skyllberg, 2011).
The present study, however, revealed no correlations between between DOC content of the F1 extracts and the mercury levels in the extracts. Core K3, which yielded more DOC in its F1 extracts, consistently had lower levels of water-extractable mercury (see table 3.3 for DOC results, figure 3.3 for representations of F1 concentrations). The levels rather seem determined by the absolute amount of mercury in the samples, of which a low percentage (up to 4 %, as in sample K2-10) was leached during the F1 step. Between 0.2 and 4.1 % of total extracted mercury were extracted in F1.

Sequential F1 extracts Sequential water extracts shed more light to the speciation of the F1 pool. Wallschläger et al. (1996) have observed during sequential F1 extractions that mercury was still present in the second and further extraction steps at a low percentage of the total aqua regia-extractable mercury. The authors suggested that the sequential water extracts were not *"extracting preexisting stable species, but rather remove species from an equilibrium, which is then readjusted for the next extraction"* (Wallschläger et al., 1996). When the supernatant is filtered and removed, a new equilibrium would be reached with the fresh H_2O_{MQ}.
This would be one possible explanation for the observed mercury concentrations in the sequential F1 extracts of this study (see table 3.2 and figure 3.4). From figure 3.4, it can be seen that the amount of mercury that is extracted from the sample after 18 h of equilibration sinks from step to step. In the sense of Wallschläger et al. (1996), this may be interpreted as new equilibria at lower concentrations, due to the fact that less mercury is left in the sample. Even if looking at the percentage of mercury extracted relative to the pool of mercury that is still left in the sample ('$\%_{\text{residual}}$', see table 3.2), the percentage extracted decreases. The equilibrium can thus not be explained solely in relation to the total mercury present in the soil. Another explanation could be that it takes a longer time for the Hg^0 trapped in the soil and adsorbed to particles to diffuse into solution and subsequently oxidize. The extraction procedure included shaking of the samples, which induces mechanical stress and

may cause more tightly bound mercury to be mobilized into the aqueous phase. All extracts were on the shaker for 18 $\pm$ 4 hours. The extracts were then centrifuged and filtered, as described in section 2.4.5. As extract F1D was treated differently, with two days passing before centrifuging and two weeks passing before filtering, one could expect more mercury to be dissolved in it, relative to the extracts which hat shorter exposer to the extractant solution. This was not the case: F1D fit well into the concentration ranges of the extracts before and after. One possible reason for this would be an equilibrium of the aqueous with the solid phase, as suggested by Wallschläger et al. (1996). Another possibility to be considered is the degassing of mercury from the solution, as the mercury in solution was not stabilized with $BrCl$. PE vials have been shown to be permeable to Hg^0 vapor and not suited for long-term storage of un-acidified Hg^0 samples (Yu and Yan, 2003). In this case, the mercury concentration would have been higher previous to the concentration measurement, but during the two weeks of down-time, more mercury would have been lost from the sample than would have been leached from the soil due to the longer equilibration time.

$F2_{Opt}$, 0.5 M HNO_3

Functionally defined as the 'labile, bioavailable pool' by Fernández-Martínez and Rucandio (2013), it leaches species that are weakly sorbed to sediment and soil surfaces, associated with ligands and free Hg^{II} species. Since the pH of this mercury pool ($\sim$ pH 1.1, see table 3.4) was lower than that of $F2_{Bloom}$, it can be assumed that HgO and $HgSO_4$, which have been shown to dissolve mainly in Bloom's 'stomach acid' extract, also appear in this fraction (Bloom et al., 2003).Since PTD had shown that they are not present in the Bad Krozingen samples, they were treated as absent from the samples. In case any mercury was associated to carbonates, it would dissolve in this section as carbonates dissolved completely in the $F2_{Opt}$ step according to the pH measurement results (table 3.4). Mercury carbonate phases have been documented to be extremely rare in nature and to mostly occur as secondary alterations to cinnabar ore in silica-carbonate deposits (Roberts et al., 2001; Varekamp and Buseck, 1984), thus it was considered unlikely by the author that they would occur in the present samples in significant amounts. Additionally, Hg^0 that leached from cavities in the soil and subsequently oxidized to Hg^{II} may be found in cases where Hg^0 was detected by thermo-desorption, as was the case for sample K2-8.

$F3_{Opt}$, 6 M HNO_3

Extractions conducted with $\geq$ 6 M HNO_3 target all mercury except HgS, as described by Hall et al. (2005). The 12 M HNO_3 step of Bloom et al. (2003) is defined as dissolving

elemental Hg^0 and Hg-species bound to Fe- and Mn-oxides. Since the $F3_{Bloom}$ step, aimed at extracting the organo-chelated fraction, was omitted, this fraction should include Hg_2Cl_2, Hg bound to humic acids and CH_3Hg, as well. Bloom et al. (2003) have shown that at their tested concentration of 44 $^{mg}/_{kg}$ Hg^0 in the extracted sample, the vast majority of metallic mercury dissolved in 12 M HNO_3.
However, sequential PTD of sample K2-8 showed that such a near-perfect leach of Hg^0 in $F3_{Opt}$ was not the case. From figure 3.8, it is visible that some elemental Hg^0 was still present in sample K2-8 after the treatment. While some Hg^0 is removed during the extraction steps, no single step proves to be selective for it. In sample K3-3, where only a peak of 'matrix-associated Hg^{II}' was detected, it was shown that >90 % of this peak were only removed during F4, the aqua regia leach. This is contrary to literature studies (Bloom et al., 2003; Fernández-Martínez and Rucandio, 2013; Hall et al., 2005) which have found that 6–12 M HNO_3 extraction steps leach all mercury species except sulfides and silicates.

$F4_{Opt}$, aqua regia

The operationally defined 'residual' or 'refractory' pool should extract the Hg sulfides left in the samples (Hall et al., 2005, e.g.). Only some samples of this study had the characteristic HgS peak at 350 °C in their thermo-desorption temperature curves and were expected to show that a significant amount mercury was leached in this step. However, in all samples, a significant amount of mercury was extracted in F4. In core K2, at least 34% of all mercury was leached in F4 in all measured samples. In core K3, at least 52 % of all mercury was extracted in F4. There was no single sample in the whole dataset where the HgS peak made up even 10 % of the total mercury detected. This is a significant discrepancy and means that the mercury in F4 must mostly also be 'matrix-bound' or be present in some form which volatilizes at $\sim$ 200 °C. Based on the contrasting information between the present Optimized SEP results and literature, no information on the bonding of this species could be given.
PTD 'after F4' on the residual soil has shown a small release of mercury still; however, this was only a factor of 4 times above background levels and was undertaken on 10-100 times larger amounts of soil. The extraction is considered complete and this PTD result is no longer considered. The scheme in figure 4.2 visualizes all information on speciation that can be obtained based on the PTD and Optimized SEP results, as just discussed.

4.1.3 Summary: Mercury speciation of samples in this thesis

F1 is the easiest Optimized SEP pool to constrain chemically, since extensive information is available on H_2O solubility of mercury phases and it is the first step and the soil is still

unaltered by any extracting solutions. In addition, a series of sequential F1 extracts was undertaken. The remnants of the unaltered contaminant species $HgCl_2$ that are not sorbed to the soil or transformed are expected to be extracted in F1, due to their high water solubility. Other expected species are Hg^{II} stemming from $HgCl_2$ dissociation, in various complexes expected at the high pH, such as $Hg(OH)_2^0$ and DOC. The relative contribution of Hg^0, where present in the samples, can be debated. It is assumed that Hg^0 oxidizes to Hg^{II} when in contact with the O_2-containing F1 solution. Based on the results of the sequential F1 extracts, it is assumed that the majority of $HgCl_2$ leaches in F1A, while Hg^0 represents the bulk of the further F1B–G extracts, as it is supplied slowly, by diffusion, and oxidized during the 18h equilibration time of the extraction. However, arguments that call for a more differentiated view of the sequential F1 extracts were also discussed. **F2** is assumed to contain weakly sorbed Hg^{II} species, which cannot be strictly chemically defined for the lack of knowledge from literature and this study. Together, F1 and F2 represent the more mobile and bioavailable fractions. **F3** is thought to contain mercury bound to crystalline oxides, bound to particulate organic matter and also, were previously detected by PTD, the Hg^0 which has not yet diffused from the sample. However, based on the available information, it is difficult to find a meaningful chemical distinction of F3 from **F4**, since it was found that F4 contained significantly more than just the sulfidic-bound mercury which it was described in literature to contain. They will be called the 'tightly bound' or 'refractory' pools in the following chapters. This study clearly demonstrates the importance of using several available methods when determining speciation. SEP speciation of this study should always be interpreted with respect to the PTD results; in samples with significant amounts of Hg^0, elemental mercury has to be expected in virtually every fraction.

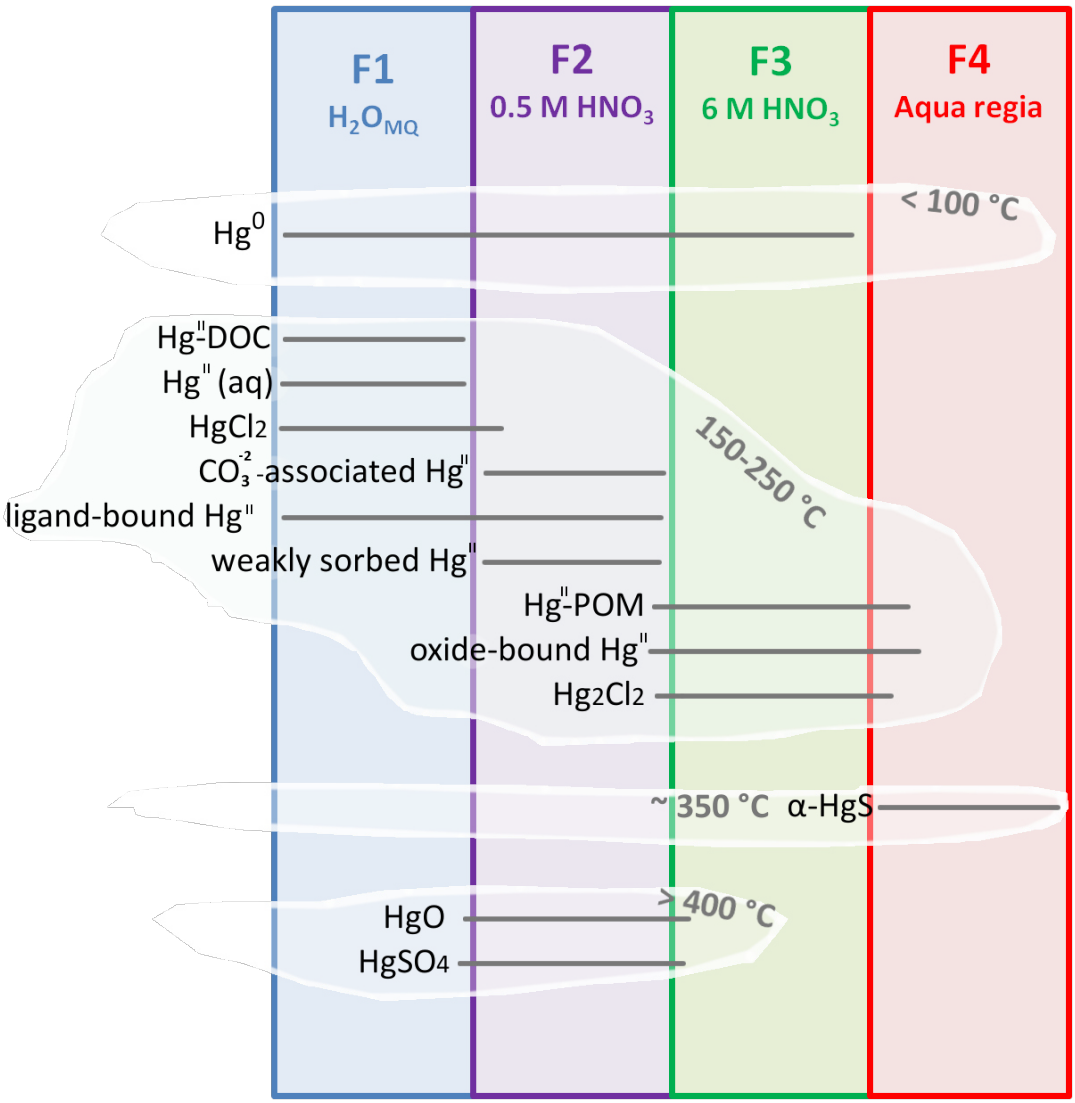

FIG. 4.2 Qualitative scheme showing the likely distribution of mercury species in the different extracts of Optimized SEP, based on literature review and measurements conducted during this study. Bloom et al. (2003); Fernández-Martínez and Rucandio (2013); Hall et al. (2005)

4.2 Interpreting mercury stable isotope results

4.2.1 Mercury isotopic signature of contamination source

Stable isotope ratios of mercury are a promising tool to track processes which transform mercury species: Every transformation of the original contamination that separates a portion of the contaminant from the original contamination by sorbing to particles, transforming to a different mercury compound, or leaving the system, is likely changing the isotopic signature of the original pool. Thus, comparing signatures that are present in the soil to the bulk signature of the contamination, a lot of information is potentially gained about the modifications that have taken place in the soil system.
To assess – and possibly quantify – fractionation that has taken place in a specific pool of mercury, it is necessary to know the isotopic signature of the original contamination. Unfortunately, no stock of the original $HgCl_2$ sublimate in Bad Krozingen was available for measurement for this study and it was necessary to find a suitable and reasonable estimate for it. Different authors have used different approaches to estimating source signatures for their study sites in the past, e.g. utilizing their studies' most contaminated sample as a baseline (Liu et al., 2011). Industrial mercury is mainly obtained from cinnabar ore and contemporarily produced industrial Hg^0 is reported to have a similar signature to its ore due to near-quantitative retorting (Sun et al., 2016). Historically, this has not been the case and up to 40% of the contained mercury was released into the atmosphere as gaseous Hg^0 (Sun et al., 2016), although there is no direct evidence of this causing fractionation in the resulting Hg^0(l) significantly fractionating both product and gaseous mercury to be found in literature (Jan Wiederhold, pers. comm.). This makes ore signatures uncertain source signatures for industrial mercury. To establish a reliable estimate that could be used also for the interpretation of this dataset, Dr. Jan Wiederhold, Andrew Grigg and the author conducted a literature survey which examined all published isotope ratio values of industrial mercury reported in publications until 2016. Figure 4.3 visualizes the collected data. Three types of data were considered: liquid Hg^0 intended for industrial use, cinnabar ores, and sediments polluted by industrial processes.

Cinnabar ore As for mercury ore data, the wealth of data as well as the variability of recorded signatures were much greater for the other two sample types. Only cinnabar ores were considered, as they are the primary source for the production of liquid Hg^0 (UNEP, 2013a). 22 different ore data from 11 different publications were recorded. The ores stem from historical and current mines in Latin America (Cooke et al., 2013), the large mines of Almadén, Spain and Idrija, Slovenia (Foucher et al., 2009; Gray et al., 2013a; Jiménez-

Moreno et al., 2016), mines in the USA Blum et al. (2014); Gehrke et al. (2011); Stetson et al. (2009); Wiederhold et al. (2013) and the Wanshan mine in China (Feng et al., 2013; Yin et al., 2013). In addition, Hintelmann and Lu (2003) compiled a dataset of different mines in Europe and North America. The mean δ^{202}Hg signature was -0.46 $\pm$ 0.56 ‰ (1 SD, n=22), MIF Δ^{199}Hg of the same dataset amounted to 0.01 $\pm$ 0.11 ‰ and is thus negligible. It is noteworthy, though, that the world's two most important *HgS* mines, Almaden in Sain and Idrija in Slovenia, both display small negative Δ^{199}Hg values.

Contaminated sediments Mercury isotope data on contaminated sediments is the most heterogeneous group of data used for this literature survey. Only sediments indicated as industrially contaminated were considered. These stemmed from the USA, China, 6 European countries and Japan (Balogh et al., 2015; Bartov et al., 2013; Bonsignore et al., 2015; Das et al., 2015; Donovan et al., 2016, 2013; Gray et al., 2015; Guédron et al., 2016; Lepak et al., 2015; Liu et al., 2011; Perrot et al., 2010; Rua-Ibarz et al., 2016; Sonke et al., 2010; Wiederhold et al., 2013; Yin et al., 2016). The average signature for industrially contaminated sediments amounted to a slightly more negative δ^{202}Hg value of -0.61 $\pm$ 0.37 ‰(1 SD, n=27). The MIF Δ^{199}Hg signature was -0.01 $\pm$ 0.12 ‰.

Industrial Hg^0 For liquid industrial Hg^0, 6 literature accounts of measurements were found and two laboratory stock chemicals were measured at the University of Vienna. An average δ^{202}Hg signature of -0.51 $\pm$ 0.3 ‰(1 SD, n=8) was found. MIF Δ^{199}Hg of the same dataset was 0.00 $\pm$ 0.03 ‰(Blum et al., 2014; Estrade et al., 2009; Gray et al., 2013a,b; Laffont et al., 2011; Mead et al., 2013; Sonke et al., 2008). For further discussion, this value of -0.51 $\pm$ 0.30 ‰ δ^{202}Hg and no MIF will be referred to as the the 'source signature'.

4.2.2 Comparing core mercury isotope data to the source signature

Assuming that the mercury source in Bad Krozingen also displayed a value of around -0.5 ‰ δ^{202}Hg and did not display any MIF prior to its application in the kyanization hall, it is now possible to compare the measured bulk sample values with this estimate. Depth profiles of the bulk isotope signatures in K2 are displayed in figures 3.10 and 3.11. It was mentioned already in the results section 3.4 that the most contaminated samples of the dataset, containing up to 800 $^{mg}/_{kg}$ mercury, exhibited also the lightest δ^{202}Hg signatures. These values fall well within the range of the possible source signature. Samples K2-6 to 9 and K2-11 display values between -0.42 ‰ (K2-8) and -0.29 ‰ (K2-11). Assuming that the light signatures are closer to the original sublimate's signature and are less fractionated relative to the heavier ones, then the most contaminated samples can be considered the 'least evolved' samples of

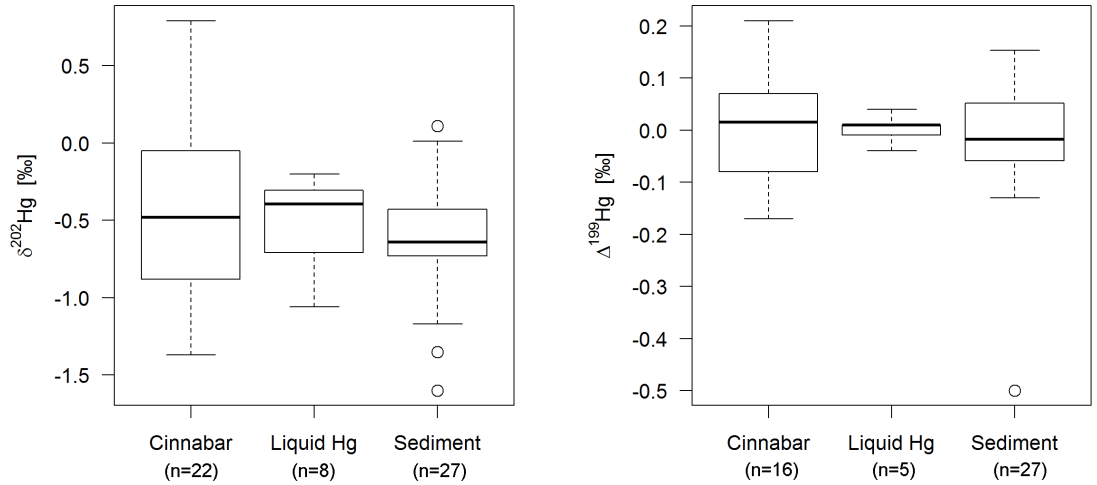

FIG. 4.3 Boxplots of the estimated source signature, as determined through a literature survey of reported values for cinnabar (HgS) ore, liquid Hg^0 and sediment contaminated with industrial mercury. The left panel shows δ^{202}Hg signatures, the right panel shows Δ^{199}Hg signatures. Ore data: Blum et al. (2014); Cooke et al. (2013); Feng et al. (2013); Foucher et al. (2009); Gehrke et al. (2011); Gray et al. (2013a); Hintelmann and Lu (2003); Jiménez-Moreno et al. (2016); Stetson et al. (2009); Yin et al. (2013); Hg^0 data: Blum et al. (2014); Estrade et al. (2009); Gray et al. (2013a,b); Laffont et al. (2011); Mead et al. (2013); Sonke et al. (2008); Sediment data: (Balogh et al., 2015; Bartov et al., 2013; Bonsignore et al., 2015; Das et al., 2015; Donovan et al., 2016, 2013; Gray et al., 2015; Guédron et al., 2016; Lepak et al., 2015; Liu et al., 2011; Perrot et al., 2010; Rua-Ibarz et al., 2016; Sonke et al., 2010; Wiederhold et al., 2015; Yin et al., 2016)

the dataset: They are likely to have experienced the least loss of mercury to the atmosphere and other sinks. Regarding Δ^{199}Hg, the differences between the samples are small, and most samples lie within the standard deviation of 0.00 $\pm$ 0.04 ‰ Δ^{199}Hg, although their mean was slightly lower, at -0.07 ‰, though, due to the outlier of -0.23 ‰ (K2-6). They were all within the standard deviation of or lighter than the assumed source signature.

Core K3 is located farther away from the contamination source and the mercury in it stems mostly from the movement of soil during the construction of residential areas after the kyanization plant was closed down. The levels of contamination are one order of magnitude lower in K3 than in K2. With the lightest sample of core K3 having a bulk δ^{202}Hg value of -0.12 ‰ (K3-5), none of them fall within the 1 SD range for industrial liquid Hg^0 of -0.51 $\pm$ 0.3 ‰. Light isotopes have been preferentially lost to other mercury pools. K3's Δ^{199}Hg signature displays a mean of -0.03 ‰ and thus lies within the standard deviation of the mean value of 0.00 ‰, albeit also on the slightly negative side.

4.2.3 Mercury isotope variations between the Optimized SEP fractions

Now that the bulk signatures of the samples have been discussed in section 4.2.2, the fractionation between the extracted fractions will be discussed in more detail. 4.1.2 elaborated the constraints that can be placed on the speciation of the Optimized SEP pools. Now, we look at their δ^{202}Hg ratios, that were introduced in figure 3.12. To see trends pertaining to the fractions, rather than to the bulk signature of the samples more clearly, the isotope values were normalized by subtracting the SEP pool signatures from the respective bulk signature in figures 4.4 and 4.5.

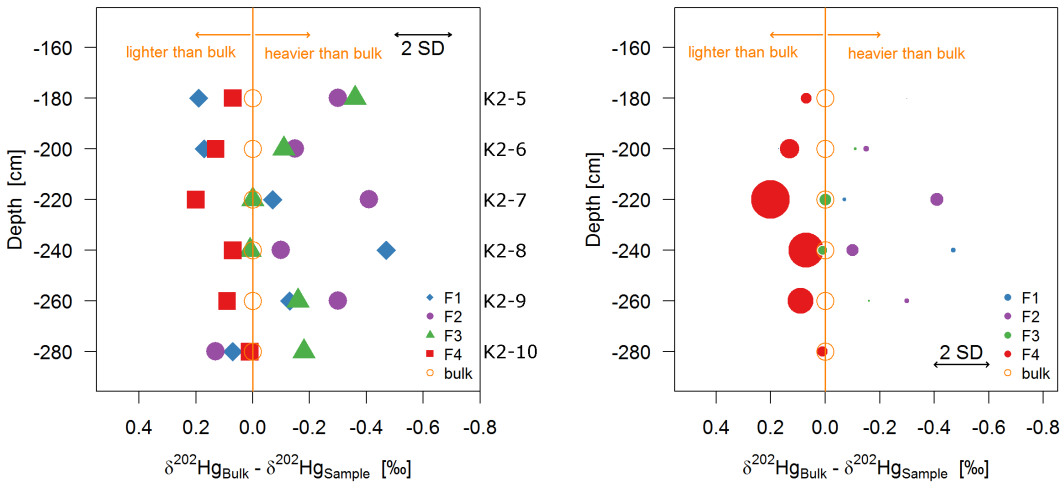

FIG. 4.4 In this figure, δ^{202}Hg results for K2 are plotted relative to the calculated bulk of the sample (vertical orange 0-line). By factoring out the variation in bulk signature, systematic enrichment of light isotopes is visible in 'F4' and enrichment of heavy isotopes is visible in 'F2' and 'F3'. In the right panel, the symbols are scaled to the amount of mercury in the pools, showing that smaller pools are more strongly fractionated from the bulk. Note that the plotted 2 SD refers to the measured data and does not take into account error propagation through the subtraction calculation.

F4 This most tightly bound fraction, indeed, consistently displayed δ^{202}Hg signatures that were lighter than the bulk sample. In the most contaminated samples (220-280cm, K2-7 to 9), it represents the overall lightest fraction, while in the less contaminated samples above and below the hotspot, the more mobile pools of F1 and F2 display even lighter signatures on the relative scale. Without normalization, as seen in figure 3.12, the F4 pools remain the overall lightest samples, reaching a minimum δ^{202}Hg signature of -0.57 $\pm$ 0.10‰ (K2-7, 230cm). The F4 pool signatures of all samples except the lowermost K2-10 sample fall within the range of industrial mercury of -0.51 $\pm$ 0.31‰.

It has been shown in laboratory experiments that Hg^{II} species sorbed to thiol-or goethite

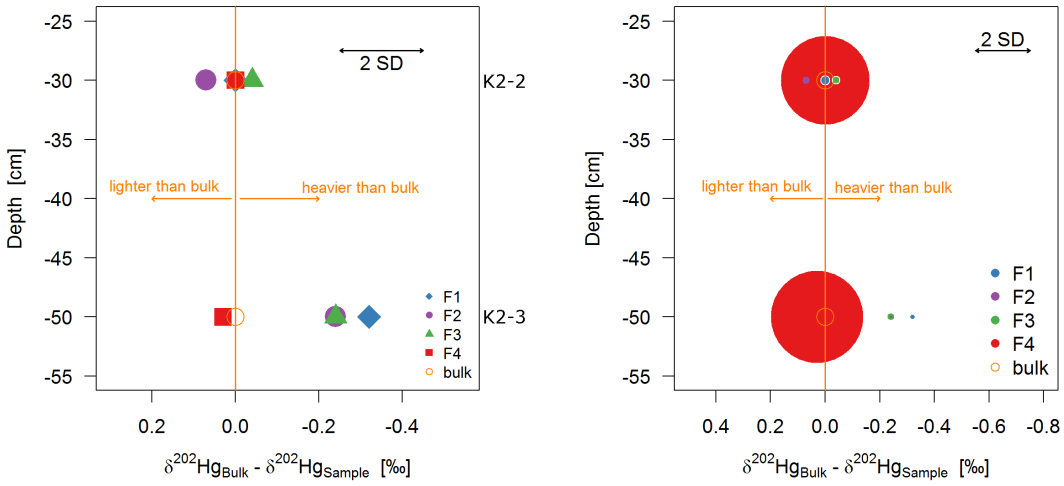

FIG. 4.5 δ^{202}Hg results for K3 are plotted relative to the calculated bulk of the sample (vertical orange 0-line). On the right panel, symbols are scaled to the amount of mercury extracted in the plotted pools. Note that the plotted 2 SD refers to the measured data and does not take into account error propagation through the subtraction calculation.

mineral surfaces are enriched in light isotopes (Jiskra et al., 2012; Wiederhold et al., 2010) in the case of equilibrium fractionation, fitting well with the fact that this pool is enriched in light isotopes relative to the others. This and other processes will be discussed in detail in section 4.3.

F3 This fraction was in all cases heavier or equal to the bulk signature. It was lightest ('closest to the bulk signature') in the most contaminated samples (K2-7 to 8, 220-260 cm), and heaviest ('farthest from the bulk signature') in the least contaminated samples. Bloom et al. (2003) stated that this pool should contain most of the samples' Hg^0, as discussed in 4.2. According to the PTD results (figure 3.6), elemental mercury should be present in significant amounts in samples K2-8 to 10 (240-300 cm). The δ^{202}Hg signatures of the Hg^0 containing samples contrasted with the K2-5 to 7, which contain mostly matrix-bound Hg^{II}. The presence of elemental mercury does not seem to influence the isotopic signature of F3.

F2 This fraction is isotopically heavier than the bulk signature of the samples in all samples but the lowermost K2-10 (280-300 cm). Likely comprising weakly sorbed, ligand-bound Hg^{II}, Hg^0 which diffused from the soil particles and oxidized to Hg^{II} and possibly Hg bound to carbonates, this fraction is relatively mobile. It may have been in solution longer than F4 and F3, which may have undergone reactions that preferentially removed heavy ^{202}Hg from the pool.

The very light signature relative to the bulk in the lowermost K2-10 sample (280-300 cm)looks curious in the normalized plot 4.4. To some extent, the extreme-looking signature is a consequence of plotting, though: looking at figure 3.12, which contains the actual values, it lies within the δ^{202}Hg range of all other F2-extracted mercury pools in core K2 with the relatively heavy value of -0.03 $\pm$ 0.10‰.

F1 This fraction is the most complex to interpret: it progresses from very light pools in the samples with lower contamination (K2-5 to 6, K2-10) to samples with extremely heavy signatures in the most contaminated samples (K2-7 to 9). As established in section 4.1.3, the F1 extracts are expected to contain dissolved $HgCl_2(aq)$, $Hg^{II}(aq)$ and Hg^{II} bound to various ligands such as chlorides, OH-groups and DOC. $Hg^0(aq)$ may also be present, but has a relatively low solubility. Assuming 0.15% (w/w) thiols on the amount of DOC measured, as suggested by Skyllberg (2011) (see table 3.3), it was calculated how much of the extracted mercury of each sample could be bound in $Hg(SR)_2$-DOC complexes. This calculation, whose results are presented in 4.1, revealed that samples where available DOC-thiol groups exceed the total mercury in F1, exhibit the heaviest δ^{202}Hg signatures. Samples with high amounts of water-extractable mercury, such as K2-6 to 9 (200-300cm) have more mercury than thiol-groups, even assuming their maximum saturation. The δ^{202}Hg signatures seem to correlate with the amount of mercury bound to thiol groups: in K2-8, where only 5.5% of the water-soluble mercury could be bound to thiol-DOC even considering full saturation of these groups, exhibited the heaviest F1 signature (0.12 $\pm$ 0.05 ‰) of the dataset. Samples K2-6 and K2-7, with maximum thiol-bound Hg of 42 and 26 % respectively, exhibit δ^{202}Hg signatures lying between. Wiederhold et al. (2010) found preferential enrichment of light isotopes in Hg^{2+} sorbed to thiol resin, indicating that when an excess of mercury is present in the soil, the light isotopes are preferentially bound to thiol-groups on DOC. A possible explanation for the difference in δ^{202}Hg signatures for samples that may contain only DOM-bound mercury and those containing an excess of mercury may be the following: The samples containing a great excess of mercury may represent those which contain the unspecifically, weakly bound, and 'evolved' pool of mercury - short, the substrate from which light isotopes are preferentially removed in order to form stronger bonds, i.e. with DOM. The F1 extracts containing less mercury only contain the more tightly bound DOM-associated mercury, which is strongly enriched in light isotopes in comparison to the 'excess' F1 extracts.The F1 pools with heavy signatures would ergo represent the most evolved pool of isotopes that is left after light isotopes have evaporated (Blum et al., 2014), sorbed to oxides, organic matter phases and bound by ligands.

TABLE 4.1 The table shows the calculation of the estimated maximum amount of thiol-DOC bound mercury for each sample, based on measured DOC concentrations (see section 3.2 and table 3.3 therein), an estimated thiol-content of 0.15% (w/w) and the assumption that all mercury will form $Hg(SR\text{-}DOM)_2$ complexes, as suggested by Skyllberg (2011). SR ... thiol group, DOM ... dissolved organic matter, DOC ... dissolved organic carbon.

Name	**Hg in F1 solution** [μg/L]	**DOC in F1 solution** [μg/L]	**SR groups 0.15% (w/w) DOC** [nmol/L]	**$Hg(SR\text{-}DOM)_2$** [nmol/L]	**Hg_{max} bound to SR** [μg/L]	**Hg_{max} bound to SR** [%]
H_2O_{MQ}	0.0	824.3	37.9	19.0	38.0	
K2-5a	15.1	1267.0	58.3	29.1	58.5	100.0
K2-6a	153.6	1391.0	64.0	32.0	64.2	41.8
K2-7a	406.2	2274.0	104.6	52.3	104.9	25.8
K2-8a	882.6	1052.0	48.4	24.2	48.5	5.5
K2-9a	122.4	1104.0	50.8	25.4	50.9	41.6
K2-10a	20.8	1044.0	48.0	24.0	48.2	100.0
K2-11a	5.4	956.2	44.0	22.0	44.1	100.0
K2-12a	11.4	1247.0	57.4	28.7	57.5	100.0
K3-2a	40.4	2974.0	136.8	68.4	137.2	100.0
K3-3a	21.4	2433.0	111.9	56.0	112.3	100.0
K3-4a	11.0	2196.0	101.0	50.5	101.3	100.0
K3-5a	10.5	2042.0	93.9	47.0	94.2	100.0

4.3 Tracing processes with mercury stable isotopes

4.3.1 Processes inducing mercury isotope fractionation

It has been well established during the past 15+ years that not only do mercury isotope ratios vary throughout Earth's mercury pools (see e.g the data collection in Blum et al. (2014)), but also that these variations are caused by fractionation during biogeochemical transformations. These transformations are studied in a growing body of literature – either witnessed in nature, or determined via controlled laboratory experiments (Bergquist and Blum, 2009). Fractionation experiments have mostly focused on the kinetically controlled reduction of Hg^{II} to Hg^0, which is known to take place biotically and abiotically, through a variety of pathways (Bergquist and Blum, 2009; Pannu, 2012). Studied biotic reactions include microbial reduction, methylation and demethylation of Hg^{II} (Kritee et al., 2008). Abiotic reactions studied include photoreduction of Hg^{II} and photodegradation of MeHg (Blum and Bergquist, 2007; Zheng and Hintelmann, 2009), as well as non-photochemical reduction (Zheng and Hintelmann, 2010), volatilization (Zheng et al., 2007), and evaporation (Estrade et al., 2009) of metallic Hg^0. Equlibrium fractionation factors have been experimentally determined for equilibrium between metallic Hg^0 and Hg^0 vapor (Estrade et al., 2009) and for complexation of Hg^{II} with thiol resin (Wiederhold et al., 2010). While laboratory conditions and the studied processes differ widely, it can be generalized that for kinetically controlled reduction, the δ^{202}Hg of the produced Hg^0 is generally lighter than the original Hg^{II}. Biotic reduction and (de)methylation have been shown to induce only MDF (Kritee et al., 2008; Rodríguez-González et al., 2009). On the other hand, abiotic photochemical processes have been shown to induce significant MIF, both depleting and enriching the product Hg^0 in odd-mass isotopes relative to the even-mass isotopes. A small MIF effect has also been shown for non-photochemical reduction of Hg^{II} (Zheng and Hintelmann, 2010). As for equilibrium fractionation studies, studies of Hg^0 volatilization, Hg^{II} complexation have found an enrichment of heavy δ^{202}Hg in the substrate with the product enriched in light mercury isotopes (Estrade et al., 2009; Wiederhold et al., 2010). Photooxidation is the only process presently known to induce Δ^{200}Hg anomalies ('even-mass MIF') (Chen et al., 2012), but there has not been experimental proof of the mechanism at the time of writing.

4.3.2 Mercury reduction pathways in soil

Hg^{II} reduction in soils has been extensively discussed in the past years. While multiple pathways, such as the ones investigated above for isotope fractionation, are known, their relative contributions to the total mercury emissions from soils are not well constrained.

Physico-chemical soil parameters (texture, pH, organic carbon, substrate Hg concentration) as well as climate parameters (solar irradiation, soil moisture, soil temperature) are thought or have been shown to exert an influence on the Hg^0 fluxes from soils to the atmosphere. According to Pannu (2012), there are few well-constrained flux studies available which study these processes specifically. While mercury bound to organic substances is bound tightly as Hg^{II} unless the organic matter decomposes, weakly bound Hg^{II}, that is adsorbed to negatively charged soil particles is easily removed by cation exchange, and may be reduced via the biotic or abiotic processes discussed above. Abiotic processes include photoreduction with sunlight or redox reactions involving humic and fulvic acid Allard and Arsenie (1991). Higher levels of soil moisture due to precipitation or pesticide application have been shown to increase reduction of Hg^{II}, although the mechanistic reason for this is still debated (Lindberg et al., 1999; Pannu, 2012). Soil temperature and radiation have a well documented positive influence on the Hg flux from soil to its environment (Choi and Holsen, 2009; Scholtz et al., 2003, f.ex.). The role of organic matter for mercury reduction is as varied as the structure of its molecules; different types of complexing can keep mercury bound to the soil in its divalent form and expecially thiol functional groups are known for their extraordinarily high affinity for complexing mercury, and thus preventing redox reactions or methylation processes (Skyllberg, 2011). Dissolved organic matter also controls photochemical reduction, which may result in significant positive or negative MIF based on the ligands Hg^{II} is bound to (Garcia et al., 2005), and also plays a significant role in dark abiotic mercury reduction, which induces significant MDF and small MIF Jiskra et al. (2015); Zheng and Hintelmann (2010). Microorganisms may reduce Hg^{II} directly or indirectly (Pannu, 2012), but they have been shown to contribute significantly to the total mercury flux in experiments comparing sterilized soils to untreated ones (Pannu, 2012; Schlüter, 2000).

4.3.3 Tracing processes in Bad Krozingen soil

The soil in BK has not been characterized in terms of the quality of its organic matter, nor does the author of this study have information on the microbial activity, and soil temperature of the site. The ongoing reduction of Hg^0, however, is manifested through high amounts of metallic mercury detected in the most contaminated samples of core K2, as well as the mercury vapor measurements conducted by Schöndorf et al. (1995). As discussed in the preceding sections, it is not possible to constrain the elemental Hg^0 present in the soil samples to one of the Optimized SEP fractions. Hence, the Hg^0-containing samples are discussed separately from the rest.

Notably, they display significantly lighter δ^{202}Hg signatures than samples in K2 which did not display the PTD peaks associated with Hg^0. This fits well with the observed fractionation

induced by mercury reduction: The reduced Hg^0 pool, whether it is dissolved in the soil solution or in gaseous state, is relatively lighter than the oxidized Hg^{II} pool. From this angle, samples containing no Hg^0 can be viewed as samples where reduction has also taken place - hence the 'heavy' δ^{202}Hg signature - but the product of the reaction, Hg^0, has left the sample by some process of mass transfer, such as evaporation, degassing or leaching to other layers. Evaporation in particular is known to further fractionate the Hg^0 pool by preferentially removing lighter isotopes to the gaseous phase, which would further the effect of enriching heavy isotopes.

K3, which does not contain any evidence of Hg^0 according to PTD analyses, is significantly heavier in its δ^{202}Hg values. This fits with the concept of a more evolved pool of mercury; according to the bulk signatures having shifted to heavy values, reduction of Hg^{II} species to Hg^0 has already taken place, and the product was lost to the atmosphere or other soil layers.

Considering the reduction processes listed above, and considering their common characteristic of preferably reducing light isotopes in a MDF manner, only one process can be excluded to have happened: photoreduction. Photoreduction is known to induce significant odd-mass MIF. The direction of MIF is dependent on the ligands that mercury is bound to in the soil organic matter. In natural waters, the enrichment of odd-mass isotopes in the aqueous phase has been observed while even-mass isotopes were preferentially reduced (Blum and Bergquist, 2007). The Δ^{199}Hg anomalies in all studied samples were so slight that it couldn't explain the reduction of > 50% of a sample's total mercury as was observed in K2-8 and K2-10 (see 3.6). Dark abiotic reduction, on the other hand, has been reported to induce a maximum Δ^{199}Hg MIF fractionation of -0.3 ‰ in samples where 70 % of the substrate Hg^{II} had reacted (Zheng and Hintelmann, 2010).

Having discussed the bulk sample signatures, which display variations between different samples, we can now turn to the variations within the samples and look at isotopic variations between the Optimized SEP pools. As established in multiple chapters before (section 3.4, section 4.2.2), there are trends in both δ^{202}Hg and Δ^{199}Hg between the extracted pools. Most generally, F3 and F4, the refractory pools, display lighter δ^{202}Hg signatures than F1 and F2, the more mobile pools. When looking at isotopic differences within single samples, transformations which do not cause mass transfer out of the sample, such as sorption and complexation by particulate organic matter, can be considered. Wiederhold et al. (2010) have studied equilibrium fractionation between Hg^{II} species and thiols and Jiskra et al. (2012) investigated sorption of Hg^{II} to goethite. In both cases, it was observed that the substrate was enriched according to MDF in heavy isotopes with fractionation in the range of -0.4 – -0.6 ‰ δ^{202}Hg, while the complexed/sorbed species was comparably lighter. Indeed, the

refractory pools reflect these findings and display significantly lighter δ^{202}Hg signatures than the mobile pools. This is not to say that most mercury is bound by sorption to goethite in this soil. Not all sorption mechanisms have been experimentally studied for mercury isotope fractionation and it is not known which the prevailing sorption mechanisms in this study are. But seeing the experimentally studied trends reflected in this set of field data gives one confidence in the overall variation of isotopes. Especially F1 displays striking differences in fractionation between samples where binding to DOC may explain the total mercury amount in this fraction, and betwee samples where such a surplus of mercury was extracted in F1 that thiol groups on DOC do not suffice as binding partners. This suggests that mercury bond to thiols is isotopically light, but the surplus mercury, which did not bind to the preferred sites,a dn is still mobile ad extracted in F1, is heavy. This makes sense considering that all mechanisms discussed in this work remove light isotopes from the aqueous Hg^{II} pool.

Precipitation of Hg^{II} as HgS is another possible process taking place in the soil. Smith et al. (2015) have studied the mercury isotope fractionation during precipitation of $\beta - HgS$ from different Hg^{II}-containing solutions and found that the precipitate is enriched in light isotopes relative to the supernatant in equilibrium. MDF with an enrichment factor of -0.63 ‰ in ^{202}Hg occurred. The only sample with significant HgS content according to PTD was K3-3 (see 3.7). *HgS* is only extracted in the aqua regia step, F4. The Optimized SEP yielded >90 % of total mercury in this pool, it thus did not prove to be very selective for sample K3-3. Still, comparing the δ^{202}Hg values of the sample with that of the sample K3-2, which did not display a significant HgS peak during PTD, striking differences are visible in the fractionation between the extracted pools. In K3-3, F4 represents the lightest pool, which is in accordance with the assumption that it includes HgS that is light compared to the solution it precipitated from. K3-2, not containing HgS, is actually the only of all sequentially extracted samples in which F4 is the heaviest of all fractions.

Looking at variation in the MIF signatures (especially figure 3.11, left panel), it is striking that the F2 pool consistently displays the highest negative Δ^{199}Hg anomalies which are consistent, again, in their magnitude with the fractionation observed during abiotic dark reduction. The MIF observed in complexation by thiols is caused by nuclear field shift (NFS), which is characterized by a Δ^{199}Hg/Δ^{201}Hg slope of 1.6. Figure 4.6 shows that especially the F2 pool samples plot along this line. These are strong indicators that mercury in F2, the weakly sorbed mercury, is most active in the reduction process. It has to be kept in mind, however, that the standard errors attached to the Δ^{199}Hg measurements are quite large for such detailed analysis. The differences seem to be consistent, but in most cases, the standard deviations of the measured values between F2 and F3 overlap.

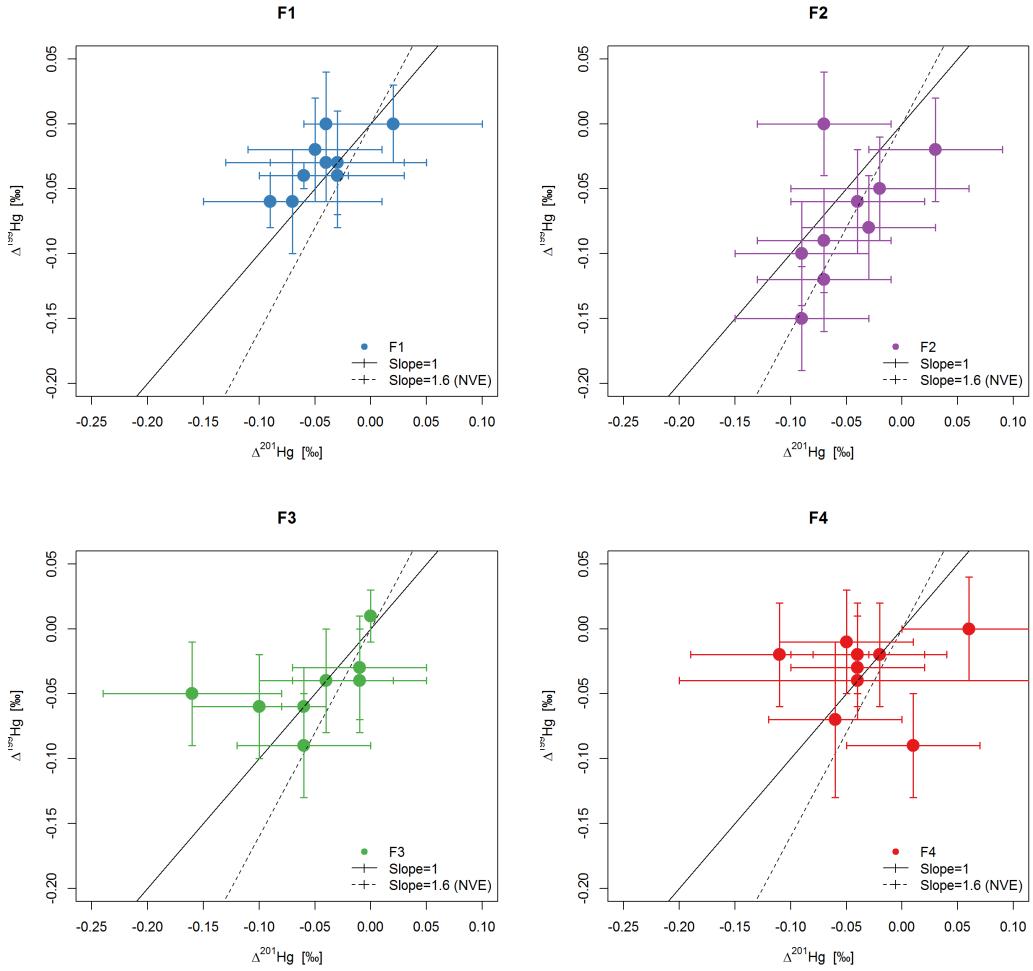

FIG. 4.6 Scatterplot of $\Delta^{199}Hg$ vs $\Delta^{201}Hg$; The extracted fractions of all samples are plotted in separate panels. Error bars represent 2 SD based on reproducibility of the secondary standard of the measuring session.

Lastly, but very interestingly, the mercury isotope fractionation observed in the sequential F1 extracts is worth discussing. As established in section 3.2, the concentrations of the sequential extracts consistently decrease from the first to the last extraction step, even though extract F1D had a significantly longer equilibration time (338 hours after centrifugation) than the standard 18 $\pm$ 4 hours. Looking at the samples' δ^{202}Hg signatures, all of them are enriched in heavy isotopes compared to the bulk sampe. With progressing extraction, δ^{202}Hg of the samples moves towards lighter values, but even the 7th extract is still >0.2 ‰ heavier than the bulk sample. However, F1D is the heaviest sample of the whole dataset, displaying a value of +0.58 $\pm$ 0.09 ‰, well above the +0.18 $\pm$ 0.09 ‰ of the F1A. This may be due to the loss of isotopically heavy Hg^0 to the atmosphere via evaporation and degassing from the vial.

Chapter 5

Conclusion

The aim of this thesis was to understand mercury transformations in soil, and trace them via mercury stable isotope analysis. Two soil cores from the $HgCl_2$-contaminated field site in Bad Krozingen, Germany were collected: One from the source of the contamination, where the impregnated poles were stacked for drying and $HgCl_2$ dripped onto the ground; the second from the border of the facility, where the contamination is only secondary, from the movement of soil during construction of the housing blocks. Both cores were analyzed for their total mercury content and mercury speciation according to PTD. The highest-contaminated samples were sequentially extracted, and mercury stable isotopes were measured on the extracts. To conclude this thesis and contextualize the data which was produced in the process, let us revisit the questions defined in the thesis objectives (section 1.8).

Question 1: *Is sequential extraction a suitable - and sufficiently specific - tool to divide the soil mercury pool into portions for mercury stable isotope analysis?*

The combination of PTD and the Optimized SEP revealed differences in mercury speciation between the two cores and also variations at different depths. According to PTD, only the most contaminated samples in K2 contained Hg^0, and only the most contaminated samples in K3 contained evidence for HgS. The majority of mercury in both cores was matrix-bound Hg^{II}. The Optimized SEP divided the total mercury in the samples into different pools. As discussed extensively in section 4.1.2, it is oftentimes difficult to assign mercury compounds to these extracted pools and only an operational definition of their mercury content can be given. However, PTD and SEP provided useful information on the mobility of mercury present in the soil. Also, the presence of certain species could be excluded. While this information is not sufficient to identify the exact chemical species of mercury, it is sufficient to reveal the presence of elemental Hg^0 and mercury sulfides, and also contains information

on the bioavailablility and mobility of the soil mercury. With this information, the Optimized SEP pools could be interpreted in terms of how strongly bound the contained mercury was, and stable isotope results could be interpreted on this basis.

Question 2: *Do the stable isotopes of mercury vary significantly over the soil cores of the studied site, the different depths, and also the extracted fractions?*

The answer to question 2 is clearly: Yes! Especially δ^{202}Hg values did vary significantly - both between cores and bulk samples, and between the sequentially extracted pools of the same sample. Comparing the stable isotope values to the estimated source signature, the two cores K2 and K3 could clearly be distinguished as closer to the assumed source signature (K2) and more evolved (K3). In some sequentially extracted samples, the δ^{202}Hg values differed by more than -0.6 ‰(2 SD = 0.09 ‰) between the extracted pools. This is remarkable considering that only one source of mercury, the $HgCl_2$ from kyanization, is known - even though it has to be stated that its original isotopic signature could only be assumed based on literature values. This piece of information is also relevant information for potential source tracing studies, where mixing between two isotopically different sources of contamination in the environment is studied, and any observed signatures in a field sites are interpreted as mixtures of those original source signatures. An approach like this would not hold true for this field site, and likely would not for other contaminated sites. The fractionation of the isotopic signatures of mercury in any similar field site would have to be taken into account. In the more than 60 years since the closing of the kyanization plant, the mercury chloride signature has fractionated to an extent that simple source tracing would not be a valid approach.

Question 3: *Can observed variation in mercury stable isotopes be attributed to biogeochemical processes which have been reported in literature?*

Even though it was not possible in most cases to determine the exact chemical speciation of the mercury in the soil, other than determining whether elemental Hg^0 was present or not, and how tightly the mercury was bound to the soil matrix, general trends in stable isotope fractionation could still be observed. As most processes which remove mercury from the aqueous phase by sorption, precipitation, or reduction and degassing preferentially remove light isotopes, extracted pools with heavy δ^{202}Hg signatures were interpreted as 'more evolved' and as pools which acted as substrate. Pools with light isotopic signatures compared to the bulk signatures were interpreted as pools which either contain strongly bound mercury, where the majority of mercury stemmed from a transformation reaction - even if this reaction could not exactly be identified. The residual F4 fraction was isotopically

light and these findings were consistent with literature suggesting that both sorption to oxides, complexation by soil-thiols and precipitation of HgS preferentially incorporates light isotopes into the solid phase. Fraction F2 being consistently isotopically heavy, it was proposed that this is the fraction which is the basis for further transformation reactions: this ligand-bound and unspecifically adsorbed mercury is reduced, precipitated or more tightly complexed through various reactions occurring in the environment, which differentiated this pool to its current isotopic signature. Isotope analysis could also show that the composition of F1 is distinctly different in the 'hotspot' most contaminated samples and the moderately contaminated samples. While the moderately contaminated samples showed light isotopic signatures that were in line with the assumed signature of mercury bound to thiols of DOC, signatures of samples where the amount of mercury exceeded the supply of DOC-thiols displayed heavy signatures. The author hypothesizes that these heavy signatures stem from $HgCl_2$ in solution, which evolved as various reduction -, sorption- and complexation reactions removed lighter isotopes from it. This pool, which seemed to be poorly or not bound at all to the soil particles, was thought to progress through the soil profile to greater depths, where it will evolve further, to even heavier signatures, until the last mobile fraction enters the groundwater. This assumption is consistent with groundwater data from Bad Krozingen measured by Jan Wiederhold that show significantly heavy signatures.
It was not possible to quantify specific processes, since most transformations remove light isotopes according to mass-dependent fractionation from the original mercury pool and store it in other pools. It would be interesting to calculate the original source signature by estimating the loss to the atmosphere and back-calculating based on the experimentally determined fractionation factor of evaporation. Even without doing that, it can be said that the estimated source signature seems realistic in the light of the measured data. It is likely lighter than the lightest sample, so likely lower than -0.43 ‰.

Outlook

This thesis has demonstrated so far that there is enormous potential to use mercury isotopes as tracers for mercury transformations in soil. To move towards the identification of exact pathways and their quantification, more work has to be done. Firstly, the missing signature of the original contamination source poses a problem, since the confidence intervals of any estimate for this signature are naturally very large, making any attempt of quantification less precise. This could be done at a different field site. Secondly, it could be discussed how the exact transformation processes could be identified by a different technique than stable isotopes, to ensure better quality control on the transformations. To study the phases present in the soil and thus achieve even better constraints on its mercury speciation, more precise,

but infrastructure-intensive spectroscopic methods such as X-ray Adsorption Fine Structure (XAFS) or X-ray Adsorption Near Edge Structure (XANES) Spectroscopy could be applied. To better understand the exact pathways that facilitate mercury phase transformations, laboratory experiments using contaminated soil from Bad Krozingen could be conducted; for example, incubation of the soil at different conditions, to study Hg reduction, and the mercury isotope fractionation it induces. This would help to further constrain and quantify the relative contributions of different reactions to the overall stable isotope signature. Ideally, the sum of these data would lead to a model which could then be applied to study mercury isotope fractionation in similar contaminated systems.

References

Allard, B. and Arsenie, I. (1991). Abiotic reduction of mercury by humic substances in aquatic system — an important process for the mercury cycle. *Water Air & Soil Pollution*, 56(1):457–464.

AMAP/UNEP (2013). Technical background report for the Global Mercury Assessment 2013. Technical report, Arctic Monitoring and Assessment Programme, Oslo, Norway / UNEP Chemicals Branch, Geneva, Switzerland.

Bacon, J. R. and Davidson, C. M. (2008). Is there a future for sequential chemical extraction? *The Analyst*, 133(1):25–46.

Balogh, S. J., Tsui, M. T. K., Blum, J. D., Matsuyama, A., Woerndle, G. E., Yano, S., and Tada, A. (2015). Tracking the fate of mercury in the fish and bottom sediments of Minamata Bay, Japan, using stable mercury isotopes. *Environmental Science & Technology*, 49(9):5399–5406.

Barringer, J. L., Szabo, Z., and Reilly, P. A. (2013). Occurrence and mobility of mercury in groundwater. In *Current Perspectives in Contaminant Hydrology and Water Resources Sustainability*, 118–138. InTech.

Bartov, G., Deonarine, A., Johnson, T. M., Ruhl, L., Vengosh, A., and Hsu-Kim, H. (2013). Environmental impacts of the Tennessee Valley Authority Kingston coal ash spill. 1. Source apportionment using mercury stable isotopes. *Environmental Science & Technology*, 47(4):2092–2099. PMID: 23157719.

Bavec, Š. and Gosar, M. (2016). Speciation, mobility and bioaccessibility of Hg in the polluted urban soil of Idrija (Slovenia). *Geoderma*, 273:115 – 130.

Begu, E., Shlyapnikov, Y., Stergarsek, A., Frkal, P., Kotnik, J., and Horvat, M. (2016). A method for semi-continuous measurement of dissolved elemental mercury in industrial and natural waters. *International Journal of Environmental Analytical Chemistry*, 96(7):609–626.

Bergquist, B. A. and Blum, J. D. (2009). The odds and evens of mercury isotopes: Applications of mass-dependent and mass-independent isotope fractionation. *Elements*, 5(6):353–357.

Biester, H. and Scholz, C. (1997). Determination of mercury binding forms in contaminated soils: mercury pyrolysis versus sequential extractions. *Environmental Science & Technology*, 31(1):233–239.

Bloom, N. S., Preus, E., Katon, J., and Hiltner, M. (2003). Selective extractions to assess the biogeochemically relevant fractionation of inorganic mercury in sediments and soils. *Analytica Chimica Acta*, 479(2):233–248.

Blum, J. D. and Bergquist, B. A. (2007). Reporting of variations in the natural isotopic composition of mercury. *Analytical and Bioanalytical Chemistry*, 388(2):353–359.

Blum, J. D., Sherman, L. S., and Johnson, M. W. (2014). Mercury isotopes in earth and environmental sciences. *Annual Review of Earth and Planetary Sciences*, 42:249–269.

Bollen, A., Wenke, A., and Biester, H. (2008). Mercury speciation analyses in $HgCl_2$-contaminated soils and groundwater–implications for risk assessment and remediation strategies. *Water research*, 42(1-2):91–100.

Bonsignore, M., Tamburrino, S., Oliveri, E., Marchetti, A., Durante, C., Berni, A., Quinci, E., and Sprovieri, M. (2015). Tracing mercury pathways in Augusta Bay (southern Italy) by total concentration and isotope determination. *Environmental Pollution*, 205:178 – 185.

Boucher, O., Jacobson, S. W., Plusquellec, P., Dewailly, É., Ayotte, P., Forget-Dubois, N., Jacobson, J. L., and Muckle, G. (2012). Prenatal methylmercury, postnatal lead exposure, and evidence of attention deficit/hyperactivity disorder among Inuit children in Arctic Québec. *Environmental Health Perspectives*, 120(10).

Brookins, D. G. (1988). *Mercury*, 58–59. Berlin, Heidelberg: Springer Berlin Heidelberg.

Chen, J., Hintelmann, H., Feng, X., and Dimock, B. (2012). Unusual fractionation of both odd and even mercury isotopes in precipitation from Peterborough, ON, Canada. *Geochimica et Cosmochimica Acta*, 90:33 – 46.

Choi, H.-D. and Holsen, T. M. (2009). Gaseous mercury emissions from unsterilized and sterilized soils: The effect of temperature and UV radiation. *Environmental Pollution*, 157(5):1673 – 1678. Special Issue Section: Ozone and Mediterranean Ecology: Plants, People, Problems.

Clever, H. L., Johnson, S. A., and Derrick, M. E. (1985). The solubility of mercury and some sparingly soluble mercury salts in water and aqueous electrolyte solutions. *Journal of Physical and Chemical Reference Data*, 14(3):631–680.

Cooke, C. A., Hintelmann, H., Ague, J. J., Burger, R., Biester, H., Sachs, J. P., and Engstrom, D. R. (2013). Use and legacy of mercury in the Andes. *Environmental Science & Technology*, 47(9):4181–4188. PMID: 23597056.

Coufalík, P. and Komárek, J. (2014). The use of thermal desorption in the speciation analysis of mercury in soil, sediments and tailings. *Journal of Analytical Chemistry*, 69(12):1123–1129.

Das, R., Landing, W., Bizimis, M., Odom, L., and Caffrey, J. (2015). Mass independent fractionation of mercury isotopes as source tracers in sediments. *Procedia Earth and Planetary Science*, 13:151 – 157.

Donovan, P. M., Blum, J. D., Singer, M. B., Marvin-DiPasquale, M., and Tsui, M. T. (2016). Methylmercury degradation and exposure pathways in streams and wetlands impacted by historical mining. *Science of The Total Environment*, 568:1192 – 1203.

Donovan, P. M., Blum, J. D., Yee, D., Gehrke, G. E., and Singer, M. B. (2013). An isotopic record of mercury in San Francisco Bay sediment. *Chemical Geology*, 349–350:87 – 98.

Drott, A., Björn, E., Bouchet, S., and Skyllberg, U. (2013). Refining Thermodynamic Constants for Mercury(II)-Sulfides in Equilibrium with Metacinnabar at Sub-Micromolar Aqueous Sulfide Concentrations. *Environmental Science & Technology*, 47(9):4197–4203. PMID: 23470118.

Estrade, N., Carignan, J., Sonke, J. E., and Donard, O. F. (2009). Mercury isotope fractionation during liquid–vapor evaporation experiments. *Geochimica et Cosmochimica Acta*, 73(10):2693 – 2711.

Feng, X., Yin, R., Yu, B., and Du, B. (2013). Mercury isotope variations in surface soils in different contaminated areas in Guizhou Province, China. *Chinese Science Bulletin*, 58(2):249–255.

Fernández-Martínez, R. and Rucandio, I. (2013). Assessment of a sequential extraction method to evaluate mercury mobility and geochemistry in solid environmental samples. *Ecotoxicology and Environmental Safety*, 97:196–203.

Fitzgerald, W. and Lamborg, C. (2014). *Geochemistry of mercury in the environment*, 11 edition. Elsevier Ltd.

Foucher, D. and Hintelmann, H. (2006). High-precision measurement of mercury isotope ratios in sediments using cold-vapor generation multi-collector inductively coupled plasma mass spectrometry. *Analytical and Bioanalytical Chemistry*, 384(7):1470–1478.

Foucher, D., Ogrinc, and Hintelmann, H. (2009). Tracing mercury contamination from the Idrija mining region (Slovenia) to the Gulf of Trieste using Hg isotope ratio measurements. *Environmental Science & Technology*, 43(1):33–39. PMID: 19209581.

Fry, B. (2006). Mixing. In *Stable Isotope Ecology*, 119–182. Springer New York.

Garcia, E., Amyot, M., and Ariya, P. A. (2005). Relationship between DOC photochemistry and mercury redox transformations in temperate lakes and wetlands. *Geochimica et Cosmochimica Acta*, 69(8):1917 – 1924.

Gehrke, G. E., Blum, J. D., and Marvin-DiPasquale, M. (2011). Sources of mercury to San Francisco Bay surface sediment as revealed by mercury stable isotopes. *Geochimica et Cosmochimica Acta*, 75(3):691 – 705.

Gray, J. E., Metre, P. C. V., Pribil, M. J., and Horowitz, A. J. (2015). Tracing historical trends of Hg in the Mississippi River using Hg concentrations and Hg isotopic compositions in a lake sediment core, Lake Whittington, Mississippi, USA. *Chemical Geology*, 395:80 – 87.

Gray, J. E., Pribil, M. J., and Higueras, P. L. (2013a). Mercury isotope fractionation during ore retorting in the Almadén mining district, Spain. *Chemical Geology*, 357:150 – 157.

Gray, J. E., Pribil, M. J., Metre, P. C. V., Borrok, D. M., and Thapalia, A. (2013b). Identification of contamination in a lake sediment core using Hg and Pb isotopic compositions, Lake Ballinger, Washington, USA. *Applied Geochemistry*, 29:1 – 12.

Guédron, S., Amouroux, D., Sabatier, P., Desplanque, C., Develle, A.-L., Barre, J., Feng, C., Guiter, F., Arnaud, F., Reyss, J. L., and Charlet, L. (2016). A hundred year record of industrial and urban development in French Alps combining Hg accumulation rates and isotope composition in sediment archives from Lake Luitel. *Chemical Geology*, 431:10 – 19.

Hall, G. E. M., Pelchat, P., and Percival, J. B. (2005). The design and application of sequential extractions for mercury, Part 1. Optimization of HNO_3 extraction for all non-sulphide forms of Hg. *Geochemistry: Exploration, Environment, Analysis*, 5:107–113.

Hintelmann, H. (2010). 11 Organomercurials. Their Formation and Pathways in the Environment. In *Organometallics in Environment and Toxicology: Metal Ions in Life Sciences*, volume 7, 365–401. The Royal Society of Chemistry.

Hintelmann, H. and Lu, S. (2003). High precision isotope ratio measurements of mercury isotopes in cinnabar ores using multi-collector inductively coupled plasma mass spectrometry. *Analyst*, 128:635–639.

Hintelmann, H. and Zheng, W. (2011). *Tracking geochemical transformations and transport of mercury through isotope fractionation*, 293–327. John Wiley & Sons, Inc.

Hocsman, A., Nezio, S. D., Charlet, L., and Avena, M. (2006). On the mechanisms of dissolution of montroydite [HgO(s)]: Dependence of the dissolution rate on pH, temperature, and stirring rate. *Journal of Colloid and Interface Science*, 297(2):696 – 704.

Huber, M. L., Laesecke, A., and Friend, D. G. (2006). The vapor pressure of mercury. Technical report, National Institute of Standards and Technology.

Irrgeher, J. and Prohaska, T. (2015). Application of non-traditional stable isotopes in analytical ecogeochemistry assessed by MC ICP-MS - A critical review. *Analytical and Bioanalytical Chemistry*.

Jiménez-Moreno, M., Barre, J. P., Perrot, V., Bérail, S., Martín-Doimeadios, R. C. R., and Amouroux, D. (2016). Sources and fate of mercury pollution in Almadén mining district (Spain): Evidences from mercury isotopic compositions in sediments and lichens. *Chemosphere*, 147:430 – 438.

Jiskra, M., Wiederhold, J. G., Bourdon, B., and Kretzschmar, R. (2012). Solution speciation controls mercury isotope fractionation of Hg(II) sorption to goethite. *Environmental Science and Technology*, 46(12):6654–6662.

Jiskra, M., Wiederhold, J. G., Skyllberg, U., Kronberg, R.-M., Hajdas, I., and Kretzschmar, R. (2015). Mercury deposition and re-emission pathways in boreal forest soils investigated with Hg isotope signatures. *Environmental Science & Technology*, 49(12):7188–7196. PMID: 25946594.

Kim, C. S., Bloom, N. S., Rytuba, J. J., and Brown, G. E. (2003). Mercury speciation by X-ray absorption fine structure spectroscopy and sequential chemical extractions: A comparison of speciation methods. *Environmental Science & Technology*, 37(22):5102–5108. PMID: 14655695.

Kirby, A., Rucevska, I., Yemelin, V., Cooke, C., Simonett, O., Novikov, V., and Hughes, G. (2013). Mercury, Time To Act. UNEP Government Report, Geneva, Switzerland.

Kritee, K., Blum, J. D., and Barkay, T. (2008). Mercury stable isotope fractionation during reduction of Hg(II) by different microbial pathways. *Environmental Science & Technology*, 42(24):9171–9177.

Laffont, L., Sonke, J. E., Maurice, L., Monrroy, S. L., Chincheros, J., Amouroux, D., and Behra, P. (2011). Hg speciation and stable isotope signatures in human hair as a tracer for dietary and occupational exposure to mercury. *Environmental Science & Technology*, 45(23):9910–9916. PMID: 22003970.

Leermakers, M., Baeyens, W., Quevauviller, P., and Horvat, M. (2005). Mercury in environmental samples: Speciation, artifacts and validation. *Trends in Analytical Chemistry*, 24(5):383–393.

Leermakers, M., Lansens, P., and Baeyens, W. (1990). Storage and stability of inorganic and methylmercury solutions. *Fresenius' Journal of Analytical Chemistry*, 336(8):655–662.

Lenguin-Hoppe, R. (2000). Altlasten in der Parksiedlung in Bad Krozingen. Website. http://www.roudel.org/CDROM/DEUTSCH/THEMEN/BADKROZ/BADKROZ1.HTM. Accessed: 2017-03-15.

Leopold, K., Foulkes, M., and Worsfold, P. (2010). Methods for the determination and speciation of mercury in natural waters—A review. *Analytica Chimica Acta*, 663(2):127–138.

Lepak, R. F., Yin, R., Krabbenhoft, D. P., Ogorek, J. M., DeWild, J. F., Holsen, T. M., and Hurley, J. P. (2015). Use of stable isotope signatures to determine mercury sources in the Great Lakes. *Environmental Science & Technology Letters*, 2(12):335–341.

Leybourne, M. I., Bloom, L., and Coughlin, B. (2016). Hg in rocks , soils and sediments : Speciation and implications for sample processing and analysis. *EXPLORE Newsletter for the Association of Applied Geochemists*, (171):1–17.

Lindberg, S. E., Zhang, H., Gustin, M., Vette, A., Marsik, F., Owens, J., Casimir, A., Ebinghaus, R., Edwards, G., Fitzgerald, C., Kemp, J., Kock, H. H., London, J., Majewski, M., Poissant, L., Pilote, M., Rasmussen, P., Schaedlich, F., Schneeberger, D., Sommar, J., Turner, R., Wallschläger, D., and Xiao, Z. (1999). Increases in mercury emissions from desert soils in response to rainfall and irrigation. *Journal of Geophysical Research: Atmospheres*, 104(D17):21879–21888.

Liu, J., Feng, X., Yin, R., Zhu, W., and Li, Z. (2011). Mercury distributions and mercury isotope signatures in sediments of Dongjiang, the Pearl River Delta, China. *Chemical Geology*, 287(1–2):81 – 89.

Mead, C., Lyons, J. R., Johnson, T. M., and Anbar, A. D. (2013). Unique Hg stable isotope signatures of compact fluorescent lamp-sourced Hg. *Environmental Science & Technology*, 47(6):2542–2547. PMID: 23373764.

Mikac, N., Foucher, D., Niessen, S., Lojen, S., and Fischer, J.-C. (2003). Influence of chloride and sediment matrix on the extractability of HgS (cinnabar and metacinnabar) by nitric acid. *Analytical and Bioanalytical Chemistry*, 377(7-8):1196–1201.

Mishra, B., O'Loughlin, E. J., Boyanov, M. I., and Kemner, K. M. (2011). Binding of Hg(II) to high-affinity sites on bacteria inhibits reduction to Hg(0) by mixed Fe(II)/(III) phases. *Environmental Science & Technology*, 45(22):9597–9603. PMID: 21913727.

Navrátil, T., Shanley, J., Rohovec, J., Hojdová, M., Penížek, V., and Buchtová, J. (2014). Distribution and pools of mercury in Czech forest soils. *Water, Air, & Soil Pollution*, 225(3):1829.

Nichols, J. W., Ambrose, R. B., Cubbison, C., Fairbrother, A., Keating, M. H., Mahaffey, K. R., Mukerjee, D., Rice, G. E., Reismann, D. J., Schoeny, R., Swartout, J., and Troyer, M. (1997). Mercury Study Report To Congress, Volume 6 Ecological Assessment For Anthropogenic Mercury Emissions In The United States. Report To Congress 6, US EPA.

NIST . Certificate of Analysis: Standard Reference Material 3133, Mercury (Hg) Standard Solution.

Pannu, R. (2012). *Quantifying mercury reduction kinetics in soils*. PhD thesis, University of Saskatchewan.

Parliament, E. (2001). Decision No 2455/2001/EC of the European Parliament and of the Council of 20 November 2001 establishing the list of priority substances in the field of water policy and amending Directive 2000/60/EC. *Official Journal of the European Communities*, L 331/1.

Perrot, V., Epov, V. N., Pastukhov, M. V., Grebenshchikova, V. I., Zouiten, C., Sonke, J. E., Husted, S., Donard, O. F. X., and Amouroux, D. (2010). Tracing sources and bioaccumulation of mercury in fish of Lake Baikal Angara River using Hg isotopic composition. *Environmental Science & Technology*, 44(21):8030–8037. PMID: 20942479.

Pirrone, N., Cinnirella, S., Feng, X., Finkelman, R. B., Friedli, H. R., Leaner, J., Mason, R., Mukherjee, a. B., Stracher, G. B., Streets, D. G., and Telmer, K. (2010). Global mercury emissions to the atmosphere from anthropogenic and natural sources. *Atmospheric Chemistry and Physics*, 10(13):5951–5964.

Rauret, G., López-Sánchez, J. F., Sahuquillo, A., Rubio, R., Davidson, C., Ure, A., and Quevauviller, P. (1999). Improvement of the BCR three step sequential extraction procedure prior to the certification of new sediment and soil reference materials. *Journal of environmental monitoring : JEM*, 1(1):57–61.

Ravichandran, M. (2004). Interactions between mercury and dissolved organic matter—a review. *Chemosphere*, 55(3):319 – 331.

Reis, A., Coelho, J., Rodrigues, S., Rocha, R., Davidson, C., Duarte, A., and Pereira, E. (2012). Development and validation of a simple thermo-desorption technique for mercury speciation in soils and sediments. *Talanta*, 99:363 – 368.

Reis, A. T., Coelho, J. P., Rucandio, I., Davidson, C. M., Duarte, A. C., and Pereira, E. (2015). Thermo-desorption: A valid tool for mercury speciation in soils and sediments? *Geoderma*, 237–238:98 – 104.

Richard, J.-H., Bischoff, C., Ahrens, C. G., and Biester, H. (2016). Mercury (II) reduction and co-precipitation of metallic mercury on hydrous ferric oxide in contaminated groundwater. *Science of The Total Environment*, 539:36–44.

Risher, J. (2003). Elemental mercury and inorganic mercury compounds: human health aspects. Technical report, World Health Organization, Geneva.

Roberts, A. C., Groat, L. A., Raudsepp, M., Ercit, T. S., Erd, R. C., Moffatt, E. A., and Stirling, J. A. (2001). Clearcreekite, a new polymorph of $Hg_3^{1+}(CO_3)(OH)\cdot 2H_2O$, from the Clear Creec claim, San Benito County, California. *The Canadian Mineralogist*, 39(3):779–784.

Rodríguez-González, P., Epov, V. N., Bridou, R., Tessier, E., Guyoneaud, R., Monperrus, M., and Amouroux, D. (2009). Species-specific stable isotope fractionation of mercury during Hg(II) methylation by an anaerobic bacteria (Desulfobulbus propionicus) under dark conditions. *Environmental Science & Technology*, 43(24):9183–9188. PMID: 19924895.

Rua-Ibarz, A., Bolea-Fernandez, E., Maage, A., Frantzen, S., Valdersnes, S., and Vanhaecke, F. (2016). Assessment of Hg pollution released from a WWII submarine wreck (U-864) by Hg isotopic analysis of sediments and Cancer pagurus tissues. *Environmental Science & Technology*, 50(19):10361–10369.

Scheffer, W. and Schachtschabel, P. (2010). Anorganische Komponenten der Böden – Minerale und Gesteine. In *Lehrbuch der Bodenkunde*, H.-P. Blume, G. W. Brümmer, R. Horn, E. Kandeler, I. Kögel-Knabner, R. Kretzschmar, K. Stahr, and B.-M. Wilke, eds., chapter 2, 7–49. Heidelberg: Spektrum Akademischer Verlag.

Schlüter, K. (2000). Review: evaporation of mercury from soils. An integration and synthesis of current knowledge. *Environmental Geology*, 39(3):249–271.

Scholtz, M., Heyst, B. V., and Schroeder, W. (2003). Modelling of mercury emissions from background soils. *Science of The Total Environment*, 304(1–3):185 – 207. Pathways and processes of mercury in the environment. Selected papers presented at the sixth International Conference on Mercury as Global Pollutant, Minamata, Japan, Oct. 15-19, 2001.

Schöndorf, T., Egli, M., Biester, H., Mailahn, W., and Rotard, W. (1999). Distribution, bioavailability and speciation of mercury in contamintated soil and groundwater of a former wood impregnation plant. In *Mercury Contaminated Sites*, R. Ebinghaus and E. Al., eds. Springer Berlin Heidelberg.

Schöndorf, T., Heinrichsmeier, K., Biester, H., and Achstetter, U. (1995). Neue Wege und Erfahrungen bei der Erkundung einer Bodenbelastung durch Quecksilber in einer Wohnsiedlung. *TerraTech*, 5:31–35.

Schroeder, W. H. and Munthe, J. (1998). Atmospheric mercury—An overview. *Atmospheric Environment*, 32(5):809 – 822.

Schuster, E. (1991). The behavior of mercury in the soil with special emphasis on complexation and adsorption processes - A review of the literature. *Water Air & Soil Pollution*, 56(1):667–680.

Skyllberg, U. (2010). Mercury biogeochemistry in soils and sediments. In *Synchrotron-Based Techniques in Soils and Sediments*, B. Singh and M. Gräfe, eds., volume 34 of *Developments in Soil Science*, chapter 13, 379 – 410. Elsevier.

Skyllberg, U. (2011). Chemical speciation of mercury in soil and sediment. In *Environmental Chemistry and Toxicology of Mercury*, 219–258. Hoboken, NJ, USA: John Wiley & Sons, Inc.

Smith, R. S., Wiederhold, J. G., and Kretzschmar, R. (2015). Mercury isotope fractionation during precipitation of metacinnabar (β-HgS) and montroydite (HgO). *Environmental Science and Technology*, 49(7):4325–4334.

Sonke, J. E., Schäfer, J., Chmeleff, J., Audry, S., Blanc, G., and Dupré, B. (2010). Sedimentary mercury stable isotope records of atmospheric and riverine pollution from two major European heavy metal refineries. *Chemical Geology*, 279(3–4):90 – 100.

Sonke, J. E., Zambardi, T., and Toutain, J.-P. (2008). Indirect gold trap-MC-ICP-MS coupling for Hg stable isotope analysis using a syringe injection interface. *Journal of Analytical Atomic Spectrometry*, 23:569–573.

Stetson, S. J., Gray, J. E., Wanty, R. B., and Macalady, D. L. (2009). Isotopic variability of mercury in ore, mine-waste calcine, and leachates of mine-waste calcine from areas mined for mercury. *Environmental Science & Technology*, 43(19):7331–7336. PMID: 19848142.

Sun, R., Streets, D. G., Horowitz, H. M., Amos, H. M., Liu, G., Perrot, V., Toutain, J.-P., Hintelmann, H., Sunderland, E. M., and Sonke, J. E. (2016). Historical (1850–2010) mercury stable isotope inventory from anthropogenic sources to the atmosphere. *Elementa*, 4(91):1–15.

Templeton, D. M., Ariese, F., Cornelis, R., Danielsson, L.-G., Muntau, H., van Leeuwen, H. P., and Lobinski, R. (2000). Guidelines for terms related to chemical speciation and fractionation of elements. Definitions, structural aspects, and methodological approaches (IUPAC Recommendations 2000). *Pure and Applied Chemistry*.

Tessier, A., Campbell, P. G. C., and Bisson, M. (1979). Sequential extraction procedure for the speciation of particulate trace metals. *Analytical Chemistry*, 51(7):844–851.

Ullrich, S. M., Tanton, T. W., and Abdrashitova, S. A. (2001). Mercury in the aquatic environment: A review of factors affecting methylation. *Critical Reviews in Environmental Science and Technology*, 31(3):241–293.

UNEP (2013a). Global Mercury Assessment 2013: Sources, emissions, releases, and environmental transport. Technical report, UNEP Chemicals Branch, Geneva.

UNEP (2013b). Minamata Convention on Mercury - Text and Annexes. 69.

Ure, A. M. (1991). Trace element speciation in soils, soil extracts and solutions. *Microchimica Acta*, 104(1):49–57.

US-EPA (1995). Mercuric chloride ($HgCl_2$); CASRN 7487-94-7. Website. https://cfpub.epa.gov/ncea/iris2/chemicalLanding.cfm?substance_nmbr=692. Accessed: 2017-03-16.

Varekamp, J. C. and Buseck, P. R. (1984). The speciation of mercury in hydrothermal systems, with applications to ore deposition. *Geochimica et Cosmochimica Acta*, 48(1):177 – 185.

Wallschläger, D., Desai, M. V. M., and Wilken, R.-D. (1996). The role of humic substances in the aqueous mobilization of mercury from contaminated floodplain soils. *Water, Air, and Soil Pollution*, 90(3):507–520.

WHO (2011). Ten chemicals of major public health concern. Website. www.who.int/ipcs/assessment/public_health/chemicals_phc/en/. Accessed: 18.05.2017.

Wiederhold, J. G. (2015). Metal stable isotope signatures as tracers in environmental geochemistry. *Environmental Science & Technology*, 49(5):2606–2624. PMID: 25640608.

Wiederhold, J. G., Cramer, C. J., Daniel, K., Infante, I., Bourdon, B., and Kretzschmar, R. (2010). Equilibrium mercury isotope fractionation between dissolved Hg(II) species and thiol-bound Hg. *Environmental Science and Technology*, 44(11):4191–4197.

Wiederhold, J. G., Skyllberg, U., Drott, A., Jiskra, M., Jonsson, S., Björn, E., Bourdon, B., and Kretzschmar, R. (2015). Mercury isotope signatures in contaminated sediments as a tracer for local industrial pollution sources. *Environmental Science & Technology*, 49(1):177–185.

Wiederhold, J. G., Smith, R. S., Siebner, H., Jew, A. D., Brown, G. E., Bourdon, B., and Kretzschmar, R. (2013). Mercury isotope signatures as tracers for Hg cycling at the new idria Hg mine. *Environmental Science and Technology*, 47(12):6137–6145.

Yin, R., Feng, X., and Shi, W. (2010). Application of the stable-isotope system to the study of sources and fate of Hg in the environment: A review. *Applied Geochemistry*, 25(10):1467 – 1477.

Yin, R., Feng, X., Wang, J., Bao, Z., Yu, B., and Chen, J. (2013). Mercury isotope variations between bioavailable mercury fractions and total mercury in mercury contaminated soil in Wanshan Mercury Mine, SW China. *Chemical Geology*, 336:80–86.

Yin, R., Lepak, R. F., Krabbenhoft, D. P., and Hurley, J. P. (2016). Sedimentary records of mercury stable isotopes in Lake Michigan. *Elementa*, 4(86).

Yu, L.-P. and Yan, X.-P. (2003). Factors affecting the stability of inorganic and methylmercury during sample storage. *Trends in Analytical Chemistry*, 22(4):245 – 253.

Zheng, W., Foucher, D., and Hintelmann, H. (2007). Mercury isotope fractionation during volatilization of Hg(0) from solution into the gas phase. *Journal of Analytical Atomic Spectrometry*, 22:1097–1104.

Zheng, W. and Hintelmann, H. (2009). Mercury isotope fractionation during photoreduction in natural water is controlled by its Hg/DOC ratio. *Geochimica et Cosmochimica Acta*, 73(22):6704 – 6715.

Zheng, W. and Hintelmann, H. (2010). Nuclear field shift effect in isotope fractionation of mercury during abiotic reduction in the absence of light. *The Journal of Physical Chemistry A*, 114(12):4238–4245. PMID: 20192261.

Appendix A

Bloom Extraction Test

F1: 25mL H_2O_{MQ}, 18 h in overhead shaker, centrifuged at 3000 rpm for 15 min, filtered through cellulose acetate syringe filter, 0.8 mL 0.2 M $BrCl$ added

F2: 0.1 M HCl + 0.1 M acetic acid, 18h in overhead shaker, centrifuged at 3000rpm for 15min, filtered through 0.45 μm cellulose acetate syringe filter, 0.8 mL 0.2 M $BrCl$ added

F3: 1 M KOH, 18 h in overhead shaker, centrifuged at 3000 rpm for 15 min, filtered through 0.45μm cellulose acetate syringe filter, 3.060 mL 0.2 M $BrCl$ added

F4: 12M HNO_3, 18 h in overhead shaker, centrifuged at 3000 rpm for 15 min, filtered through 0.45μm PTFE syringe filter 0.4 mL 0.2 M $BrCl$ added

F5: 13 mL aqua regia, 18 h in overhead shaker, centrifuged at 3000 rpm for 15 min, 8 mL H_2O_{MQ} added, filtered through 0.45μm PTFE syringe filter

TABLE A.1 Test of Bloom's 5-step extractoin protocol (Bloom et al., 2003) on dried material of drilling core E6 of the Bad Krozingen site. 'N2711' ... NIST 2711 'Montana soil" standard. 'E6_7' and 'E6_7f' represent the same sample from core E6, where the sample without suffix was milled, the sample marked 'f' was not. 'BK 3026' represents the highest contaminated sample from previous Bad Krozingen soil samples and is believed to be the sample most similar to the contamination source.

	F1		F2		F3		F4		F5		Total
Name	**% Hg in F1 [%]**	**Hg conc. [mg/kg]**	**% Hg in F2 [%]**	**Hg conc. [mg/kg]**	**% Hg in F2B [%]**	**Hg conc. [mg/kg]**	**% Hg in F2 [%]**	**Hg conc. [mg/kg]**	**% Hg in F5 [%]**	**Hg conc. [mg/kg]**	**In sample [mg/kg]**
N2711	0.65	0.03	0.00	0.00	1.79	0.10	76.40	4.10	21.17	1.14	5.36
E6_7f	2.58	0.15	41.81	2.50	6.24	0.37	33.46	2.00	15.91	0.95	5.98
E6_7f			56.90	7.59			35.28	4.70	7.81	1.04	13.33
E6_7			38.40	2.02			52.67	2.77	8.93	0.47	5.26
BK 3026			0.02	0.02			93.41	108.59	6.57	7.63	116.25

F1: H_2O_{MQ}
F2: 0.1M HCl + 0.1M CH_3COOH
F3: 1M KOH
F4: 12M HNO_3
F5: aqua regia

Appendix B

Sequential extraction data

TABLE B.1 Mercury concentration results of the First Sequential Extraction. Concentrations are wet weight concentrations. (Water content mesurements for determination of dry weight concentrations of the samples can be found in table 3.1 of section 3.2).

Name	F1		F2		F2B		F4		F5		Total In sample [mg/kg]
	% Hg in F1 [%]	Hg conc. [mg/kg]	% Hg in F2 [%]	Hg conc. [mg/kg]	% Hg in F2B [%]	Hg conc. [mg/kg]	% Hg in F2 [%]	Hg conc. [mg/kg]	% Hg in F5 [%]	Hg conc. [mg/kg]	
N2711	0.68	0.03	0.08	0.04	0.01	0.00	95.29	4.85	3.94	0.20	5.13
K2-5	0.18	0.10	10.47	5.59	8.60	4.59	72.96	38.92	7.78	4.15	53.34
K2-6	2.42	2.70	7.42	8.29	18.20	20.34	65.69	73.42	6.28	7.02	111.78
K2-7	1.78	10.39	9.69	56.59	18.44	107.63	59.34	346.35	10.75	62.74	583.70
K2-8a	1.87	10.69	3.98	22.78	6.31	36.15	66.08	378.50	21.77	124.68	572.80
K2-8b	4.44	18.73	6.06	25.61	8.89	37.53	64.23	271.20	16.38	69.16	422.22
K2-8c	2.48	11.40	4.62	21.21	7.48	34.36	66.57	305.75	18.84	86.54	459.26
K2-9	2.24	3.80	4.17	7.09	3.42	5.82	70.81	120.38	19.36	32.92	170.02
K2-10	4.58	0.65	1.24	0.18	0.04	0.01	87.85	12.55	6.29	0.90	14.29
K2-11	3.63	0.52	1.96	0.28	0.02	0.00	86.20	12.45	8.19	1.18	14.44
K2-12	2.98	0.13	0.89	0.04	0.00	0.00	90.90	4.08	5.23	0.23	4.49
K3-2a	1.11	0.60	1.16	0.63	1.64	0.89	89.63	48.51	6.46	3.50	54.12
K3-2b	1.30	1.14	0.80	0.71	1.11	0.98	88.09	77.58	8.70	7.66	88.06
K3-2c	0.98	1.41	0.86	1.23	2.32	3.33	87.60	125.76	8.24	11.83	143.55
K3-3	0.55	0.33	0.03	0.02	0.02	0.01	95.07	57.42	4.33	2.62	60.40
K3-4	0.05	0.10	0.01	0.01	0.01	0.01	99.77	187.31	0.17	0.32	187.74
K3-5	0.45	0.07	0.02	0.00	0.03	0.01	95.42	15.10	4.09	0.65	15.82

F1: 25 mL H_2O_{MQ}, 18 h in end-over-end shaker, centrifuged at 3000 g for 15 min, filtered through 0.45 μm cellulose acetate syringe filter, 0.025 mL 0.2 M $BrCl$ added.

F2: 25 mL 0.01 M HCl + 0.1 M CH_3COOH, 18 h in end-over-end shaker, centrifuged at 3000 g for 15 min, filtered through 0.45 μm cellulose acetate syringe filter, 0.025 mL 0.2 M $BrCl$ added.

F2B: repetition of F2, to dissolve residual carbonate present in sample, and consequently lower the pH to similar values as described by Bloom et al. (2003).

F3: 25 mL 12 M HNO_3, 18 h in end-over-end shaker, centrifuged at 3000 g for 15 min, filtered through 0.45 μm PTFE syringe filter, 0.4 mL 0.2 M $BrCl$ added.

F4: 12 mL aqua regia (8 mL HCl, 3 mL HNO_3, 1 mL 0.2 M $BrCl$ in concentrated HCl), 18 h in lateral shaker, 8 mL H_2O_{MQ} added, centrifuged at 3000 g for 15 min, filtered through 0.45 μm PTFE syringe filter.

TABLE B.2 Mercury concentration results of the Optimized Sequential Extraction.Concentrations are wet weight concentrations. (Water content mesurements for determination of dry weight concentrations of the samples can be found in table 3.1 of section 3.2).

	F1		F2		F3		F4		Total
Name	**% Hg in F1 [%]**	**Hg conc. [mg/kg]**	**% Hg in F2 [%]**	**Hg conc. [mg/kg]**	**% Hg in F3 [%]**	**Hg conc. [mg/kg]**	**% Hg in F4 [%]**	**Hg conc. [mg/kg]**	**In sample [mg/kg]**
N2711	0.97	0.06	0.20	0.01	3.83	0.22	95.00	5.48	5.77
N2711	0.72	0.04	0.23	0.01	2.89	0.17	96.16	5.50	5.72
K2-5c	1.97	0.61	10.72	3.30	8.52	2.63	78.78	24.28	30.82
K2-6c	2.09	2.99	21.69	31.08	28.00	40.12	48.22	69.09	143.27
K2-7c	1.73	12.87	16.69	123.91	47.15	350.14	34.43	255.73	742.65
K2-8z	2.13	13.49	16.30	103.41	39.13	248.24	42.44	269.20	634.35
K2-8aa	3.21	17.65	19.17	105.31	39.10	214.76	38.51	211.55	549.26
K2-8ab	2.35	14.70	16.83	105.41	40.60	254.23	40.22	251.82	626.17
K2-8ac		13.65		105.58		238.29			357.52
K2-8ad		16.19		138.35					154.54
K2-8ae		15.22							15.22
K2-9c	0.22	0.38	12.96	22.00	16.59	28.15	70.23	119.19	169.71
K2-10c	4.08	1.03	1.13	0.28	6.73	1.69	88.06	22.14	25.14
K2-11c	3.35	0.17	2.59	0.13	4.58	0.23	89.48	4.42	4.94
K2-12c	3.06	0.14	1.28	0.06	5.93	0.27	89.73	4.03	4.49
K3-2c	2.61	1.70	1.85	1.20	9.55	6.21	85.99	55.91	65.02
K3-3u	1.03	0.69	0.17	0.11	8.51	5.66	90.29	60.09	66.55
K3-3v	0.88	0.48	0.07	0.04	8.42	4.60	90.63	49.45	54.56
K3-3w	1.20	0.71	0.05	0.03	8.39	5.01	90.37	53.96	59.72
K3-3x		0.61		0.03		4.78			5.41
K3-3y		0.46		0.03					0.49
K3-3z		0.30							0.30
K3-4c	2.73	0.26	3.11	0.30	20.44	1.97	73.71	7.12	9.65
K3-5c	1.82	0.31	0.24	0.04	44.11	7.55	53.83	9.21	17.12

F1: 25 mL H_2O_{MQ}, 18 h in end-over-end shaker, centrifuged at 3500 rpm (2360 g) for 15 min, filtered through cellulose acetate syringe filter, 0.250 mL 0.2 M $BrCl$ added

F2: 25 mL 0.5 M HNO_3, 18 h in end-over-end shaker, centrifuged at 3500 rpm (2360 g) for 15 min, filtered through 0.45μm cellulose acetate syringe filter, 0.250 mL 0.2 M $BrCl$ added

F3: 25 mL 6 M HNO_3, 18 h in end-over-end shaker, 25 mL H_2O_{MQ} added, centrifuged at 3000 g for 15 min, filtered through 0.45 μm cellulose acetate syringe filter, 0.500 mL 0.2 M $BrCl$ added

F4: 12 mL aqua regia (8 mL HCl, 3 mL HNO_3), 1 mL 0.2 M $BrCl$ in concentrated HCl, 18 h in end-over-end shaker, 36 mL H_2O_{MQ} added, centrifuged at 3000 g (HeroLab) for 15 min, filtered through 0.45 μm cellulose acetate syringe filter

Appendix C

Mercury stable isotope data tables

C.1 Mercury stable isotopes, Optimized SEP

TABLE C.1 Mercury stable isotope data collected from core K3 during Optimized SEP. Where standard deviations are given, they refer to repeat measurements of the samples. Standard deviations of all other samples can be taken from table C.3, either from the overall variability of the 'Fluka' standard or the specific session which the samples were measured in.

Sample Name	Sample Depth [cm]	Sample Type	Pool Size [%]	n	δ^{202}Hg [‰]	2 SD [‰]	$\Delta^{199}Hg$ [‰]	2 SD [‰]	$\Delta^{200}Hg$ [‰]	2 SD [‰]	$\Delta^{201}Hg$ [‰]	2 SD [‰]	$\Delta^{204}Hg$ [‰]	2 SD [‰]	Date
K3-02	**30**	**F1**	**2.61**	**3**	**0.01**	**0.05**	**0.00**	**0.03**	**-0.02**	**0.13**	**0.02**	**0.08**	**0.00**	**0.07**	**November 2016**
		F2	1.85		-0.06		0.00		-0.13		-0.07		0.00		15 November 2016
		F4	9.55	2	0.05	0.10	0.01	0.02	0.04	0.03	0.00	0.00	0.00	0.04	November 2016
		F5	85.99		0.01		-0.03		0.14		-0.04		-0.01		29 November 2016
		bulk calc	*100.00*		*0.01*		*-0.03*		*0.12*		*-0.03*		*-0.01*		
		Bulk	**100.00**		**-0.06**		**0.01**		**0.02**		**-0.01**		**-0.01**		**18 July 2016**
K3-03	50	F1	1.03		0.34		-0.02		-0.03		-0.05		0.02		17 November 2016
		F2	0.17		0.26		-0.02		-0.21		0.03		-0.08		18 November 2016
		F4	8.51		0.26		-0.03		0.03		-0.01		0.02		28 November 2016
		F5	90.29		-0.01		-0.09		0.04		0.01		-0.03		17 November 2016
		bulk calc	*100.00*		*0.02*		*-0.08*		*0.04*		*0.01*		*-0.02*		
		Bulk	**100.00**		**0.08**		**-0.10**		**-0.04**		**-0.04**		**0.01**		**19 July 2016**
K3-04	**70**	**Bulk**	**100.00**		**-0.03**		**-0.02**		**-0.02**		**-0.01**		**0.02**		**18 July 2016**
K3-05	**140**	**Bulk**	**100.00**		**-0.12**		**-0.02**		**0.02**		**-0.01**		**-0.01**		**18 July 2016**

TABLE C.2 Mercury stable isotope data collected from core K2 during Optimized SEP. Where standard deviations are given, they refer to repeat measurements of the samples. Standard deviations of all other samples can be taken from table C.3, either from the overall variability of the 'Fluka' standard or the specific session which the samples were measured in.

Sample Name	Sample Depth [cm]	Sample Type	Pool Size [%]	n	$\delta^{202}Hg$ [‰]	2 SD [‰]	$\Delta^{199}Hg$ [‰]	2 SD [‰]	$\Delta^{200}Hg$ [‰]	2 SD [‰]	$\Delta^{201}Hg$ [‰]	2 SD [‰]	$\Delta^{204}Hg$ [‰]	2 SD [‰]	Date
K2-04	**70**	**Bulk**	**100.00**	**1**	**-0.22**		**-0.01**		**0.09**		**-0.02**		**-0.01**		**14 July 2016**
K2-05	180	F1	1.97	3	-0.34	0.06	-0.04	0.01	0.03	0.07	-0.06	0.04	0.00	0.06	Fall 2016
		F2	10.72		0.15		-0.10		-0.03		-0.09		0.05		21 December 2016
		F4	8.52		0.21		-0.06		-0.11		-0.10		0.02		21 December 2016
		F5	78.78	2	-0.22	0.08	-0.07	0.06	-0.05	0.11	-0.06	0.06	-0.02	0.14	Fall 2016
		bulk calc	*100.00*		*-0.01*		*-0.15*		*-0.07*		*-0.05*		*-0.07*		
		Bulk	**100.00**		**-0.14**		**-0.17**		**-0.12**		**-7.00**		**0.06**		**14 July 2016**
K2-06	200	F1	2.09		-0.47		-0.03		-0.01		-0.03		0.01		28 November 2016
		F2	21.69		-0.15		-0.09		-0.03		-0.07		0.02		28 November 2016
		F4	28.00		-0.19		-0.04		0.03		-0.01		-0.02		28 November 2016
		F5	48.22		-0.43		-0.02		-0.01		-0.04		-0.07		28 November 2016
		bulk calc	*100.00*		*-0.30*		*-0.04*		*0.00*		*-0.04*		*-0.04*		
		Bulk	**100.00**		**-0.36**		**-0.23**		**0.13**		**-0.10**		**0.06**		**14 July 2016**
K2-07	220	F1	1.73	2	-0.30	0.03	0.00	0.04	0.00	0.06	-0.04	0.01	0.02	0.13	Fall 2016
		F2	16.69		0.04		-0.15		-0.07		-0.09		0.02		20 December 2016
		F4	47.15		-0.37		-0.04		-0.05		-0.04		-0.03		20 December 2016
		F5	34.43		-0.57		-0.01		-0.05		-0.05		-0.01		20 December 2016
		bulk calc	*100.00*		*-0.37*		*-0.05*		*-0.05*		*-0.05*		*-0.01*		
		Bulk	**100.00**		**-0.38**		**0.00**		**0.10**		**-0.05**		**0.00**		**14 July 2016**
K2-08 F1 extract	240	F1A	*10037*		0.18		-0.11		0.11		-0.05		-0.01		29 November 2016
		F1B	*6510*		0.13		-0.05		0.13		-0.01		-0.04		29 November 2016
Fract.size		F1C	*6246*		-0.05		-0.05		-0.03		-0.07		-0.02		29 November 2016
is given		F1D*	*3611*		0.58		-0.06		0.08		-0.03		0.00		20 December 2016
in ng_{Hg} / g_{soil}		F1E	*3560*		-0.21		-0.03		0.10		-0.05		0.00		20 December 2016
		F1F	*2858*		-0.03		-0.02		-0.03		-0.07		0.01		20 December 2016
		F1G	*2693*	2	-0.15	0.04	-0.02	0.02	0.04	0.17	-0.07	0.06	-0.02	0.01	December 2016
K2-08aa		F1	3.21	2	0.12	0.05	-0.06	0.02	-0.11	0.23	-0.09	0.00	0.00	0.05	November 2016
		F2	19.17		-0.25		-0.08		-0.15		-0.03		0.03		16 November 2016
		F4	39.10		-0.36		-0.04		0.02		-0.01		-0.01		16 November 2016
		F5	38.51		-0.42		-0.02		0.03		-0.02		0.03		16 November 2016
		bulk calc	*100.00*		*-0.35*		*-0.04*		*-0.01*		*-0.02*		*0.02*		
		Bulk	**100.00**	**3**	**-0.43**	**0.02**	**-0.02**	**0.07**	**0.00**	**0.06**	**-0.05**	**0.02**	**0.00**	**0.02**	**July 2016**
K2-08z		F1	2.13		0.08		-0.06		0.01		-0.07		0.03		14 November 2016
		F2	16.30		-0.28		-0.05		0.13		-0.02		0.04		15 November 2016
		F4	39.13		-0.45		-0.05		0.03		-0.16		0.00		15 November 2016
		F5	42.44		-0.55		-0.02		0.02		-0.11		-0.05		15 November 2016
		bulk calc	*100.00*		*-0.45*		*-0.04*		*0.04*		*-0.11*		*-0.01*		
		Bulk	**100.00**	**3**	**-0.43**	**0.02**	**-0.02**	**0.07**	**0.00**	**0.06**	**-0.05**	**0.02**	**0.00**	**0.02**	**July 2016**
K2-09	260	F1	0.22		-0.11		-0.04		0.02		-0.03		0.02		28 November 2016
		F2	12.96		0.06		-0.12		0.01		-0.07		0.00		28 November 2016
		F4	16.59		-0.08		-0.09		-0.05		-0.06		-0.04		28 November 2016
		F5	70.23		-0.33		0.00		0.08		0.06		-0.12		28 November 2016
		bulk calc	*100.00*		*-0.24*		*-0.03*		*0.05*		*0.02*		*-0.09*		
		Bulk	**100.00**		**-0.29**		**-0.07**		**0.06**		**-0.05**		**-0.01**		**14 July 2016**
K2-10	280	F1	4.08	2	0.03	0.05	-0.03	0.03	0.02	0.14	-0.04	0.09	0.00	0.03	November 2016
		F2	1.13		-0.03		-0.06		-0.02		-0.04		0.03		18 November 2016
		F4	6.73	2	0.28	0.01	-0.06	0.03	0.03	0.08	-0.06	0.02	0.00	0.05	November 2016
		F5	88.06	2	0.09	0.08	-0.04	0.01	0.06	0.00	-0.04	0.16	0.01	0.03	November 2016
		bulk calc	*100.00*		*0.10*		*-0.04*		*0.06*		*-0.04*		*0.01*		
		Bulk	**100.00**		**0.07**		**-0.10**		**0.21**		**-0.08**		**-0.03**		**14 July 2016**
K2-11	**300**	**Bulk**	**100.00**		**-0.33**		**-0.02**		**-0.03**		**-0.07**		**0.02**		**18 July 2016**
K2-12	**320**	**Bulk**	**100.00**		**-0.25**		**0.02**		**0.04**		**-0.05**		**0.01**		**18 July 2016**

* F1D equilibrated 2 weeks instead of 18 +/- 4 hrs

TABLE C.3 The 'ETH-Fluka'standard was repeatedly measured in all sessions which provide data to this thesis. Based on its variability, the analytical precision of the mercury stable isotope measurements was determined.

Sample Name		δ^{202}**Hg**	**2 SD**	$\Delta^{199}Hg$	**2 SD**	$\Delta^{200}Hg$	**2 SD**	$\Delta^{201}Hg$	**2 SD**	$\Delta^{204}Hg$	**2 SD**	**Date**
		[‰]	[‰]	[‰]	[‰]	[‰]	[‰]	[‰]	[‰]	[‰]	[‰]	
Fluka		-1.45		0.10		0.17		0.03		0.02		14 July 2016
		-1.36		0.09		0.22		0.06		0.01		14 July 2016
		-1.36		0.05		0.00		0.03		0.00		14 July 2016
		-1.37		0.09		0.00		0.04		-0.01		18 July 2016
		-1.41		0.09		-0.02		0.04		0.02		18 July 2016
		-1.39	-1.39‰,	0.07	0.07‰,	0.04	0.05‰,	0.04	0.03‰,	0.01	0.00‰,	18 July 2016
		-1.44	2 SD	0.03	2 SD	0.01	2 SD	0.01	2 SD	-0.03	2 SD	18 July 2016
		-1.39	= 0.06‰,	0.10	=0.08‰,	-0.02	= 0.15‰,	0.02	= 0.04‰,	0.01	= 0.04‰,	19 July 2016
		-1.38	n=14	0.09	n=14	0.00	n=14	0.01	n=14	-0.02	n=14	19 July 2016
		-1.39		0.08		0.00		0.03		0.01		19 July 2016
		-1.38		0.07		0.11		0.04		0.02		19 July 2016
		-1.42		-0.03		0.08		-0.01		-0.02		20 July 2016
		-1.39		0.13		0.01		0.01		-0.05		20 July 2016
		-1.38		0.10		0.04		0.06		-0.01		20 July 2016
Fluka		-1.53		0.08		0.04		0.03		0.05		14 November 2016
		-1.59		0.07		-0.15		-0.06		0.04		14 November 2016
		-1.36	-1.44‰,	0.10	0.08‰,	0.04	-0.04‰,	0.14	0.03‰,	-0.08	-0.01‰,	14 November 2016
		-1.43	2 SD	0.08	2 SD	-0.05	2 SD	0.07	2 SD	-0.01	2 SD	15 November 2016
		-1.50	=0.24‰,	0.09	=0.04‰,	0.00	=0.15‰,	0.03	0.08‰,	0.03	=0.10‰,	15 November 2016
		-1.54	n=8	0.06	n=8	-0.14	n=8	-0.06	n=8	0.00	n=8	15 November 2016
		-1.30		0.07		-0.02		-0.02		-0.06		15 November 2016
		-1.24		0.12		-0.06		0.14		-0.05		15 November 2016
Fluka		-1.45		0.07		0.02		0.02		0.02		16 November 2016
		-1.46		0.08		0.01		0.03		-0.02		16 November 2016
		-1.36		0.09		0.05		0.02		0.06		16 November 2016
		-1.42		0.07		-0.13		0.09		-0.05		16 November 2016
		-1.36		0.06		-0.09		-0.04		-0.02		17 November 2016
		-1.42		0.08		0.07		0.02		-0.03		17 November 2016
		-1.45		0.09		0.10		0.05		0.03		17 November 2016
		-1.45		0.09		-0.04		0.03		-0.02		17 November 2016
		-1.46		0.11		-0.09		0.04		-0.02		18 November 2016
		-1.43	-1.45‰,	0.10	0.08‰,	0.03	0.01‰,	0.08	0.03‰,	0.00	0.00‰,	18 November 2016
		-1.49	2 SD	0.05	2 SD	0.08	2 SD	0.02	2 SD	-0.03	2 SD	18 November 2016
		-1.47	= 0.09‰,	0.09	= 0.04‰,	0.19	= 0.15‰,	0.03	= 0.06‰,	0.01	= 0.06‰,	18 November 2016
		-1.46	n=23	0.05	n=23	-0.03	n=23	0.06	n=23	-0.01	n=23	18 November 2016
		-1.50		0.11		-0.01		0.04		0.04		28 November 2016
		-1.44		0.08		0.05		0.02		0.02		28 November 2016
		-1.52		0.07		-0.03		0.02		-0.01		28 November 2016
		-1.48		0.07		0.04		0.02		-0.04		28 November 2016
		-1.52		0.04		-0.03		0.01		0.04		28 November 2016
		-1.50		0.07		-0.04		-0.03		0.07		28 November 2016
		-1.40		0.09		0.03		0.02		-0.01		29 November 2016
		-1.51		0.05		0.03		0.02		0.04		29 November 2016
		-1.43		0.07		-0.10		0.00		0.01		29 November 2016
		-1.40		0.09		0.00		0.02		0.01		29 November 2016
Fluka		-1.39		0.05		0.09		0.01		-0.03		20 December 2016
		-1.42		0.06		0.12		-0.01		-0.03		20 December 2016
		-1.51	-1.40‰	0.12	0.08‰	0.13	0.09‰,	0.04	0.01‰,	-0.01	0.01‰,	20 December 2016
		-1.35	2 SD	0.10	2 SD	0.03	2 SD	0.04	2 SD	0.01	2 SD	20 December 2016
		-1.37	= 0.11‰,	0.06	= 0.05‰,	0.05	= 0.13‰,	-0.01	= 0.05‰,	0.07	= 0.08‰,	20 December 2016
		-1.39	n=7	0.07	n=7	0.02	n=7	0.00	n=7	-0.03	n=7	21 December 2016
	n	-1.37		0.08		0.20		-0.02		0.05		21 December 2016
Fluka overall	52	-1.43	0.13	0.08	0.05	0.02	0.16	0.03	0.08	0.00	0.07	
Fluka 16. November - 21. December	30	-1.44	0.10	0.08	0.04	0.03	0.16	0.02	0.06	0.00	0.07	

C.2 Mercury stable isotopes, First SEP

TABLE C.4 Mercury stable isotope data collected from both cores K2 and K3 during the First SEP. Where standard deviations are given, they refer to repeat measurements of the samples. Standard deviations of all other samples can be taken from table C.3, either from the overall variability of the 'Fluka' standard or the specific session which the samples were measured in.

Sample Name	Sample Depth [cm]	Sample Type	Pool Size [%]	n	δ^{202}Hg [‰]	2 SD [‰]	$\Delta^{199}Hg$ [‰]	2 SD [‰]	$\Delta^{200}Hg$ [‰]	2 SD [‰]	$\Delta^{201}Hg$ [‰]	2 SD [‰]	$\Delta^{204}Hg$ [‰]	2 SD [‰]	Date
K2-8a	240	F1	1.87	1	0.11		-0.06		0.05		-0.07		-0.03		19 July 2016
	240	F2	3.98	1	0.35		-0.12		0.06		-0.09		0.01		19 July 2016
	240	F2B	6.31	1	0.25		-0.12		0.07		-0.09		0.02		19 July 2016
	240	F3	66.08	1	-0.40		0.02		0.00		-0.02		0.00		19 July 2016
	240	F4	21.77	1	-0.50		-0.03		-0.01		-0.04		0.04		19 July 2016
K2-9	260	F1	2.24	1	-0.08		0.00		0.16		-0.02		0.01		19 July 2016
	260	F2	4.17	1	0.20		-0.01		0.02		-0.06		0.03		19 July 2016
	260	F2B	3.42	1	0.20		-0.08		0.08		-0.07		-0.01		19 July 2016
	260	F3	70.81	1	-0.06		-0.23		-0.03		-0.12		-0.02		20 July 2016
	260	F4	19.36	1	-0.55		0.11		0.07		0.03		-0.03		20 July 2016
K3-2c	30	F1	0.98	1	0.27		0.05		0.09		0.02		-0.06		20 July 2016
	30	F2	0.86	1	0.46		-0.25		-0.08		-0.07		0.00		20 July 2016
	30	F2B	2.32	2	0.82	0.02	0.01	0.01	0.07	0.09	0.03	0.02	0.04	0.04	20 July 2016
	30	F4	8.24	1	-0.45		-0.12		-0.06		-0.07		-0.01		20 July 2016

Abstract

Understanding the speciation of mercury (Hg) in the environment is key to understanding its risk, since mercury species differ drastically in their bioavailability and toxicity. Biogeochemical reactions of Hg have been found to induce Hg stable isotope fractionation between the product and the reactant. Studying stable isotope signatures of different mercury pools thus provides an opportunity to trace the transformations of the contaminant in the soil. While this has been observed both in the field and in the laboratory, few studies have applied these findings to study transformation processes in contaminated field sites, which was the aim of this thesis. Two soil cores from a $HgCl_2$-contaminated field site in Bad Krozingen, Germany were collected: Core K2 from the source of the contamination and core K3 from the border of the facility, where the contamination is only secondary, from the movement of soil during construction of residential buildings blocks. Both cores were analyzed for their total mercury content and pyrolytic thermo-desorption (PTD) was conducted to characterize its speciation. The highest-contaminated samples were extracted according to a sequential extraction protocol (SEP). Hg stable isotopes were measured on the extracts. The combination of PTD and SEP revealed differences in speciation between the two cores and between different soil depths. Only the most contaminated samples in K2 (up to 802 $^{mg}/_{kg}$) contained Hg^0, and only the most contaminated samples in K3 (up to 100 $^{mg}/_{kg}$) contained evidence for HgS. The majority of mercury in both cores was Hg^{II}, whose exact binding forms could not be determined with the used methods. However, via stable isotope analysis, significant differences in the isotopic signatures of the cores, different depths and different extracted pools could be determined. Assuming the contamination source signature to lie within the average literature value for industrial Hg^0 of -0.45 $\pm$ 0.31 ‰ δ^{202}Hg (2 SD, n=8), the pools of refractory mercury in the most contaminated soil samples in core K2 were within that value, whereas all values in core K3 were significantly heavier, hinting at a more strongly altered mercury pool. Within the most contaminated samples, refractory, tightly bound Hg displayed the lightest signatures, whereas the more labile, 0.5 M HNO3-extractable Hg was significantly heavier. Water-extractable Hg varied widely in its Hg isotopic composition. This field study demonstrated successfully that biogeochemical transformations induce significant fractionation of Hg stable isotopes, even in a site with only a single source of contamination. The fractionation observed fit well with literature reporting fractionation factors via laboratory experiments, but quantification of the processes remains a project for further study.

Deutsche Zusammenfassung

Um das Verhalten von Quecksilber (Hg) in der Umwelt zu verstehen, ist es unumgänglich, seine Speziierung zu kennen, da sich die verschiedenen Spezies stark in ihrer Bioverfügbarkeit und Toxizität unterscheiden. Diese Prozesse in einem natürlichen System zu verstehen, ist oft eine Herausforderung. Da viele der biogeochemischen Prozesse, die in der Umwelt relevant sind, die stabilen Hg-Isotopen charakteristisch fraktionieren, sind Isotopenmessungen an verschiedenen Hg-Pools in einem System eine vielversprechende Möglichkeit, um die Umwandlungsprozesse, die stattgefunden haben, zu verstehen. Fraktionierungsfaktoren von Hg-Umwandlungsreaktionen wurden hauptsächlich durch Laborexperimente bestimmt - bis jetzt wurde das Konzept des „Process Tracing“ durch Isotopenmessungen noch nicht erfolgreich auf Feldsysteme angewandt. Diese Verknüpfung war das Ziel dieser Arbeit. An einem durch $HgCl_2$ kontaminierten Standort in Bad Krozingen, Deutschland wurden zwei Rammkernsonden gezogen. Bohrkern K2 stammt aus der am stärksten kontaminierten Zone, wo die $HgCl_2$-Lösung direkt in den Boden eingetragen wurde. K3 war sekundär durch Umlagerung des Erdreichs aufgrund von Bauarbeiten Hg-verseucht. Beide Bohrkerne wurden hinsichtlich ihres Gesamt-Hg-Gehalts analysiert und mithilfe von pyrolytischer Thermodesorption (PTD) charakterisiert. Die am stärksten kontaminierten Proben wurden nach einem optimierten sequentiellen Extraktionsprotokoll (SEP). Hg-Isotope wurden an den Komplettaufschlüssen und den sequentiellen Extrakten gemessen. Die Ergebnisse von PTD und Gesamtaufschlüssen ergaben sowohl Unterschiede der Bindungsformen von Hg zwischen den beiden Bohrkernen, als auch zwischen den verschiedenen Tiefen. Nur die höchstkontaminierten Proben in K2 (bis zu 802 $^{mg}/_{kg}$) enthielten Hg^0, und nur die am meisten kontaminierten Proben in K3 (bis zu 100$^{mg}/_{kg}$) wiesen Spuren von HgS auf. In beiden Bohrkernen war der Großteil des Hg als Hg^{II} an die Matrix gebunden und nicht näher durch PTD bestimmbar. Über Isotopenmessungen an den extrahierten Pools und Gesamtaufschlüssen konnten nicht nur zwischen Proben und Bohrkernen, sondern auch zwischen den extrahierten Fraktionen Unterschiede festgestellt werden. Die Quellensignatur, die auf Basis einer Literaturrecherche bei -0.45 $\pm$ 0.31 ‰δ^{202}Hg (2 SD, n=8) angenommen wurde, wurde als Referenz für die gemessenen Werte herangezogen. Während die meistkontaminierten Proben im Kern K2 mit diesem Wert überlappten, zeigten alle Proben aus K3 signifikant schwerere δ^{202}Hg-Werte. Das am stärksten gebundene Hg war in allen Fällen der isotopisch leichteste Pool, das mit 0.5 HNO_3 extrahierte Hg in den meisten Fällen schwer relativ zu Gesamtprobe und relativ zur vermuteten Quellensignatur. Der wasserextrahierbare Pool zeigte sich variabel. Der vorliegende Datensatz demonstriert, dass biogeochemische Prozesse an einem kontaminierten Standort signifikante Hg-Isotopenfraktionierung herbeiführen können. Die beobachtete Fraktionierung stimmt mit Literaturwerten über abiotische Reduktion von Hg und verschiedenen Sorptionsprozessen überein. Die Quantifizierung der verschiedenen Einflüsse auf die Fraktionierung bleibt allerdings der Gegenstand von zukünftigen Untersuchungen.